Modeling Long-term Morphological Development of Intertidal Flats

A Comparison among Different Modeling Approaches

Le Zhang

TU Delft
Delft University of Technology

MODELING LONG-TERM MORPHOLOGICAL DEVELOPMENT OF INTERTIDAL FLATS – A COMPARISON AMONG DIFFERENT MODELING APPROACHES

A thesis submitted to the Delft University of Technology in partial fulfillment of the requirements for the degree of

Master of Science in Civil Engineering

by

Le Zhang

5017386

October 2021

Le Zhang: *Modeling Long-term Morphological Development of Intertidal Flats – A Comparison among Different Modeling Approaches* (2021)

The work in this thesis was made in the :

Department of Hydraulic Engineering
Faculty of Civil Engineering and Geosciences
Delft University of Technology

Supervisors: Prof.dr.ir Z.B.(Zheng Bing) Wang
Dr.ir. B.C.(Bram) van Prooijen
Dr.ir. M. (Mick) van der Wegen
Drs. Q.J. (Quirijn) Lodder
Dr. Y. (Ymkje) Huismans

ABSTRACT

Estuarine intertidal flats comprise valuable ecosystems and act as an important sediment source for the adjacent salt marsh systems. However, accelerating sea-level rise threatens the mudflats and associated ecosystems, where the mudflat accretion lag behind sea level rise. A reliable forecast on the morphological developments of the mudflat under sea-level rise scenarios is of vital importance to assess sea level rise impact on the estuarine system.

Different tools exist that can predict the long-term evolution of the mudflats, viz. Delft3D, ASMITA and the hybrid model (Delft3D-ASMITA). Since the hybrid model is newly developed, the comparison among the various approaches has not yet been available. However, it is significant to know if they can produce the same results.

The research aims to compare the three modeling approaches (Delft3D, ASMITA,and the hybrid model) based on a case study in South San Francisco Bay. This comparison will reveal the strengths and weaknesses of the three approaches as well as indications where the approaches may strengthen each other.

The research is conducted in three main phases. Phase 1 consists of the sensitivity analyses in Delft3D for the case of South San Francisco Bay; Phase 2 contains the calibration of one-element and multi-element ASMITA models to reproduce the Delft3D model; Phase 3 focuses on the potential to improve the simulation efficiency of Delft3D in the hybrid model.

Model result comparison shows that, after the calibration, the ASMITA and hybrid model can efficiently simulate the same cases as in Delft3D. However, the upper part (landwards end) of the mudflat is more sensitive to the water level changes in the hybrid model due to the different sediment transport computation modules. The power indicating the relation between the equilibrium and actual morphology as well as the reference level is the important calibration coefficient to adjust the steepness of a mudflat. It can be concluded that the Delft3D model is used as the foundation to calibrate ASMITA and the hybrid model, both of which can improve the simulation efficiency with simplifications, especially in the long-term morphological development.

The study provides clear insights into the comparisons among different modelling approaches in the case of the long-term morphological developments of mudflats by the impacts of sea-level rise. It is recommended to do further research on the configuration of a 2D model and the conduction of the combination of different modeling approaches in other similar cases to confirm the validation.

ACKNOWLEDGEMENTS

First of all, I would like to express my great appreciation to all the people involved in this thesis for their time and effort. I cannot imagine it is possible to achieve the tough ride without them. I want to thank my supervisor Prof. Wang for the timely guidelines and tips during our thesis meetings to ensure my thesis was finalized as planned. Also, I want to thank Dr. van der Wegen for the help with the instructions and advice of Delft3D. In addition, I would like to thank Dr. Huismans for giving me the confidence, the instructions of ASMITA model runs, and the suggestions about the paper structure that provided me with a clear vision to write the report. Drs. Lodder and Dr. van Prooijen, thank you, always giving me constructive feedback in the progress meetings.

Furthermore, I want to thank my parents. They provided not solely the economic support but also the mental encouragement to support me through the difficulties! A special thank you to my friends in Delft, Tao, Shawn, Chen, Ni, Ziru, Fei, Anna, and Huang for providing moral support while I was anxious and sad. A special thank you to Shawn and Chen for providing academic help and career advice! Besides, I appreciate Cai for helping me design the cover of the thesis. To conclude, thank you all for making me believe that nothing is impossible!

CONTENTS

LIST OF FIGURES

LIST OF TABLES

ACRONYMS

1 INTRODUCTION

1.1 INTER-TIDAL FLATS AND *SEA LEVEL RISE (SLR)*

Inter-tidal flats, as the connection between the vegetated shores and the deep channels, inundate and become dry during a tidal cycle. A large amount of mud can accumulate in this area due to limited hydrodynamic forcing. Mudflats serve as a feeding ground for some species (e.g., fish and birds) and provide spaces for microphytobenthos (Herman et al. [1999]). In addition, inter-tidal flats can be an essential source of sediment to adjacent salt marshes (Van der Wegen et al. [2017]). Inter-tidal flats along with the marsh system also play a crucial role in flood defense by wave attenuation (Van der Wegen et al. [2019]). Moreover, due to the rich bio-diversity of the inter-tidal flats, this results in the localities of significant tourist attractions, thus increasing in local economic activities (Dissanayake et al. [2012]).

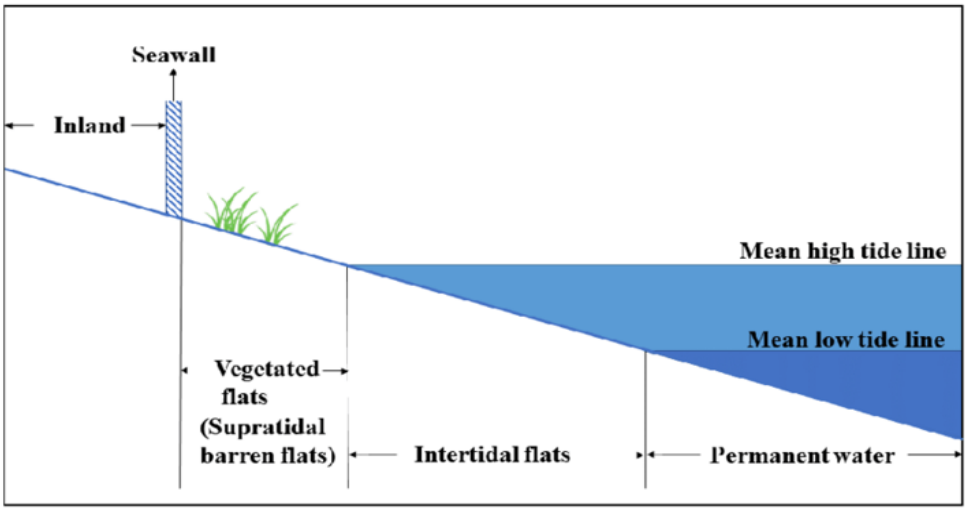

Figure 1.1: Schematization of tidal flat

SLR is one of the factors which impacts the development of intertidal flats. Fleming et al. [1998] indicates that the change in sea level relative to its present position is due to the redistribution of the seawater within the ocean basin, the geological activities in the coastal area, and the changes in the volume or shape of the oceans. Sea-level fluctuated with climate changes and reached its current level 6,000 years ago. There were slight changes in sea level between 1 and 1800 C.E. But sea level started to rise in the nineteenth century rapidly and further accelerated in the early twentieth century. Nowadays, the rate of **SLR** is beyond the level of any time in the past 200 years (Kemp et al. [2011]), and the anticipated global **SLR** rate will be at the range between 0.2 m and 2.0 m by the end of the 21st century (Parris et al. [2012]).

SLR threatens the existence of intertidal flats and associated ecosystems. If the accretion rate of inter-tidal flats cannot keep up with the **SLR** rate, the estuaries may

degenerate into deep tidal lagoons in the case of continuous reduction in the height of inter-tidal flats concerning the rising sea level. From the perspective of sediment transport, the drowning of tidal flats is due to the amount of sediment imported to the basin that cannot make up the new accommodation space gained by the rise in mean sea level (Dissanayake et al. [2012]). The anticipated **SLR** itself is historically unprecedented and involves high uncertainties that need a solid comprehension of the mudflat system dynamics, especially on a long time scale. A reliable forecast of the long-term morphological development of intertidal flats is necessary to identify potential threats and thus adopt timely approaches to reduce economic and ecological losses. This can be achieved by some possible methods in which different types of morphological models can predict the evolution of the inter-tidal flat over a long period.

1.2 MORPHOLOGICAL MODELS

Over the past 30 years, morphological modeling of mudflats has developed rapidly, along with well-established models. The section introduces these modeling approaches, which are helpful tools to do further research.

1.2.1 Delft3D

*Delft3D (**D3D**)* is a process-based model developed by Deltares which allows one- (1D), two- (2DV and 2DH), and three-dimensional (3D) simulations for coastal, river and estuarine areas. This also can discretize the study area in rectilinear, curvilinear, or spherical coordinate systems. It can carry out simulations of flows, sediment transports, waves and morphological developments. The basic structure of the model is shown in Figure 1.2. For hydrodynamics, the equations consist of the horizontal momentum equations, the continuity equation, the transport equation, and a turbulence closure model (Lesser et al. [2004]). The specific equations of sediment transport in **D3D** are in Appendix A.

To significantly improve the efficiency in the morphological calculation, the bed level changes calculated at every hydrodynamic time step are scaled up by multiplying the bed level change by a constant morphological factor. But the usage of morphological factors should allow the bed level change not to be over 10 % of the water depth (Dissanayake et al. [2012]).

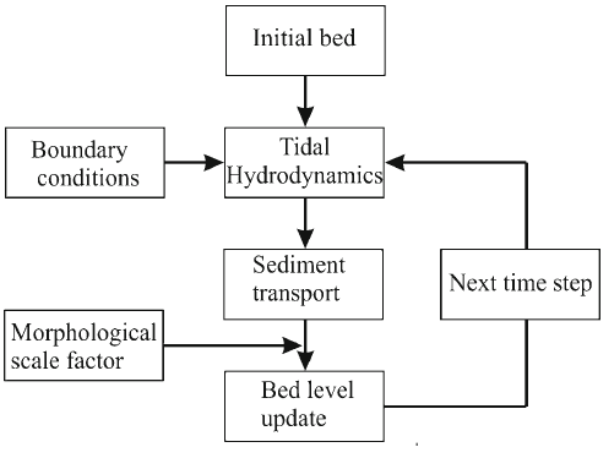

Figure 1.2: Schematised diagram of FLOW online-morphological model in **D3D**

1.2.2 ASMITA

Building the *Aggregated Scale Morphological Interaction between Tidal basin and Adjacent Coastline (**ASMITA**)* model is based on the two main assumptions: the morphological equilibrium can be defined for each element depending on the hydrodynamic conditions and morphological conditions it is subjected, and every element cannot be isolated from each other when their morphological development is considered (de Vriend [1996]).

ASMITA has a high level of spatial aggregation. The tidal basin system can always be schematized into three main morphological elements, see Figure 1.3:

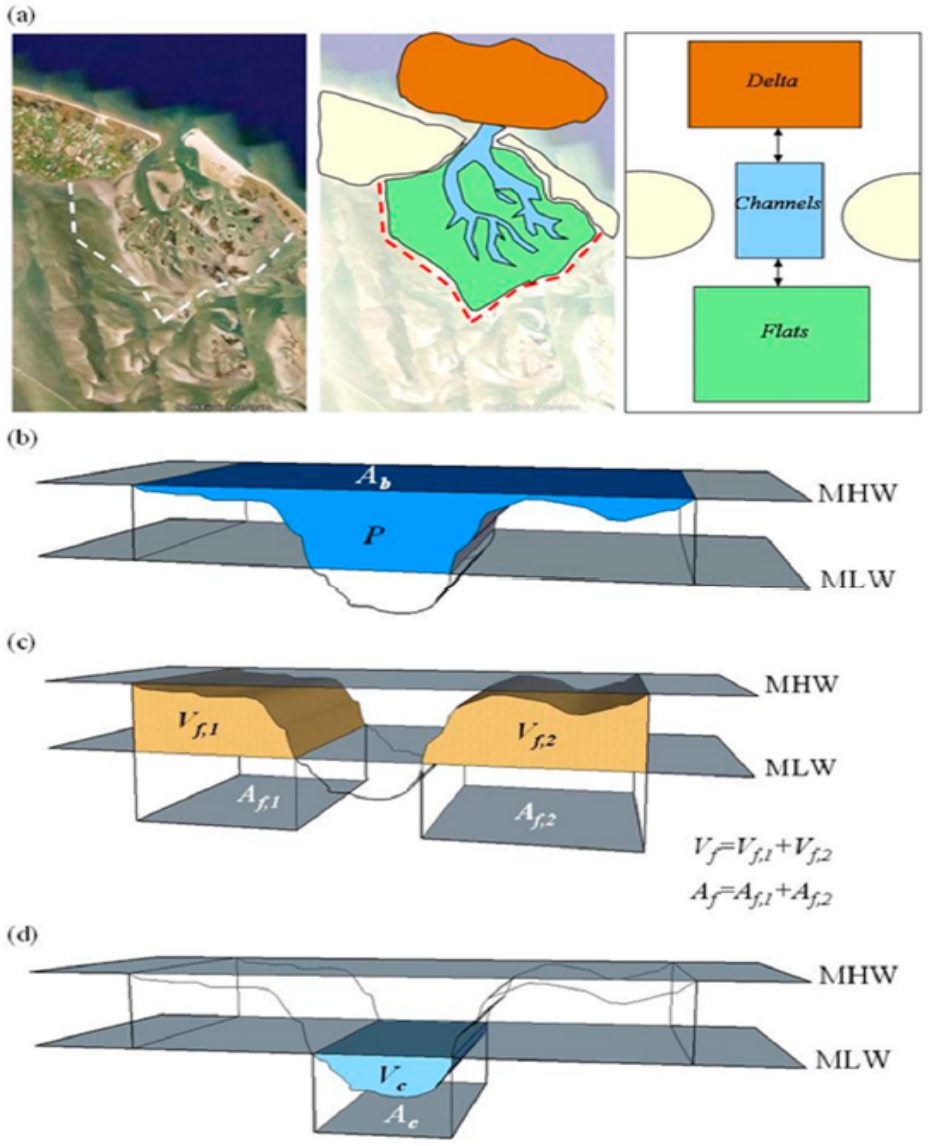

Figure 1.3: The three elements schematization in ASMITA, Lodder et al. [2019]

- Ebb delta, with its state variable V_d= total excess sediment volume relative to the undisturbed coastal bed profile $[L^3]$

- Inter-tidal flats, with its state variable V_f= total sediment volume between *Mean Low Water (**MLW**)* and *Mean High Water (**MHW**)* $[L^3]$

- Tidal channels, with its state variable V_c= total water volume below **MLW** $[L^3]$

If the morphology of the tidal basin system only is defined for the three main elements, we do not need to model the hydrodynamics in detail, instead, can use integrated hydrodynamic parameters, viz. the tidal prism (Townend et al. [2016]). For small basins where the length of basin is smaller than the tidal wave length, the water volume between **MLW** and **MHW** can be defined as the tidal prism:

$$P = A_b * H - V_f \tag{1.1}$$

In which: H is the tidal range relying on the open sea as a boundary condition and the morphological state of the inlet system. However, it is difficult to model the influences of morphological changes on the tidal range in that **ASMITA** utilizes the highly aggregated schematization. But for small basins the impact can be negligible (Wang et al. [2020]).

Due to no setting of hydrodynamic parameters in **ASMITA**, the model only applies the concentration field indicating the variation of forces - any deviation from equilibrium in terms of sediment concentration, can be related to the flow velocity, and hence cross-sectional area, or volume (Townend et al. [2016]). The sediment is regarded to be conservative in **ASMITA** model in the sense the total exchange between one element and its neighbors balances the local erosion and sedimentation. The inter-element or horizontal exchange is formulated in term of diffusive transport. For this purpose, the availability of sediment in each element is written as concentration and discrepancies in concentration across elements lead to horizontal exchange. The concentration that indicates the availability of sediment within an element, is called the local concentration, c. The demand of sediment within an element is the local equilibrium concentration, c_e (Van Goor et al. [2003]). In fact, for steady uniform flow, the vertical profile of sediment concentration, far away from the boundary, is the equilibrium concentration profile. The prescribed value of sediment concentration at the bed boundary is therefore by the definition the local equilibrium concentration. For non-cohesive sediment (sand), the equilibrium concentration or the equilibrium concentration gradient depends on the flow condition and the sediment properties and can be determined by one of many sediment transport formulas e.g. Soulsby, 1997 (Wang et al. [2020]). If all elements reach equilibrium states, the concentration of every element needs to be set as the global equilibrium concentration, c_E, which is the background concentration in the marine environment or the average concentration within the estuary if the system is close to the equilibrium, so $c_E = c_e = c$ (Townend et al. [2016]). In **ASMITA**, the equilibrium concentration is dependent on the ratio between the morphological state variables and its equilibrium value (Wang et al. [2018], Wang et al. [2020]), for example:

$$c_e = c_E(\frac{A_e}{A})^n \tag{1.2}$$

Where the equilibrium cross-sectional area A_e follows from the equilibrium relation. But here we use the simplest form, viz. the equilibrium cross-sectional area is proportional to the tidal prism, P:

$$A_e = \alpha P \tag{1.3}$$

1.2.3 Hybrid model: ASMITA-D3D

As a new long-term morphological model which is the hybridization of **ASMITA** and **D3D**, it needs to define the equilibrium bed level at every computational grid which is also the limitation of application. The hybrid model is not ready for the cases without the morphological equilibrium available. However, the hybrid model is meant to predict the effects of relative **SLR**, i.e. **SLR** plus subsidence due to e.g.

gas mining. In the hybird model, we combine the formulation in aggregated models for the sediment exchange and the aggregation level of process-based models. The basic structure of hybrid model is generalized as follows:

Hydrodynamic module

This part is not changed and tidal flow simulations will be the same as Delft3D.

Sediment transport module

Hybrid model will not consider the bed-load transport. For suspended sediment transport, the non-cohesive sediment (sand) formulation is basic. In **D3D**, the sediment exchange rate between the bed and water column can be computed as:

$$E = \gamma w_s (c_e - c) \tag{1.4}$$

where:

E = Exchange rate (erosion rate – deposition rate);

γ = Coefficient depending on $w_s/u*$ in which $u*$ is the bed shear stress velocity (Galappatti model formulation in 2DH models);

w_S = Settling velocity;

c_e = Equilibrium sediment concentration;

c = Sediment concentration.

The equilibrium concentration c_e is computed by empirical sediment transport formula, e.g. Van Rijn, in Delft3D:

$$c_e = F(u, ..., D_{50}, ...) \tag{1.5}$$

However, for hybrid model the exchange rate is obtained by:

$$E = w_s (c_e - c) \tag{1.6}$$

This can be realized by replacing the calculation of the coefficient by $\gamma = 1$. So the equilibrium concentration is:

$$c_e = c_E (\frac{h_e}{h})^n \tag{1.7}$$

Herein:

c_E = Global equilibrium concentration, as an input parameter;

h_e = Equilibrium water depth, an input quantity, spatial varying but constant in time;

h = Water depth.

Bed level module

The bed level module is kept constant. The bed level, d, changes due to morphological changes, and can be calculated using the sediment exchange between bed and water column:

$$\frac{\partial d}{\partial t} = \frac{1}{1-\epsilon} w_s (c_e - c) + \beta \tag{1.8}$$

Herein:

ϵ = the bed porosity;

β = the subsidence rate;

c = the volume concentration.

This implies that erosion happens at the positive derivative, $\frac{\partial d}{\partial t} > 0$, when the equilibrium concentration is higher than the actual ones while deposition relates to a negative derivative.

1.3 PROBLEM DESCRIPTION

Previous studies provide a solid understanding and wide perspective of the morphological developments of mudflats both in the short-term and long-term. However, most case studies were taken by only one modeling approach, **D3D** or **ASMITA**. For instance, Elmilady et al. [2019] implemented 3-D process-based model to investigate the morphological development of San Pablo Bay over 250 years. Van der Wegen et al. [2017] analyzed the impacts from **SLR** on the mudflat in South San Francisco Bay in the 1-D process-based model. Moreover, the hybrid model is newly developed. The previous research to apply all of the possible modeling approaches in the same case is not available, so it is not easy to make a contrast on their predictive behaviors. Additionally, the efficiency and quality of the model run on the development of mudflats under **SLR** in a long period may not be guaranteed by a single model. The tests of the predictive behaviors under joint actions from different modeling approaches are scarce.

1.4 OBJECTIVES AND RESEARCH QUESTIONS

This study aims to provide insights into the predictive behaviors of different modeling approaches in the case of long-term morphological evolution of mudflats under **SLR** scenarios. A transect of mudflat in South San Francisco Bay was chosen as a case study, because the historic bathymetry data set and the calibrated process-based model are available provided by Van der Wegen et al. [2017]. We aim to not only reproduce the results from **D3D** by **ASMITA** and hybrid model but also test the respective abilities of the modeling approaches on the long-term prediction of mudflat development so that it can provide a combination among three models to make an efficient prediction, and offer the methodology for performing similar forecasts in other locations.

The key objectives as described in this section can be summarized as the following research question:

What are the comparison results among process-based modelling approaches, aggregated modelling approaches and hybrid models for a case that has been modelled successfully with the process-based model D3D: the development of tidal flat cross-section profile under influence of sea-level rise?

To support the main question, the sub questions target at some important factors:

- Do the three modelling approaches of **D3D**, **ASMITA** and the hybrid model predict the same behavior of the tidal flat responding to sea-level rise?
- What are the requirements for the parameter settings in the aggregated modelling and hybrid modelling in order to reproduce quantitatively the same results as the process-based modelling?
- How far can the spatial aggregation go?
- What is the best way of combing the three modelling approaches?

1.5 THESIS OUTLINE

The thesis is separated into six main chapters: Chapter 2 provides insights in the basic information of South San Francisco Bay including the geographic information,

hydrodynamics and sediment characteristics. The methodology is introduced in Chapter 3, including the related characteristics of modelling software used in details and the setup in different modelling approaches. Chapter 4 gives the results of all model runs, which are discussed in Chapter 5. The conclusion of this thesis is provided in Chapter 6, consisting of the solutions to research questions and recommendations.

2 BACKGROUND

The chapter explicitly introduces the basic information about the research location - South San Francisco Bay comprising the morphology, hydrodynamics, and sediment characteristics. Thereby, we can develop a more profound understanding of the mudflat system in this location.

2.1 INTRODUCTION TO SOUTH SAN FRANCISCO BAY

2.1.1 Morphology

South San Francisco Bay is situated within the largest estuary on the west coast of the USA, with relatively shallow water in the San Francisco estuary. Its average depth is about 3 m and surface area is approximately 400 km^2 (Foxgrover et al. [2004]). The bathymetry for South San Francisco Bay is the main channel surrounded by broad shallow intertidal flats (Figure 2.1). The channel narrows from 1 *km* in the north to several hundred meters in the south. The depth of channel shoals from north to south is between -25 m and -5 m (Van der Wegen et al. [2017]).

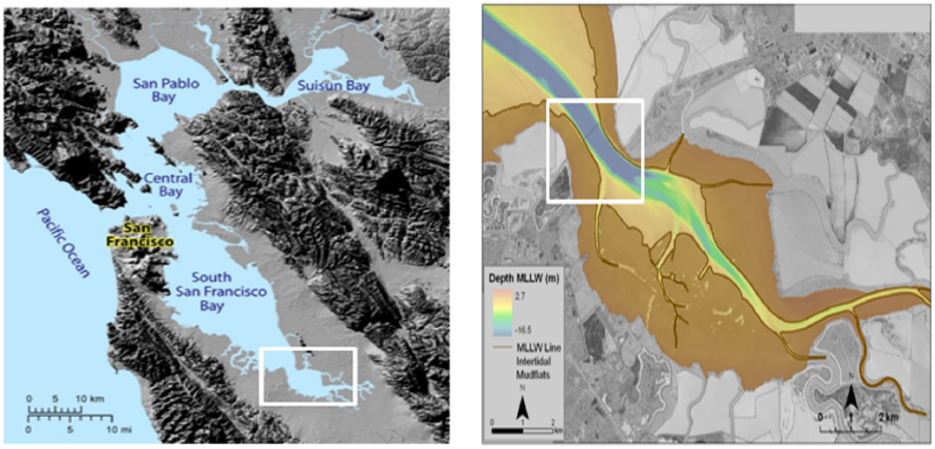

Figure 2.1: Location of Dumbarton mudflat in San Francisco Bay and location of Dumbarton mudflat in South Bay(Van der Wegen et al. [2017])

2.1.2 Hydrodynamics

The hydrodynamic forcing comes from tides, winds, and freshwater discharge from the seasonal stream (Cheng et al. [1993]). There are persistent northerly to northwesterly winds in dry summers existing in the South San Francisco Bay. During the cool wet winters, frequent storms transit the region and generate strong southerly to southeasterly winds. Meantime the storms can provide substantial rainfall to the landmass, and this induces the runoff into the bay (Conomos et al. [1985]). The varying sediment and freshwater discharge enter into the South San Francisco Bay by the small creeks and local streams during and after flooding (Schoellhamer [1996]). Although the North San Francisco Bay enables the South region to change its water

levels and flows, the mechanisms related to the water exchange and its effects on the circulation and sediment exchange between North and South San Francisco Bay are not well understood (Walters et al. [1985]).

2.1.3 Sediment Characteristics

In 2005, nearly half of mudflats in the South San Francisco Bay were in low energy, higher tide range at the south of Dumbarton Bridge (Figure 2.2). Intertidal flat with an area of 51.2 + 4.8/ - 5.8 km^2 had the gradually increasing width from 200 to 900 m from north to south. The surface sediments are primarily composed of silt with a mean grain size of about 50 μ (Van der Wegen et al. [2017]). The majority (more than 75 %) of samples are verified to be mud.

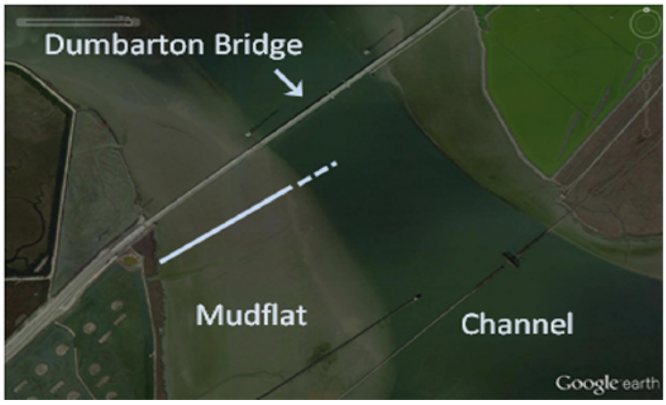

Figure 2.2: Mudflats in South San Francisco Bay in 2012 gained from Google earth. The transect in the research shown in the white line (Van der Wegen et al. [2017])

2.1.4 History

The mudflat in the western shore and south of Dumbarton Bridge is tested. From Figure 2.3, the profile is dynamic over time, with the elevation variation from about -2 to 0 **MSL**. The widening of the mudflat with the double-length accompanies net sediment import, and narrowing happens in sediment export. The mudflats around the Dumbarton Bridge are very stable between 1983 and 2005 without many net changes on the profiles (Bearman et al. [2010]).

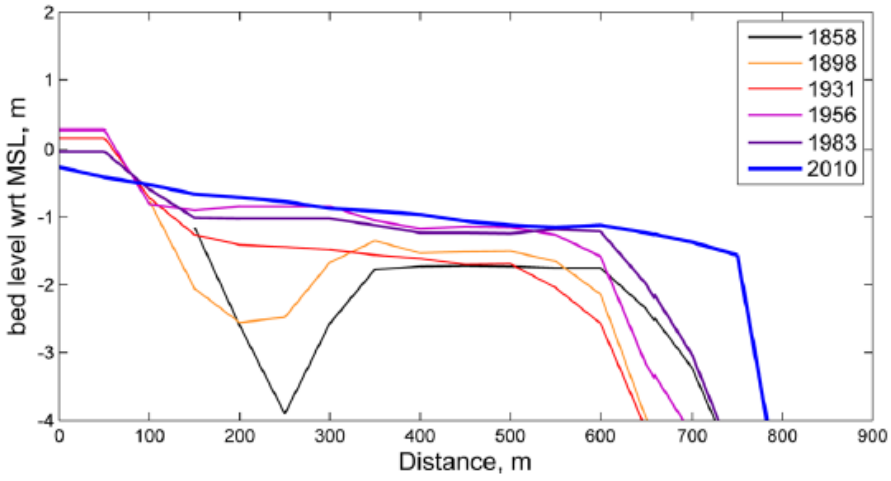

Figure 2.3: Historical profiles along the transect in Figure 2.2 (Van der Wegen et al. [2017])

3 METHODS

This thesis aims to compare the three modeling approaches in the case of the development of tidal flats under the influence of sea-level rise. This chapter explicitly describes the characteristics of different models, how the study is conducted, and the setup for the various modeling approaches.

3.1 MODELLING APPROACHES

3.1.1 Delft3D

D3D has been successfully applied for some cases so far, e.g.Van der Wegen et al. [2017], when predicting morphodynamics of inter-tidal flat under the impacts of **SLR**. However, the high complexity of the process-based model needs a lot of computational efforts, and it is difficult to determine the critical sea-level rise rate even if the model has been carefully set up and verified (Lodder et al. [2019]). The delayed response to the acceleration of **SLR** influences the exchange of sediment between the basin and coastal areas through the tidal inlet, resulting in the increase of morphological timescale with larger **SLR** rate (Wang et al. [2018]). Especially for the accelerated **SLR**, when the **SLR** rate is closer to the critical value, the achievement of a new dynamic equilibrium needs a larger time scale, and thus aggravates the computational intensive.

3.1.2 ASMITA

Predicting the critical rate of **SLR** can be achieved by the non-linearity of **ASMITA**. The traditional morphological equilibrium relation (Equation 3.3) can be expressed by the linear model assuming exponential decay of disturbances to morphological equilibrium and finding a dynamic equilibrium, but cannot obtain the critical **SLR** rate. The characteristic of non-linearity represents the limitation of sediment transport capacity in **ASMITA**. Suppose the **SLR** rate is only 40% of the critical rate. In that case, the difference between the linear and nonlinear model is negligible, suggesting that the critical SLR obtained by non-linearity of **ASMITA** and the assumption of the decrease of deviation from the morphological equilibrium by a factor of e are valid at the same time. The assumption is only applicable for the tidal basins that are not too far deviated from the morphological equilibrium (Wang et al. [2018]).

In the nonlinear model, the limit rate of **SLR**, R_c, nearly cannot be measured directly due to the response of tidal basin in the order of centuries, instead, obtained by morphological equilibrium (Lodder et al. [2019]):

$$R_c = \frac{H_e}{n * T_m} = \frac{H_e}{T} = \frac{w\delta c_E}{\delta + wA_b} \tag{3.1}$$

In which:

H_e = morphological equilibrium depth [m];

c_E = global equilibrium [-]

A_b = basin area [m^2]

δ = horizontal exchange coefficient [m^3/s]

w = settling velocity [m/s]

T = timescale which includes the vertical exchange process and horizontal exchange process:

$$T = \frac{1}{c_E}(\frac{H_e}{w_s} + \frac{H_e A_b}{\delta}) \tag{3.2}$$

T_m = morphological timescale which is the time needed for a small deviation from the morphological equilibrium to decrease by a factor e. It can be obtained after linearizing the Equation 3.3 around $H = H_e$ when $R = 0$:

$$\frac{dH}{dt} = \frac{w\delta c_E}{\delta + wA_b}[(\frac{H_e(t)}{H(t)})^n - 1] + R \tag{3.3}$$

Herein R is the sea level rise rate, and n depends on the type of sediment. In fact, the sediment in the flats is finer than channels, suggesting that different elements in the tidal basin have different responses towards **SLR**. A tidal basin with a relatively large range of sediments is less vulnerable than a system with highly sorted sediment available (Lodder et al. [2019]). When the deviation of actual water depth from its equilibrium state is equal to zero, the element reaches the state of dynamic equilibrium. It is essential to pay attention to the time process of the development towards the new dynamic equilibrium when **SLR** accelerates. Some insights into the process have already been obtained from the morphological timescale, determined by linearizing Equation 3.3 around the dynamic equilibrium which $\frac{H_e}{H}$ is constant:

$$\frac{t}{T} = \frac{1}{n(1 - \frac{R}{R_c})^{\frac{n+1}{n}}} \tag{3.4}$$

Herein t is the time after which a deviation from the dynamic equilibrium would be decreased by a factor of e. For the **SLR** rate of zero, the relationship between the morphological timescale and the timescale is the same as Equation 3.1. The timescale, t, is a variable with the change in **SLR** rate instead of constant.

However, **ASMITA** as an aggregated model relies on the combination of the expert analysis and empirical relationships developed from the observations, but also partly lacks to provide an understanding of the underlying physical mechanism (Elmilady et al. [2019]). The aggregated parameters, in part, are not measured directly but depend on the calibration which needs the data of long-term morphological development (e.g., centuries), suggesting that this is hard to apply for other lagoons and estuaries.

The physical parameters in the aggregated model can be divided into two groups:

1. The parameters can define the morphological timescale, Wang et al. [2008] provides the following suggestions that can combine the parameter setting in **ASMITA** with **D3D**:
    - The power, n, which is in the formulation of local equilibrium concentration, should be equal to an application sediment transport formula;
    - The vertical exchange coefficient, w_s, should be proportional to and of the same order of the magnitude as the settling velocity of the sediment particles;

- The inter-tidal dispersion coefficient, D, should be proportional to $\frac{u^2 H}{w_s}$ in which u is the scale of tidal flow velocity and H is the hydraulic water depth. It can be written:

$$\frac{D}{uH} = \epsilon \frac{u}{w_s} \tag{3.5}$$

With ϵ in the order of 0.1 (final value to be chosen during calibration). u needs to be in the order of 1 m/s. The cross-sectional velocity, u, can be approximated as the amplitude $\hat{u}_e$ of a sinusoidal tidal motion (Bosboom and Stive [2012]). In that case, u can be related to the tidal prism, P.

$$P = \int_0^{1/2T} A_e u dt = \int_0^{1/2T} A_e \hat{u}_e sin(\frac{2\pi}{T} t) dt = \frac{T A_e}{\pi} \hat{u}_e \tag{3.6}$$

Thus,

$$\hat{u}_e = \frac{\pi P}{A_e T} = \frac{\pi a A_b}{A_e T} \tag{3.7}$$

T = tidal period [s];

a = tidal range [m];

A_b = basin area [m^2], can be expressed by L_b in 1D model;

A_e = cross-section area [m^2].

With regards to the computation of velocity at a certain cross-section within the mudflat, the tidal prism is the water volume change between the landward end and the chosen cross-section within a tidal cycle. This implies that the velocity near the shoreline converges to zero.

- The general equilibrium concentration, c_E, is a parameter indicating the level of morphological activity in this area. This should be adjusted to express the right morphological time scale in the calibration.

In this way, there are only two calibration parameters viz.ϵ and c_E in this group. In fact, **ASMITA** works with discrete aggregated elements and uses the horizontal exchange coefficients, $\delta(m^3/s)$. The relation between dispersion coefficient, D and δ can be found:

$$\delta = \frac{DA}{L} \tag{3.8}$$

Herein A is the cross-sectional area linking the two elements, can be replaced by water depth at the junction in 1D model, and L is the distance between the midpoints of two adjacent elements.

2. The parameters can define morphological equilibrium state, e.g. α in the expression of A_e (Equation 1.3). To determine these coefficients, we need to rely on the field data and cannot reproduce from experiences gained elsewhere (Wang et al. [2018]).

3.1.3 Hybrid model

As a newly-developed model, which is the combination of **ASMITA** and **D3D**, the hybrid model is implemented in **D3D** but with more robustness. The hybrid model needs a defined **SLR** as an input (see Figure 3.1). Furthermore, defining the equilibrium morphology in the numerical grids is necessary. The input of global equilibrium concentration and the power representing the relation between equilibrium morphology and actual morphology can be specified in **.SED** file. Apart from the above setup, the hybrid model has the duplicate attribute files as **D3D** containing specific input quantities.

```
location            'General'
time-function       'non-equidistant'
reference-time      'from model'
time-unit           'minutes'
interpolation       'linear'
parameter           'time      ' unit '[min]'
parameter           'water level' unit '[m]'
records-in-table    731
 0          0
720         1.92E-06
1440        7.69E-06
2160        1.73E-05
2880        3.07E-05
3600        4.80E-05
4320        6.92E-05
5040        9.42E-05
5760        0.000122973
6480        0.000155637
```

Figure 3.1: Defining the water level changes at different points

3.2 STUDY PHASES

The research is mainly executed by three main modelling approaches, **ASMITA**, **D3D** and Hybrid models. The research phases are performed as follows:

Phase 1 analysing the methodology and results of **D3D** in South San Francisco Bay mainly based on the research of Van der Wegen et al. [2017]. As is the parameter inputting from Van der Wegen et al. [2017], the focus lays on the sensitivity analyses of the whole evolution stages to test the relative importance of different factors on the adaption process and final equilibrium state. The phase forms a base case of the research.

Phase 2 simulations with **ASMITA** to reproduce the results of **D3D**. The phase focuses on the application of different number of elements in **ASMITA** modelling approach.

Phase 3 simulations with the Hybrid model. Same as the tests in **D3D** model, the phase pays attention to the developments of mudflat from initial profile to final equilibrium state and impacts from **SLR** on the generated equilibrium profile, respectively. Differently, the setup is simplified to verify the feasibility of simulation efficiency raise in the hybrid model.

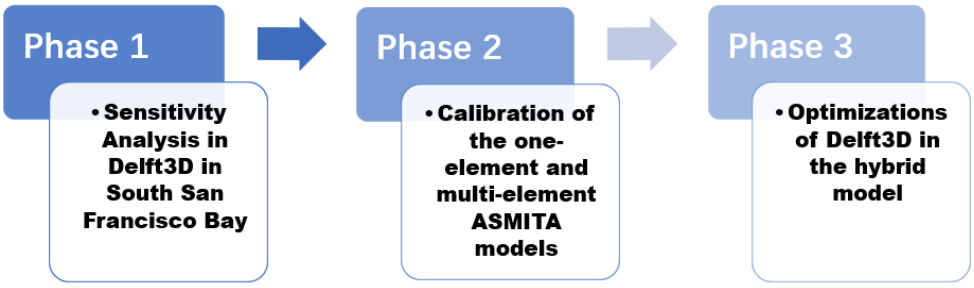

Figure 3.2: Visualisation of the study steps conducted in this research

3.3 MODEL SETUP

3.3.1 D3D

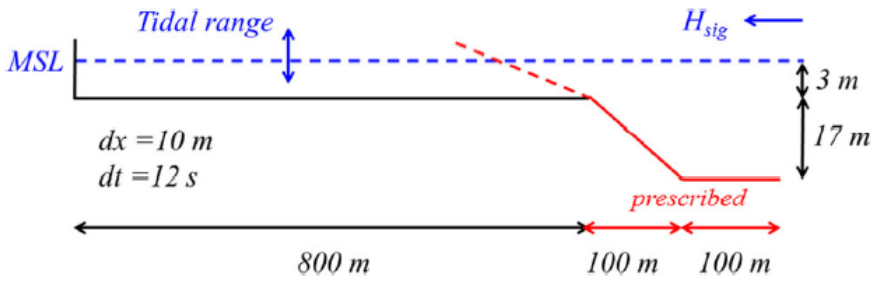

Figure 3.3: Model setup from Van der Wegen et al. [2017]

The 1D process-based model is provided in Van der Wegen et al. [2017]. The parameters used in this model can be checked in Table 3.1. The morphological factor of **100** was chosen in this research. The study applies a profile model where waves and tides enter from channel to inter-tidal flats. The first set of runs start from the initial bathymetry to simulate the 100-year evaluations of intertidal flats and subsequently carry out a sensitivity analysis by varying a range of parameters. The second set of runs (Figure 4.3) tested the impacts from different SLR rate and *Suspended Sediment Concentration (SSC)* scenarios for another 100-year on the equilibrium mudflats profile obtained in the first experiment. The main results are shown in Chapter 4. [1]

Table 3.1: Overview of model parameter variations in D3D

Parameter	Standard run	Minimum	Maximum	Observed
Tidal amplitude, $dH(m)$	0.5	0.25	0.75	About 1 m
Boundary SSC, $c(mg/l)$	45	22.5	90	On average about 30 mg/l with monthly peak between 100 and 300 mg/l and yearly peak up to 1000 mg/l
Initial mudflat depth, $dep_{ini}(m)$	3	1	5	
Diffusion coefficient, $D(m^2/s)$	10	1	20	
Significant wave height, $H_s(m)$	0.123	0.09	0.15	On average about 0.25 m with occasional peaks of 1 m
Peak wave period $T_p(s)$	2.5	2	3	
Erosion coefficient, $M(kg/m^2/s)$	5×10^{-4}	5×10^{-5}	5×10^{-3}	$1 - 5 \times 10^{-5}$
Dry bed density, $\rho_{dry}(kg/m^3)$	1200	1000	1600	
Critical erosion shear stress,$\tau_{cr,e}(Pa)$	0.25	0.15	0.35	0.05 - 2
Fall velocity, $w(mm/s)$	1	0.1	2	0.1 - 10
Morphological factor, $MF(-)$	100	25	200	

1 Here, the water depth is used as the state variable in that this is related to morphological equilibrium and equilibrium concentration as well as the procedure of drowning. Moreover, the *Mean Sea Level (MSL)* is chosen as the reference level, and this choice has consequences on the time scale and critical SLR rates.

3.3.2 ASMITA

Excel Version of ASMITA

Excel version of **ASMITA** as an initial test is to verify the feasibility to reproduce the **D3D** model run results consisting of the average profile elevation developments at different time. The related parameters setup is of vital importance to build the **ASMITA** model:

1. **Parameters determining equilibrium state**

   Figure 4.3 indicates the standard initial profile, expressed by the mean profile level with regards to **MSL**, which is **0.64 m**. If without changes in the external factor viz. **SLR**, the mudflat reaches the equilibrium state and keeps a constant level in the next 100 years. As such, the **ASMITA** model can adopt the equilibrium to calibrate the parameters related to mudflat equilibrium. The balance of tides and waves determines the equilibrium.

2. **Parameters determining morphological timescale**

   - The curve for the sudden drop 50% in **SSC** can be used to estimate the value of the power, n (Figure 4.3). This is mainly achieved by the ratio between the morphological variables and its equilibrium value:

   $$c_e = c_E(\frac{H_e}{H})^n \tag{3.9}$$

   Where the ratio of c_e/c_E is 0.5, H_e is 0.64 m and H representing the new equilibrium in the mudflat system is 0.8 m. Thus, the power, n, is **3.338**.

   - In order to simplify this model, the adaption timescale adopted in this model is constant. (Table 3.2).

Table 3.2: The adapting timescale for different cases

Morphological Timescale, T (years)	Situations
25	**SLR** 1.67, c-50 %
35	**SLR** 0.83, c-50 %
40	**SLR** 0, c-50 %
20	**SLR** 1.67
27	**SLR** 0.83

The only trick applied is the assumption on which the faster water level growth and accordingly larger storage area will facilitate the exchange of sediments between the mudflat and channel, thus lowering the adapting time.

One Element Model

The one-element model aggregates the complete mudflat as one element, and the boundary between the channel and intertidal flat is at the 750 m from the shoreline. As such, **ASMITA** model has the capacity of tracking the average elevation development of the mudflat in South San Francisco Bay. The version of **ASMITA** for one-element model is the one that regards Kragtwijk et al. [2004] as the theoretical basis.

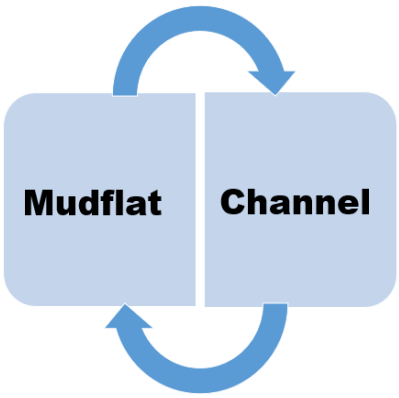

Figure 3.4: Schematic diagram of 1-element model

Table 3.3: Overview of model parameters in one element model of **ASMITA** in the case of no change in **SSC** at the boundary

Parameter	Application Value	Explanation
$\delta(m^3/s)$	0.032	**SLR** 0.83 m/century
	0.042	**SLR** 1.67 m/century
$w_s(m/s)$	0.001	adopted from **D3D** by Van der Wegen et al. [2017]
$c_E(kg/m^3)$	0.045	global equilibrium concentration
$dH(m)$	1	tidal range
n	3.338	the power in Equation 3.3
α	0.64	parameter determining equilibrium state
$\beta)$	1	parameter determining equilibrium state
$V_0(m^3)$	480	initial volume of mudflat
$A_0(m^2)$	750	initial area of mudflat

Table 3.4: Overview of model parameters in one element model of **ASMITA** in the case of 50 % **SSC** drop at the boundary

Parameter	Application Value	Explanation
$\delta(m^3/s)$	0.033	**SLR** 0.83 m/century
	0.044	**SLR** 1.67 m/century
	0.011	no **SLR**
$w_s(m/s)$	0.001	adopted from **D3D** by Van der Wegen et al. [2017]
$c_E(kg/m^3)$	0.045	global equilibrium concentration
$dH(m)$	1	tidal range
n	3.338	the power in Equation 3.3
α	0.80	parameter determining equilibrium state
$\beta)$	1	parameter determining equilibrium state
$V_0(m^3)$	480	initial volume of mudflat
$A_0(m^2)$	750	initial area of mudflat

Multi-Element Model

Despite the simple setup of the 1-element model, the aggregation level of **ASMITA** determines that this model can only predict the aggregated variables, e.g., the mean elevation of the mudflat. The local features of mudflat are, in essence, averaged out. For example, the landward-directed mudflat growth comes to a halt if the mudflat is too long, **SLR** is too large, or **SSC** drops too fast, and there will be flooding channels or ebb drainage near land by tidal flows directed along the mudflats.

To simulate the significant features as well as the general steepness of mudflats, we can separate the integral mudflat into smaller parts by increasing the number of elements in **ASMITA** and accordingly linking different elements along the mudflat to construct the complete profile in every time step. Same as the one-element model, the test code of **ASMITA** based on the principles from Kragtwijk et al. [2004] is used for the subsequent runs.

Additional tests (not shown) indicate that the calibrated parameter ϵ can be kept in the order of 0.1 when adopting larger water depth values, H. Thus, the application of water depth chooses the maximum, which one is after 100 years of evolution in **D3D**. Moreover, the prescribed bed level of channel is kept constant under impacts from **SLR** in **D3D** model. To simulate the changeless bathymetry, a method where **ASMITA** model adopts the zero settling velocity in the element representing channel part is applied. The schematization of the multi-element **ASMITA** models and the parameter setup for different elements are shown as follows:

3-element model

In the 3-element model, the channel and its slope are regarded as individual elements, and the whole mudflat is divided into two parts represented by two elements to predict the aggregated water depth on the intertidal flat.

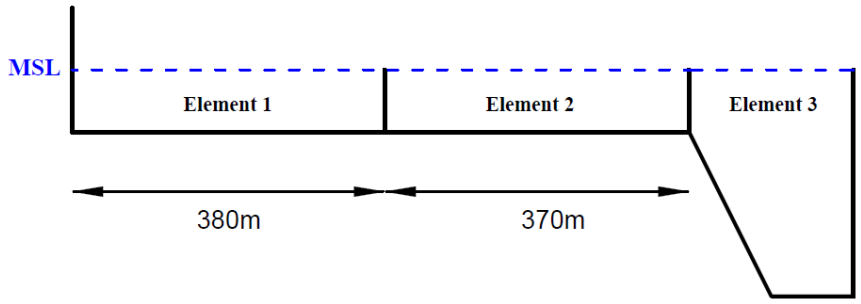

Figure 3.5: Sketch Map of 3-element model

Table 3.5: Overview of model parameters in 3-element model of **ASMITA** without changes in **SSC** at the boundary

Path	H (m)	a (m)	T (s)	L_b (m)	u (m/s)	ϵ	D (m^2/s)	δ (m^3/s)	L (m)	w_s (m/s)
0.83	m/century									
1to2	0.84	1	44700	190	0.0159	0.3	10.0637	0.0225	375	0.001
2to3	1.23	1	44700	565	0.03228	0.2	10.2564	0.0407	310	0.001
3tochannel	20.83	1	44700	875	0.00295	0.9	10.0000	1.6664	125	0
1.67	m/century									
1to2	1.01	1	44700	190	0.0132	0.9	10.0397	0.0274	375	0.001
2to3	2.07	1	44700	565	0.0192	0.2	10.1523	0.0678	310	0.001
3tochannel	21.67	1	44700	875	0.0028	0.9	10.0000	1.7336	125	0

5-element model

Adopting the same channel element setup, the whole tidal flat are specifically divided into more elements with smaller sizes.

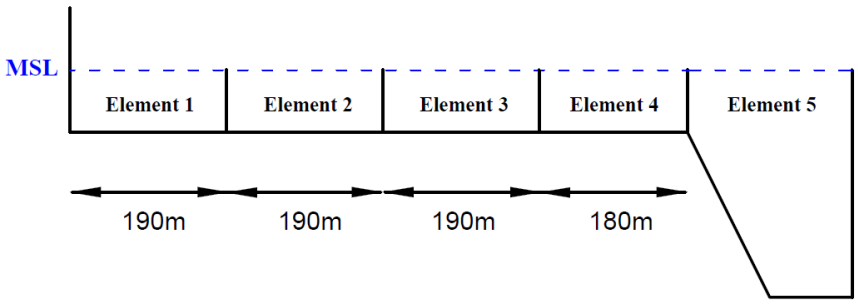

Figure 3.6: Sketch Map of 5-element model

Table 3.6: Overview of model parameters in 5-element model of **ASMITA** without changes in **SSC** at the boundary

Path	**H (m)**	**a (m)**	**T (s)**	L_b **(m)**	**u (m/s)**	ϵ	**D** (m^2/s)	δ (m^3/s)	**L (m)**	w_s **(m/s)**
0.83	m/century									
1to2	0.55	1	44700	95	0.0121	0.1	10.0081	0.0290	190	0.001
2to3	0.84	1	44700	285	0.0239	0.1	10.0478	0.0443	190	0.001
3to4	1.09	1	44700	475	0.0306	0.1	10.1022	0.0592	185	0.001
4to5	1.23	1	44700	660	0.0377	0.2	10.1749	0.0582	215	0.001
5tochannel	20.83	1	44700	875	0.0030	0.2	10.0000	1.6664	125	0
1.67	m/century									
1to2	0.76	1	44700	95	0.0088	0.1	10.0015	0.0400	190	0.001
2to3	1.01	1	44700	285	0.0198	0.1	10.0099	0.0534	190	0.001
3to4	1.21	1	44700	475	0.0276	0.1	10.0230	0.0660	185	0.001
4to5	2.07	1	44700	660	0.0224	0.1	10.0260	0.0973	215	0.001
5tochannel	21.67	1	44700	875	0.0028	0.1	10.0000	1.7336	125	0

11-element

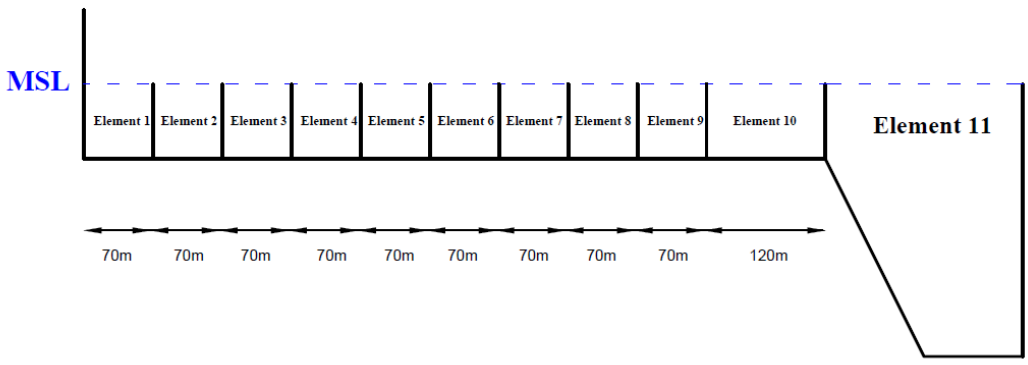

Figure 3.7: Sketch Map of 11-element model

Table 3.7: Overview of model parameters in 11-element model of **ASMITA** without changes in **SSC** at the boundary

Path	H (m)	a (m)	T (s)	L_b (m)	u (m/s)	ϵ	D (m^2/s)	δ (m^3/s)	L (m)	w_s (m/s)
0.83	m/century									
1to2	0.37	1	44700	35	0.00665	0.1	10.0016	0.0529	70	0.001
2to3	0.48	1	44700	105	0.01537	0.1	10.0113	0.0686	70	0.001
3to4	0.58	1	44700	175	0.02121	0.1	10.0261	0.0831	70	0.001
4to5	0.68	1	44700	245	0.02532	0.1	10.0436	0.0976	70	0.001
5to6	0.79	1	44700	315	0.02802	0.1	10.062	0.1136	70	0.001
6to7	0.91	1	44700	385	0.02973	0.1	10.0805	0.131	70	0.001
7to8	1	1	44700	455	0.03198	0.1	10.1023	0.1443	70	0.001
8to9	1.08	1	44700	525	0.03416	0.1	10.1261	0.1562	70	0.001
9to10	1.16	1	44700	595	0.03605	0.1	10.1508	0.1239	95	0.001
10to11	1.23	1	44700	690	0.03943	0.1	10.1912	0.0678	185	0.001
11tooutside	20.83	1	44700	875	0.00295	0.1	10	1.6664	125	0
1.67	m/century									
1to2	0.59	1	44700	35	0.00417	0.1	10.001	0.0843	70	0.001
2to3	0.69	1	44700	105	0.0107	0.1	10.0079	0.0986	70	0.001
3to4	0.78	1	44700	175	0.01577	0.1	10.0194	0.1116	70	0.001
4to5	0.88	1	44700	245	0.01957	0.1	10.0337	0.1261	70	0.001
5to6	0.97	1	44700	315	0.02282	0.1	10.0505	0.1393	70	0.001
6to7	1.06	1	44700	385	0.02553	0.1	10.0691	0.1525	70	0.001
7to8	1.13	1	44700	455	0.0283	0.1	10.0905	0.1629	70	0.001
8to9	1.2	1	44700	525	0.03075	0.1	10.1135	0.1734	70	0.001
9to10	1.26	1	44700	595	0.03319	0.1	10.1388	0.1345	95	0.001
10to11	2.07	1	44700	690	0.02343	0.1	10.1136	0.1132	185	0.001
11tooutside	21.67	1	44700	875	0.00284	0.1	10	1.7336	125	0

3.3.3 Hybrid Model

The same experiments as **D3D** are processed in hybrid model: the first series are based on the similar setup as **D3D** in Van der Wegen et al. [2017], the global equilibrium concentration c_E of 0.045, power n of 3.338 as **ASMITA** (Figure 3.8). The equilibrium bed level from the results in **D3D** is defined in the numerical grids (**Hequi.dep**). Starting from the final equilibrium profile, the second runs assess the impacts of **SLR** on the profile development, for the cases of the rate of 0.83 m/century and 1.67 m/century respectively. As is Figure 3.1, the **SLR** must be specified in the **.WLT** file. Differently, the hybrid model adopts the simplifications based on the analyses of **D3D** and **ASMITA**.

```
[SedimentFileInformation]
  FileCreatedBy   = Delft3D FLOW-GUI, Version: 3.43.05.22651
  FileCreationDate = Wed Jun 18 2014, 12:48:24
  FileVersion     = 02.00
[SedimentOverall]
  Cref          =  1.6000000e+003    [kg/m3]  CSoil Reference density for hindered settling calculations
  IopSus        = 0                  If Iopsus = 1: susp. sediment size depends on local flow and wave conditions
[Sediment]
  Name          = #Sediment mud#          Name of sediment fraction
  SedTyp        = sand                 Must be "sand", "mud" or "bedload"
  RhoSol        =  2.6500000e+003    [kg/m3]  Specific density
  CDryB         =  1.2000000e+003    [kg/m3]  Dry bed density
  IniSedThick   = #sedav.sdb#        [m]      Initial sediment layer thickness at bed (uniform value or filename)
  SedDia        = 0.0001         [m]
  FacDSS        = 1.0              [-]
  TraFrm        = 21
  CEqui         = 0.045
  HEqui         = #Hequi.dep#
  N             = 3.338
  MaxHH         = 10.0
```

Figure 3.8: Equilibrium related parameters input in hybrid model

4 RESULTS

This chapter will describe the base run results in D3D in the situation of SLR impacts on the evolution of mudflat in South San Francisco Bay and the sensitivity analysis on the factors, consisting of wave height, tidal range and SSC. Followed by ASMITA and hybrid model implemented in the same scenario, the predictive behaviors of two modeling approaches are also shown in this chapter. The specific model setup of three models can be checked in Chapter 3.

4.1 PHASE 1 - D3D RUN

Before doing further research on the case of South San Francisco Bay, it is essential to properly evaluate the previous D3D model run results. Based on this model, variations in the parameters can get insight into how factors impact the adaption timescale and the equilibrium state.

4.1.1 D3D modeling results

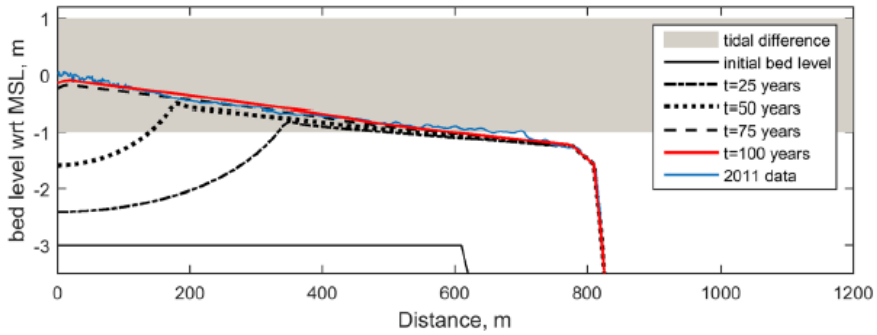

Figure 4.1: Modelled mudflat profile evolution, from Van der Wegen et al. [2017]

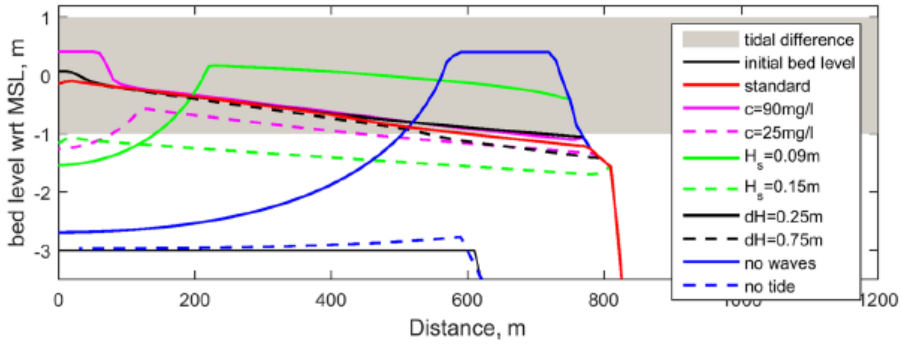

Figure 4.2: Sensitivity analysis on mudflat profile after 100 years, from Van der Wegen et al. [2017]

From Figure 4.1, it is clear that there is a gradual adaption of mudflat in South San

Francisco Bay, in which the edge of the bed near the channel began to deposit until reaching a certain level, and the land-side part slowly develops towards the final equilibrium state afterward. Wave and tide play a significant role in this evolution: the mud initially deposit at the edge of the mudflat, waves stir up the sediments into the suspended state during low water, subsequent flood flow can transport grains landward to fill up the remaining. The collective effects can prevent not only the unlimited deposition on the seaside edge (Figure 4.2, no wave case) but also stimulate the development of the complete profile (Figure 4.2, no tide case). There should be stressed that the reasons for adopting the constant boundary conditions in **D3D** are the application of the considerable time averaging of forcing states so that the seasonal variation, e.g., tides, wind, and waves, and extreme wind and waves events can be neglected.

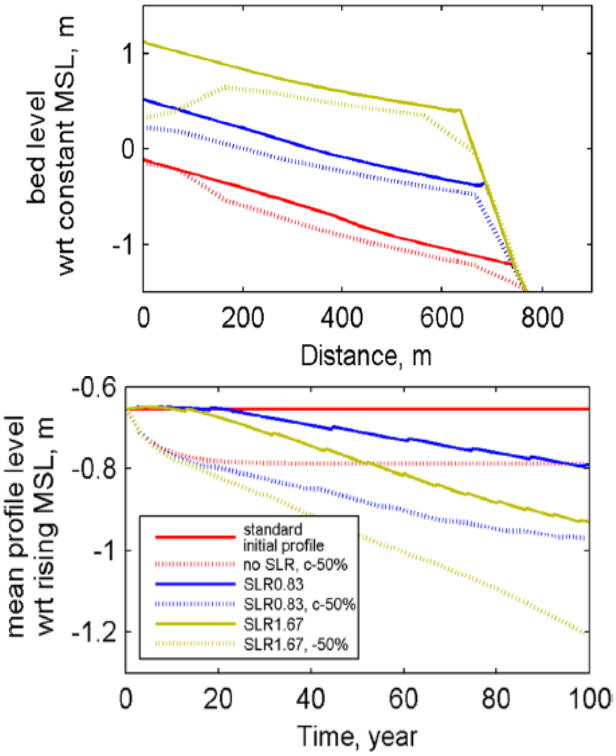

Figure 4.3: Mudflat profiles under different SLR and SSC scenarios after 100 years Van der Wegen et al. [2017]

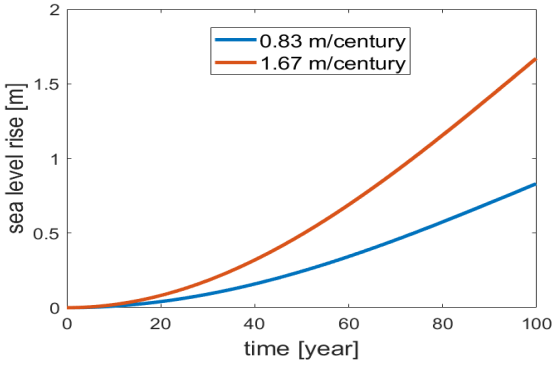

Figure 4.4: Sea level rise scenario

The second set of experiments suggest that different **SLR** rates can generate almost parallel final profiles in different levels in the case of no change in **SSC** at the boundary. Rapid **SLR** increasing enables it to create a larger storage area and input more sediments from outside. From the perspective of the mean profile level, the

accretion rate of mudflats cannot keep up with the **SLR** pace, so that the mudflat will be gradually drowned for both cases of 0.83 m/century and 1.67 m/century, which is indicated in the rising water depth from initial 0.64 m. It is worth mentioning that the increment of water level adopted a cosine function instead of linear growth (Figure 4.4). An abrupt 50% decay of **SSC** has a relatively immediate effect on the mean inter-tidal flat level and stabilizes afterward, suggesting that the system reaches a new equilibrium state (**0.8 m** wrt **MSL**).

4.1.2 Sensitivity Analysis

As is Figure 4.2, the sensitivity analyses have been performed and the final profiles of different scenarios are indicated. In this sub-section, the attention is transferred to the mean flat level evolution[1]. Thus, the adaption timescale and the final mean elevation can be directly estimated. The factors of **SSC**, wave height, and tidal range were chosen in the sensitivity experiments.

SSC

The first factor was tested is **SSC** level. Figure 4.5 shows the scenario in which the level of **SSC** drops 50 % from 45 mg/l to 22.5 mg/l.

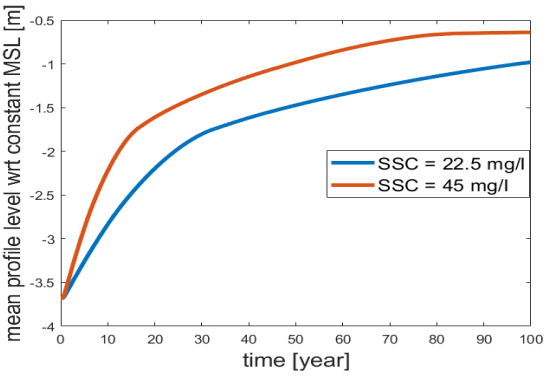

Figure 4.5: **SSC** factor impacts on the equilibrium state

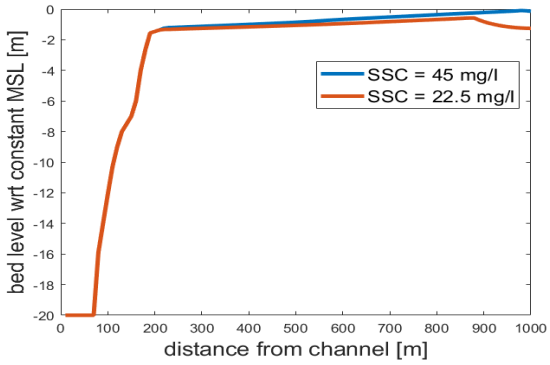

Figure 4.6: **SSC** factor impacts on the full profile in the 100th year

The case with the 50 % **SSC** decrease suggests a relatively slower development as well as lower mean level compared with the standard case. It reveals that **SSC** level not only influences the adaption timescale but also the morphological equilibrium. Moreover, Figure 4.6 indicates the breach at the landward end in the case of sudden drop in **SSC**.

1 The following set of experiments will be based on the first 100-year, i.e., start from the state, which is close to the equilibrium state without the **SLR** impact.

Wave Height

The wave heights of 0.09 m, 0.123m and 0.15m were tested to observe the impacts.

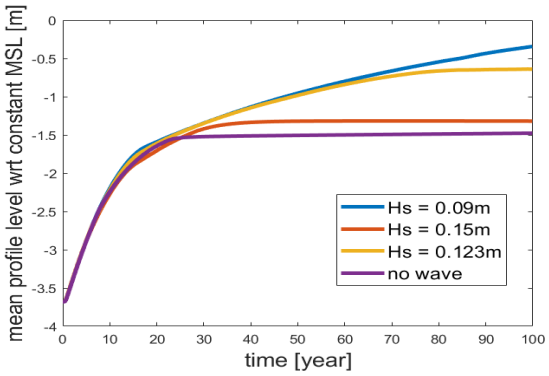

Figure 4.7: Wave height factor impacts on the equilibrium state

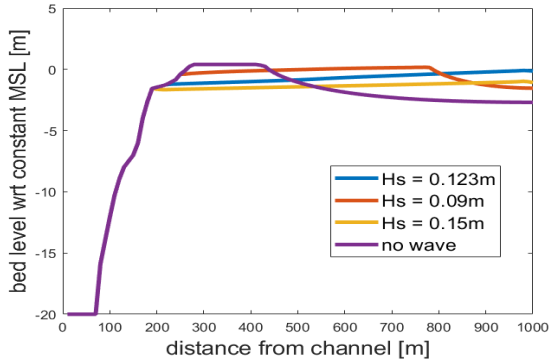

Figure 4.8: Wave height factor impacts on the full profile in the 100thyear

The mudflat profiles impacted by different wave heights keep the similar evolution within 20 years, even in the no-wave case, after which they suggest the dominant differences: more considerable wave height leads to a lower mudflat and reaches the equilibrium state faster. Accordingly, the morphological timescale and morphological equilibrium state are sensitive to wave condition in the mudflat system.

Tidal Range

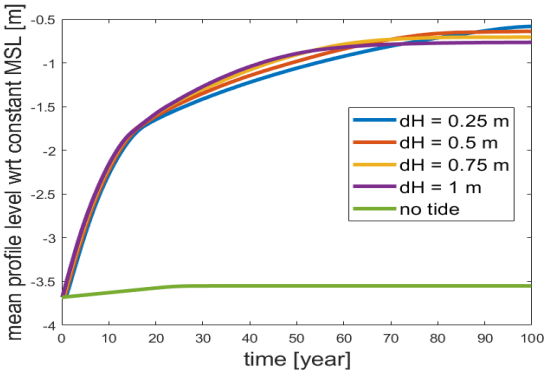

Figure 4.9: Tidal range factor impacts on the equilibrium state

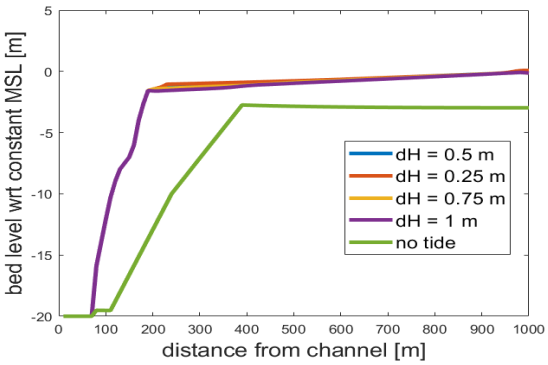

Figure 4.10: Tidal range factor impacts on the full profile in the 100th year

From Figure 4.9, variations of tidal ranges induce the similar adaption timescale and even equilibrium state, suggesting that tide influences are limited compared with other factors. However, the case of no tide gives a completely different scenario - there is nearly no change in the elevation of mudflat. The small deposition at the mudflat in the absence of tides is due to the limited diffusion transport [2].

4.2 PHASE 2 – ASMITA RUN

4.2.1 ASMITA Test

To verify the feasibility to reproduce **D3D** simulations, Excel can be utilized to do an easy experiment based on the fundamental conception of **ASMITA**. Wang et al. [2008] recommended the theoretical analysis and calibration procedures to relate the parameter setting in **ASMITA** with **D3D**, which have been specifically discussed in Chapter 3. There are two groups of parameters on the building of an **ASMITA** model that should be defined: one determines morphological equilibrium, and another determines the relevant timescales. Here considering the simplest version of **ASMITA**, i.e., one element, the evolution formula is shown as follow:

$$\frac{dH}{dt} = \frac{H_e}{T}[(\frac{H_e}{H})^n - 1] + R \tag{4.1}$$

The ratio, $\frac{H_e}{H}$ represents hydrodynamics including the tidal currents and waves, which further the accretion of mudflats.

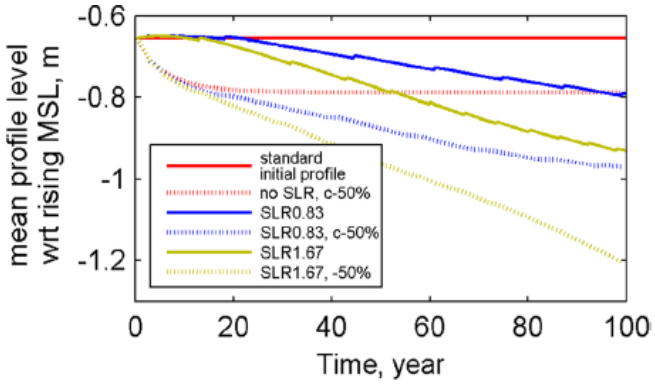

Figure 4.11: Mean profile level evolution from **D3D** version in different scenarios from Van der Wegen et al. [2017]

2 This is specifically explained in Section 4.2.2

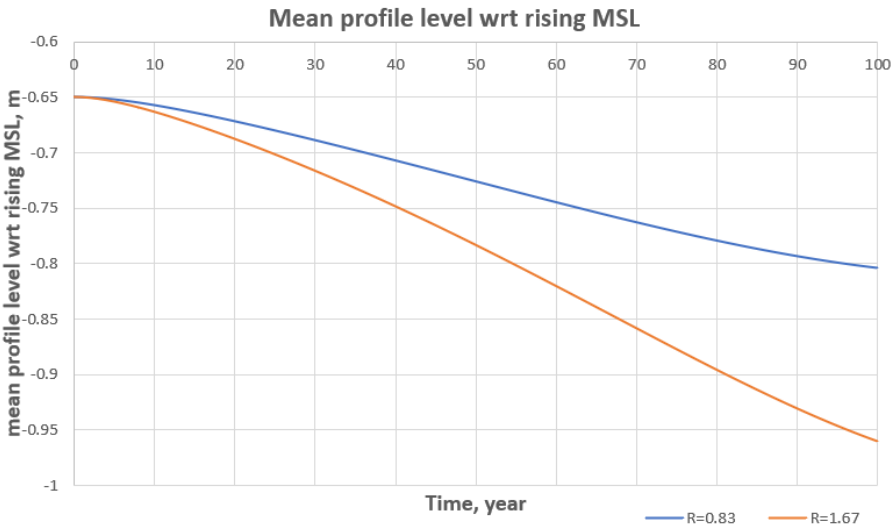

Figure 4.12: Mean profile level evolution from Excel Version of **ASMITA** in the case of no change in boundary **SSC** with the constant timescale

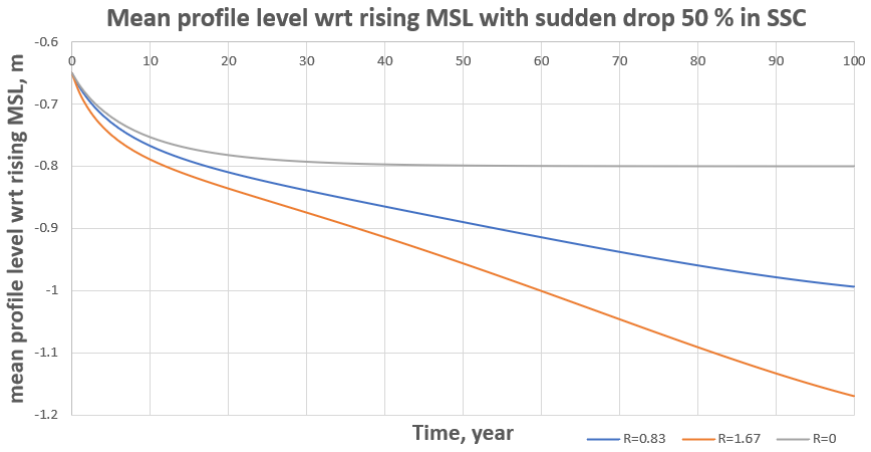

Figure 4.13: Mean profile level evolution from Excel Version of **ASMITA** in the case of 50 % drop in **SSC** at the boundary with the constant timescale

By caparison among Figure 4.12, Figure 4.13 and Figure 4.11, this suggests the high similarities between **D3D** and **ASMITA** in the case of predicting the evolution of aggregated variable of the mean profile level. From the perspective of the mean elevation, the mudflat is gradually drowned with **SLR**; the rapid decrease in the mean profile due to the initial sudden drop in **SSC** at the boundary with the following gradual drowning at a continuous rate. Thus, reproducing the predictive results of **D3D** by **ASMITA** is promising.

4.2.2 ASMITA - One Element Model

It is unrealistic to consider the constant timescale during the evolution of mudflat, while the operation results are ideal. For closing to the fact of the accelerated water level rising, this can be achieved in the version of **ASMITA** based on Kragtwijk et al. [2004]. The specific model setup was described in Table 3.3 and Table 3.4.

Equation 3.2 can be transferred into the version with the water depth as a state variable.

$$T(t) = \frac{1}{c_E}\left(\frac{H_e(t)}{w_s} + \frac{H_e(t)A_b}{\delta}\right) \tag{4.2}$$

With rising water level and SLR, the timescale is time-dependent due to the variation of H_e.

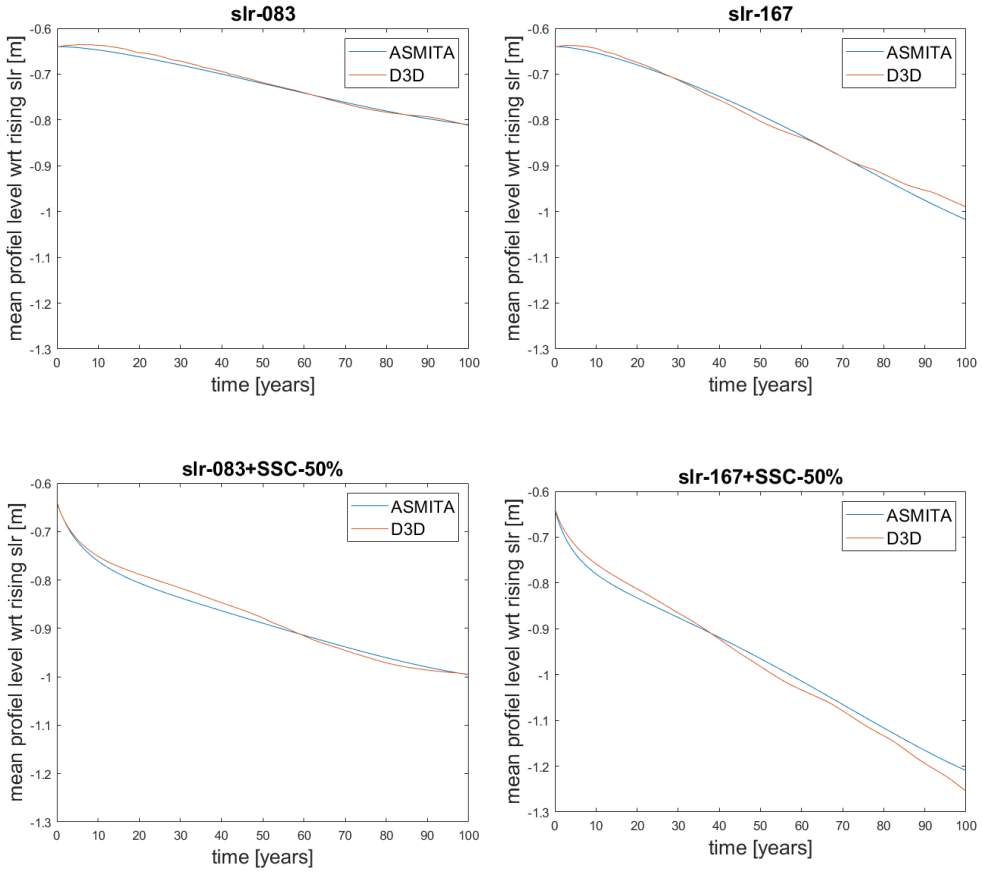

Figure 4.14: Comparisons on the average elevation evolution of mudflat between one-element model and D3D

Figure 4.14 also verifies the assumption that ASMITA can satisfactorily reproduce the evolution of aggregated variables from D3D applying physically reasonable input parameter.

The time scale, shown in Equation 4.2, can be divided into two time scales, one for the vertical exchange and one for the horizontal exchange. By using the parameters in one-element ASMITA model, the order of magnitudes for the two time scales can roughly be computed:

Table 4.1: Overview of horizontal and vertical timescale in different scenarios

Parameter	0.83m/century	1.67m/century
$\delta(m^3/s)$	0.032	0.042
n	3.338	3.338
$w_s(m/s)$	0.001	0.001
$H_0(m)$	0.65	0.65
$Vertical(year)$	1.21	1.21
$Horizontal(year)$	28.4	21.7

The calculation results show that diffusion transport dominates: the timescale of vertical transport is an order of magnitude smaller than the horizontal motion. However, the without tide case in D3D gave a different case that shows small deposition at the edge of mudflat (Figure 4.9). This is because diffusion may not be activated at the boundary, i.e., the prescribed SSC is not used in D3D, and there is no inflow to input sediments.

4.2.3 ASMITA - Multi Elements Model

The multi-element models can not only simulate the evolution of aggregated variables but also the slope of profiles and the local features.

3-element Model

Except for the subtle differences, the forecasts for the mean profile level from **ASMITA** (Figure 4.15) reveals that 3-element model of **ASMITA** has the capacity of reproducing the continuous drowning of mudflat in **D3D**.

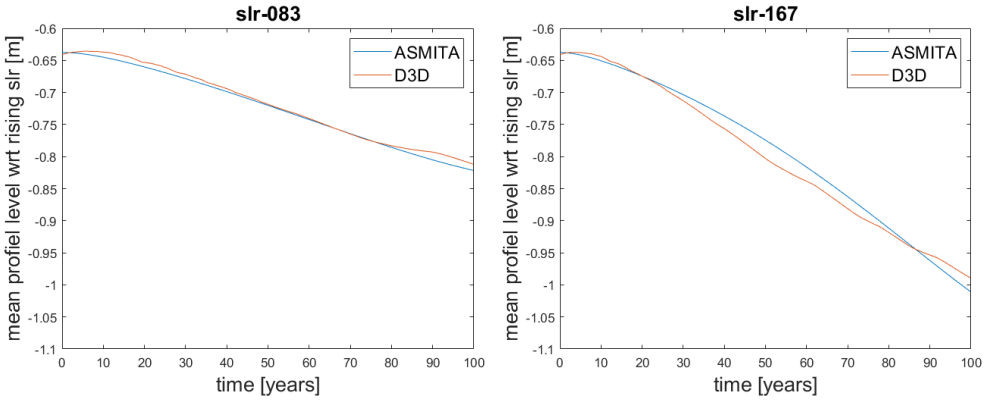

Figure 4.15: Evolution of the mean profile level in the case of 0.83 m/century and 1.67 m/century in 3-element **ASMITA** model in 3-element model

Figure 4.16 can be obtained by fitting straight lines through two midpoints of two elements representing the mudflat at different time. The lines reveal the evolutionary tendency of mudflat under the **SLR** influences. The nearly parallel accretions along the mudflat happen under **SLR** of 0.83 m/century, whereas the accretion near the shoreline dominantly slows down after 80 years in the 1.67 m/century scenarios. The limited accretion at the landward end leads to the gentler mudflat slope. This can also be observed in Figure 4.18, the closer analyses by the comparisons between **D3D** and **ASMITA** after 14, 68, 82 and 100 years.

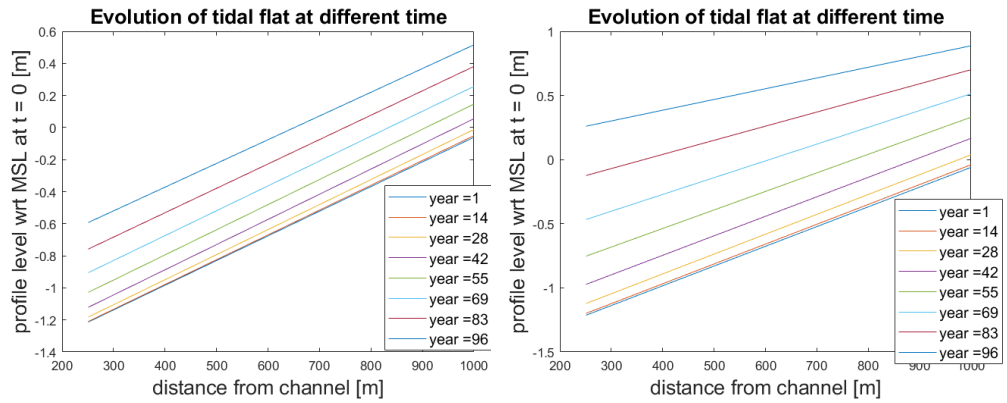

Figure 4.16: Evolution of the whole mudflat profile level under **SLR** rates of 0.83 m/century and 1.67 m/century at different time steps in 3-element **ASMITA** model

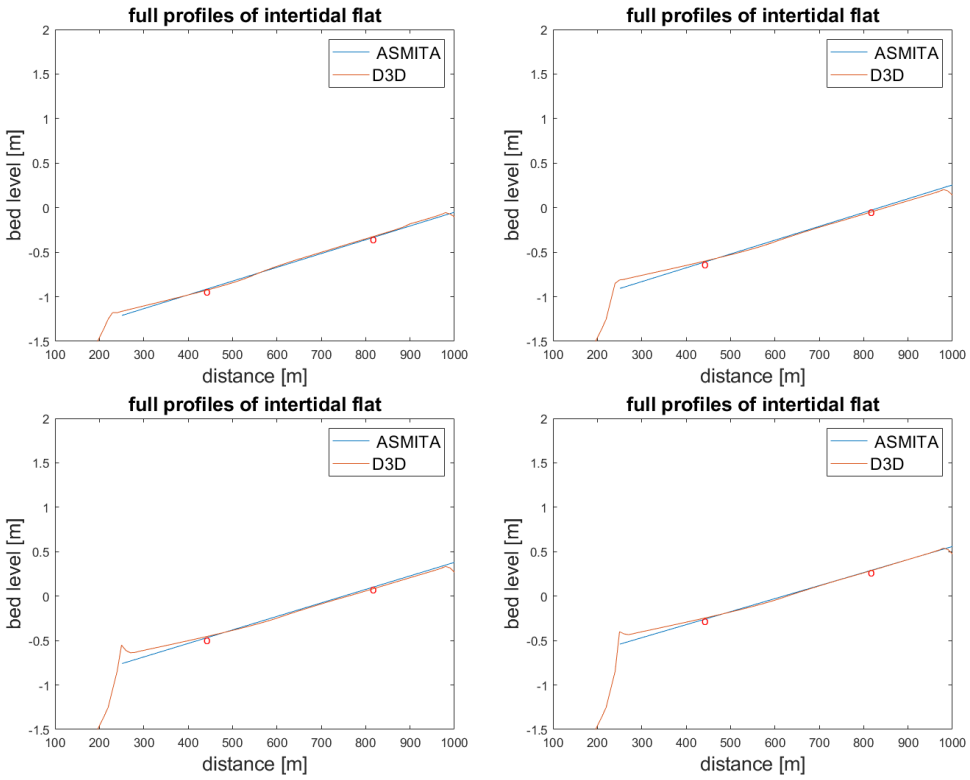

Figure 4.17: Mudflat profiles after 14, 68, 82 and 100 years under 0.83 m/century **SLR** (Red dots represent the center of elements) in 3-element model

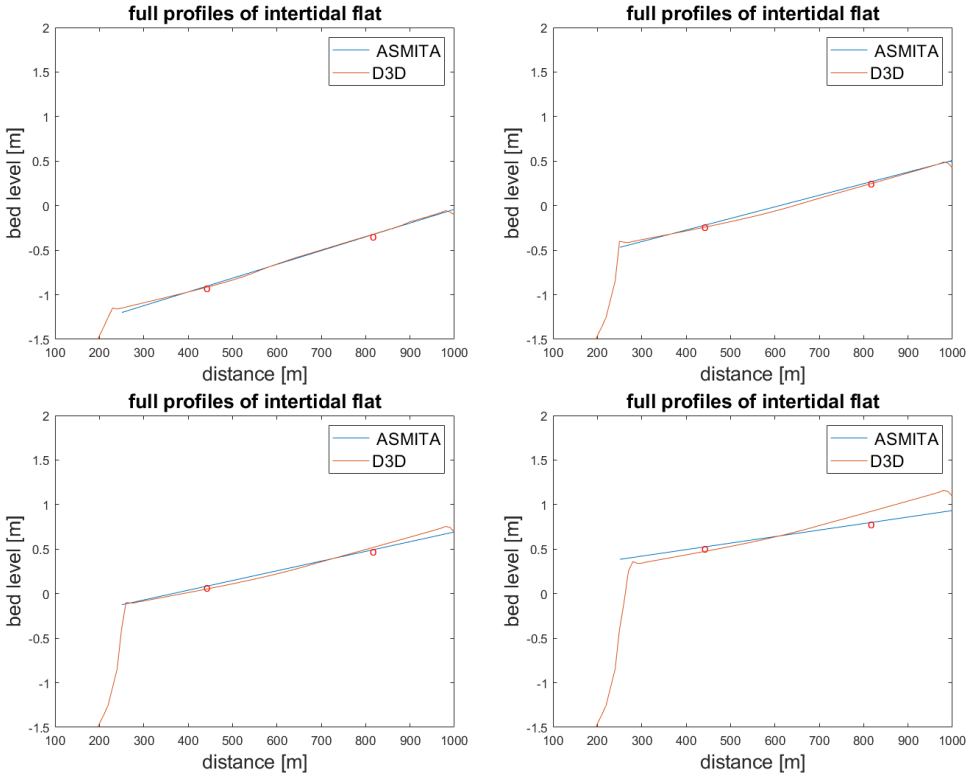

Figure 4.18: Mudflat profiles after 14, 68, 82 and 100 years under 1.67 m/century **SLR** (Red dots represent the center of elements) in 3-element model

Lower **SLR** scenarios show that the predictive results from **ASMITA** perfectly fit **D3D** in different time points. Exceptionally, the seaward edge of mudflat has a relatively faster deposition, and the limited accretion is at the landward end, leading

to gentler profiles after 80 years. The reasons are as follows. The sediment input from Element 2 to Element 1 does not have enough ability to keep up with the **SLR** to fill the extra storage area. On the contrary, there is a relatively higher sediment input efficiency from the channel to the nearby mudflat. The sediment transport in **ASMITA** modeling approach depends on the concentration differences, i.e., diffusion transport between the adjacent elements, which is represented by the horizontal exchange coefficient, δ. The computed horizontal diffusive coefficient is not large enough.

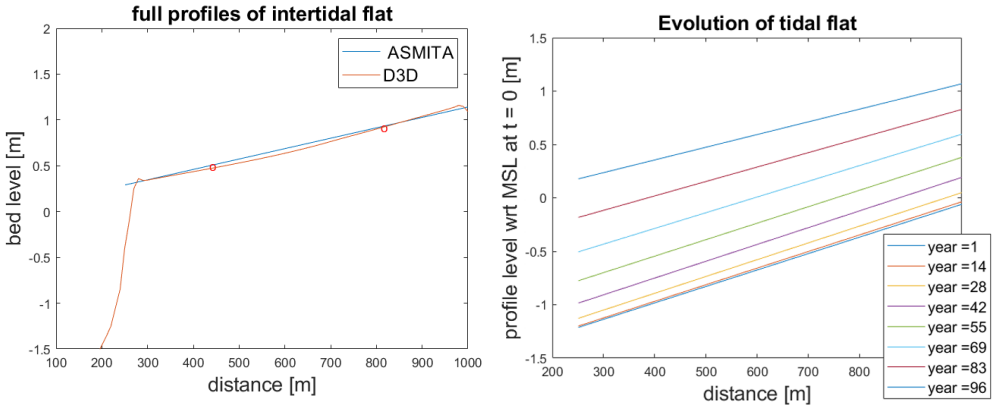

Figure 4.19: Modified mudflat profile after 100 years (Red dots represent the center of elements) and modified evolution of mudflat profiles at different time steps in 3-element model

After appropriately increasing δ by 0.01 between Element 2 and Element 1, Figure 4.19 suggests that the steepness of mudflat in **ASMITA** can maintain the same level as **D3D** even for the later stages of development. The nearly parallel profiles in the prediction of **ASMITA** indicates that larger diffusion coefficient contributes to the increase of deposition rate near the shoreline.

5-element Model

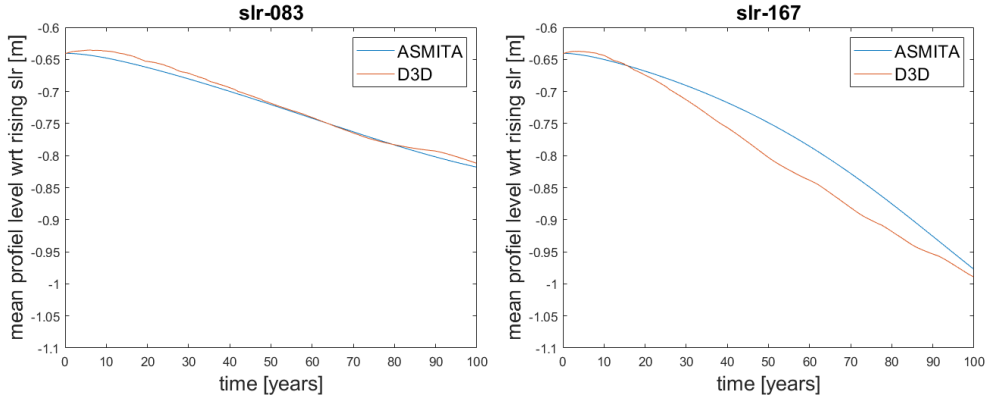

Figure 4.20: Evolution of the mean profile level in the case of 0.83 m/century and 1.67 m/century in 5-element **ASMITA** model

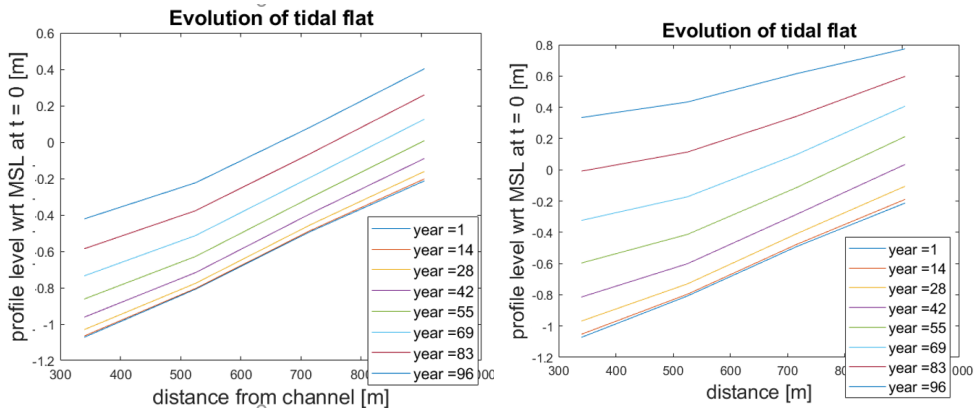

Figure 4.21: Evolution of the whole mudflat profile level in the case of 0.83 m/century and 1.67 m/century at different time steps in 5-element model

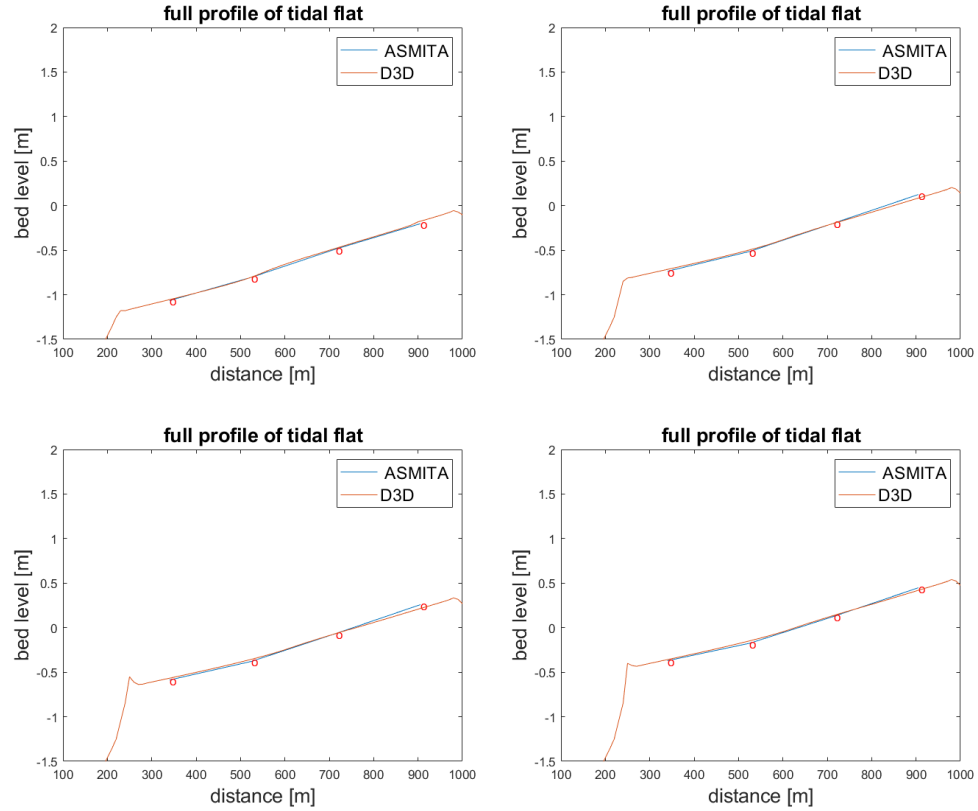

Figure 4.22: Mudflat profiles after 14, 68, 82 and 100 years under 0.83 m/century **SLR** (Red dots represent the center of elements) in 5-element model

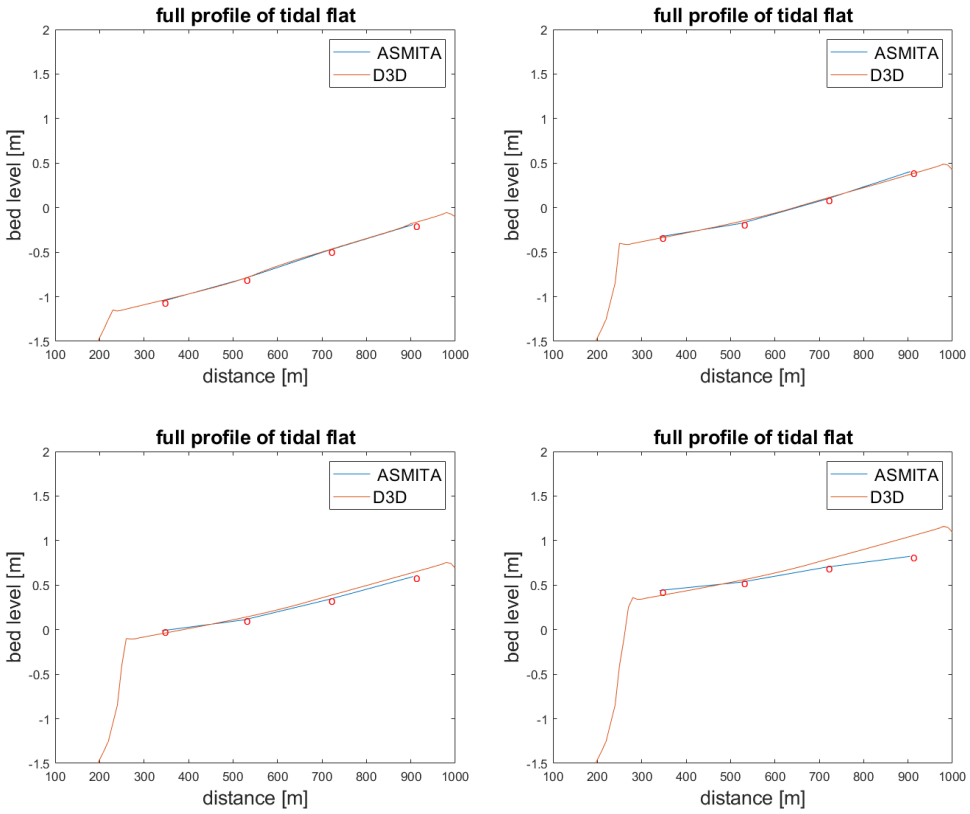

Figure 4.23: Mudflat profiles after 14, 68, 82 and 100 years under 1.67 m/century **SLR** (Red dots represent the center of elements) in 5-element model

The 5-element model separates the mudflat into four parts, which means that more data points are tracking the elevation of mudflat under **SLR** and a straight line does not represent the mudflat, instead, polyline. The tidal flat can be closer to the shape in **D3D**.

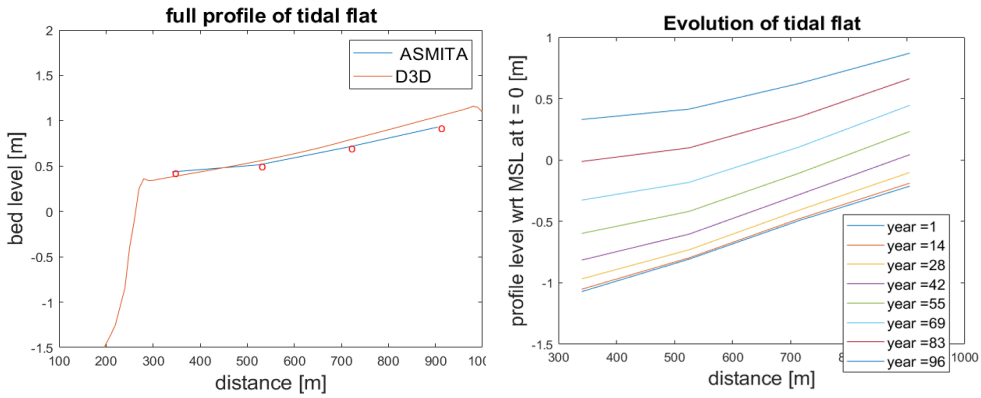

Figure 4.24: Modified mudflat profile after 100 years (Red dots represent the center of elements) and modified evolution of mudflat profiles at different time steps in 5-element model

As a 3-element model, the landward end of a tidal flat in **ASMITA** cannot catch up with the elevation of **D3D** after 80 years under the case of 1.67 m/century, which leads to the milder steepness. The same method is also adopted in 5-element model by increasing the landward δ of elements (The values between Element 1 and Element 2, Element 2 and Element 3 respectively turn into 0.053 m^3/s and 0.0632 m^3/s). Figure 4.24 indicates that the elevation is higher than the original profile

with lower horizontal exchange near the shoreline. It suggests that more sediments migrate landward, and this exaggerates the accretion degree.

11-element Model

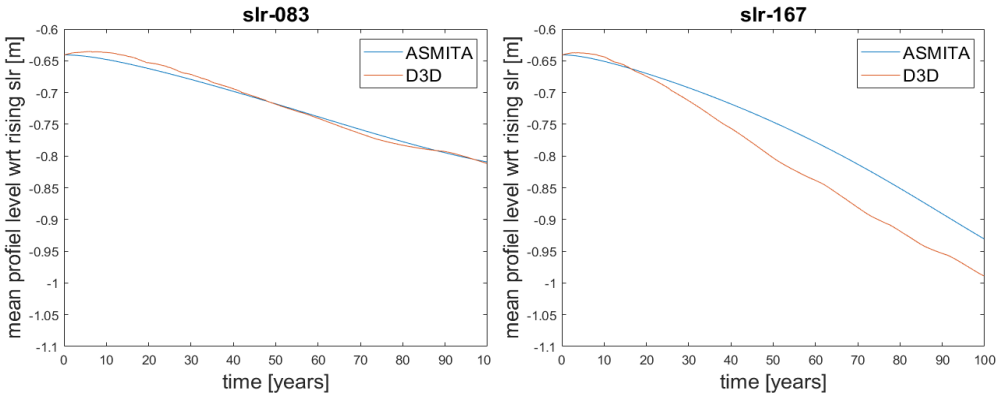

Figure 4.25: Evolution of the mean profile level in the case of 0.83 m/century and 1.67 m/-century in 11-element model

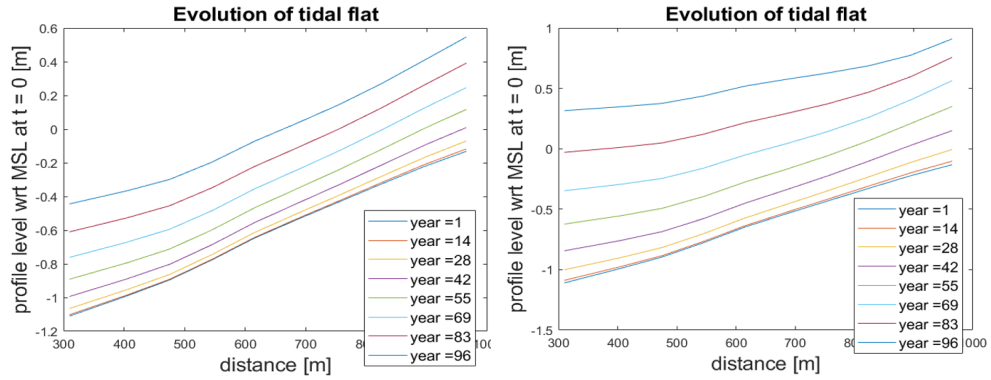

Figure 4.26: Evolution of the whole mudflat profile level in the case of 0.83 m/century and 1.67 m/century at different time steps in 11-element model

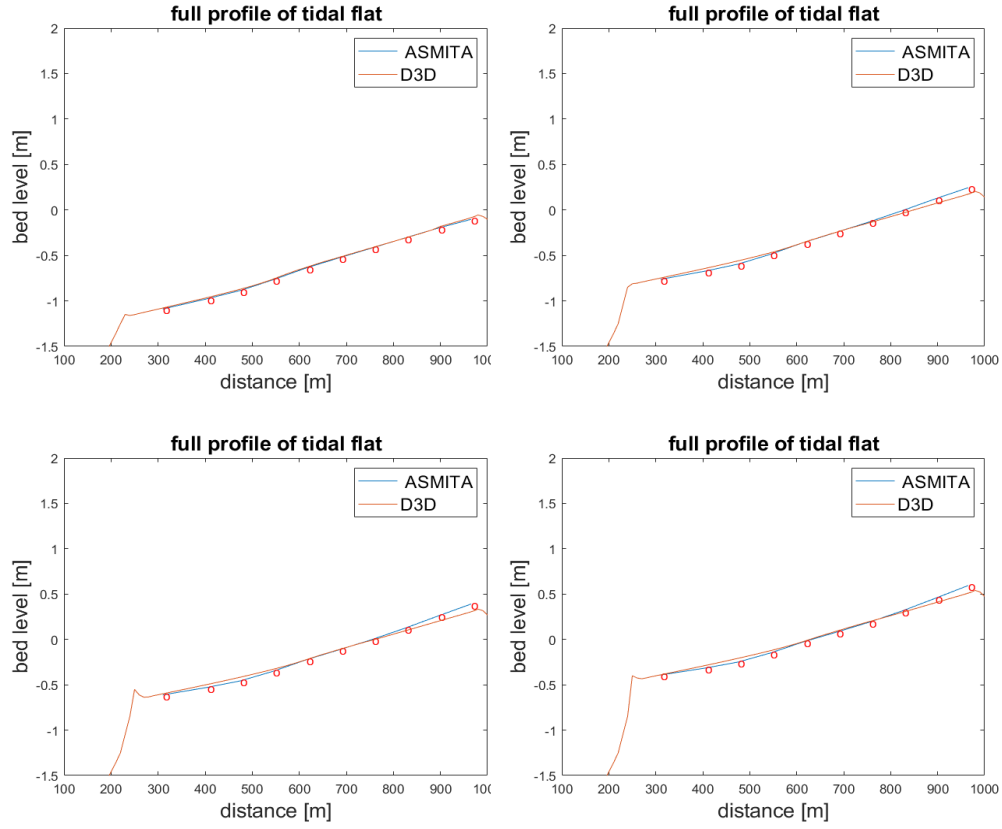

Figure 4.27: Mudflat profiles after 14, 68, 82 and 100 years under **SLR** rate of 0.83 m/century (Red dots represent the center of elements) in 11-element model

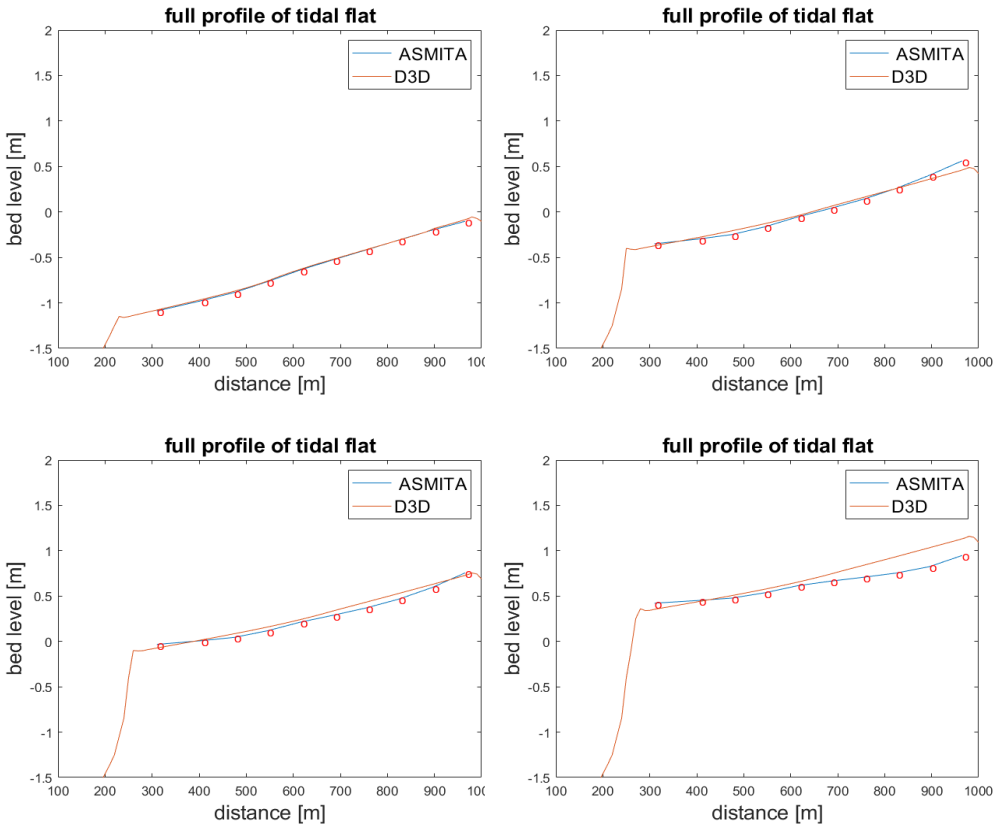

Figure 4.28: Mudflat profiles after 14, 68, 82 and 100 years under **SLR** rate of 1.67 m/century (Red dots represent the center of elements) in 11-element model

After expanding the element number in **ASMITA** to eleven, the coverage area by ten predictive dots (one of them represents the channel) on mudflat is broader, and accordingly, this can provide more detailed predictions of the mudflat. The same problem of the relative slow deposition rate near shoreline happens after about 80 years. The same method is adopted the larger δ for the elements at the landward side and relatively small δ near the channel. The specific application of δ is shown in Table 4.2. The regulated profiles better fit in the simulations in **D3D**, but more calibration efforts need to be paid in that the smaller elements do not have enough covering ability to represent the relatively wide part of mudflat near the shoreline.

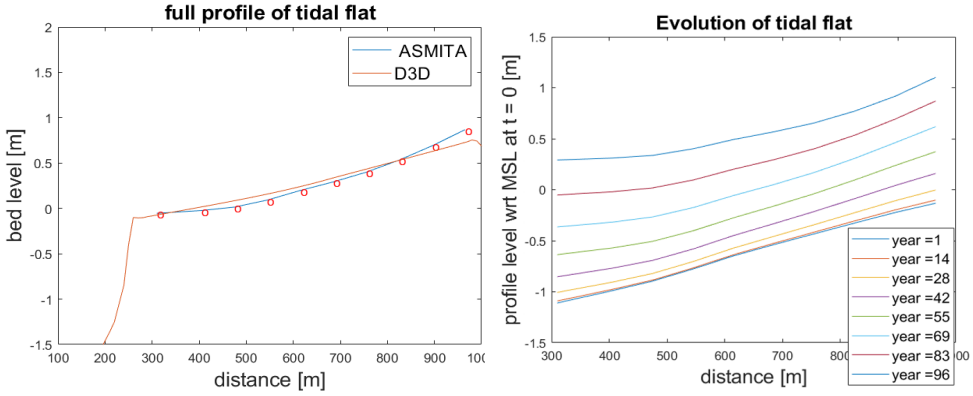

Figure 4.29: Modified mudflat profile after 100 years (Red dots represent the center of elements) and modified evolution of mudflat profiles at different time steps in 11-element model

Table 4.2: Overview of model parameters in 11-element model of **ASMITA**

Path	δ
1to2	0.15
2to3	0.16
3to4	0.182
4to5	0.187
5to6	0.19
6to7	0.192
7to8	0.193
8to9	0.196
9to10	0.133
10to11	0.1
11tooutside	1.7336

4.3 PHASE 3 – HYBRID MODEL RUN

The wave-induced shear stress does not influence the erosion and deposition in the hybrid model. The bed level changes are a function of flow-induced advection and diffusion transport and the difference between the local and equilibrium concentration. As such, the wave forcing is neglected in the hybrid model. Besides, the timescale computation in Table 4.1 suggests that the dominated transport in this mudflat system is diffusion transport. Further research can test the feasibility of applying the time average tide motion as the conception in **ASMITA** in the setup. Finally, the changes in the numerical configurations consisting of the grid-scale and time step are exerted in this section.

4.3.1 Equilibrium Profile

Before any **SLR** setup executing on the hybrid model, it is crucial to properly evaluate the adaption process and final equilibrium profile without the impacts of **SLR** in the hybrid model.

Varying Tides

The first run mainly pays attention to the process of tidal flat towards the equilibrium state without the impacts of **SLR**. A similar mean bed level of the final state is expected (Figure 4.30) because of the prescribed equilibrium in the hybrid model. However, the discrepancies happen between 20 years and 80 years.

Suppose we pay attention to the evolution of the whole tidal flat. In that case, the hybrid model can simulate the similar tendency of a deposition front gradually moving from the mudflat edge toward the landward end, except for the initial sink at the channel.

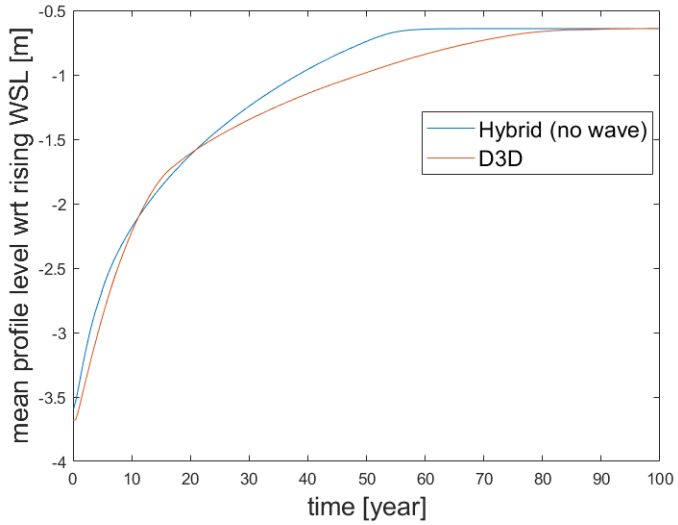

Figure 4.30: The comparison on the mean bed level between **D3D** and Hybrid model in the first run

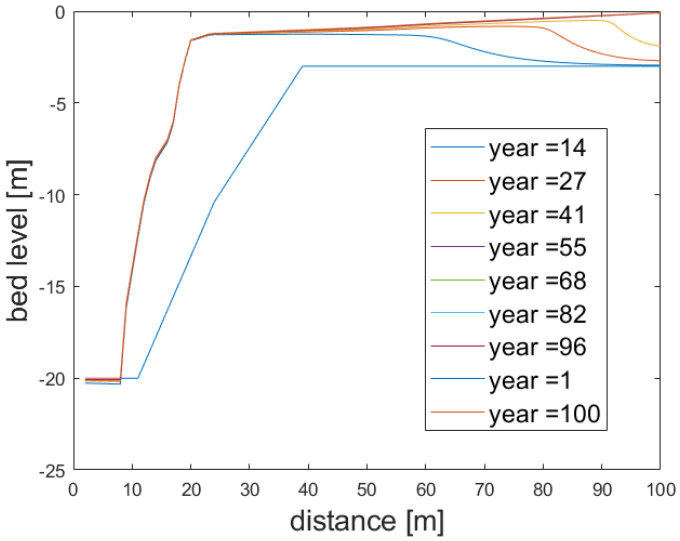

Figure 4.31: The evolution of the full profile of mudflat in the first run of the hybrid model

Time Averaging of Tide Motion

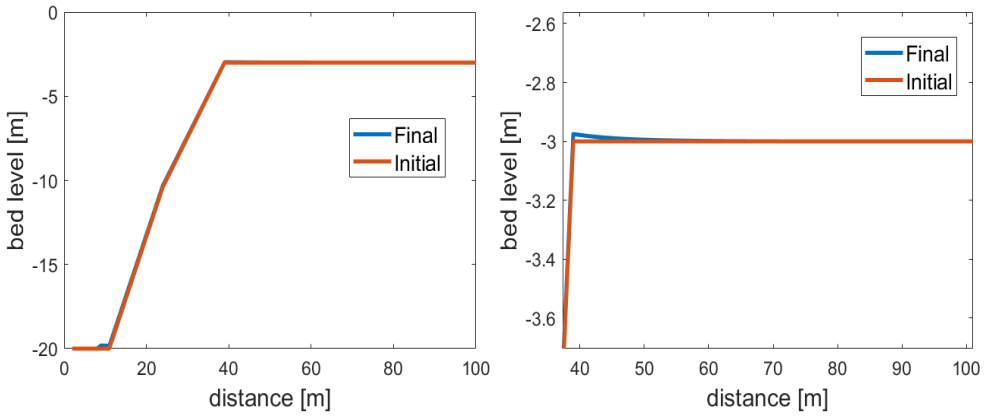

Figure 4.32: The comparison between the initial and final profiles in the case of average tides in the first run and its close-up in hybrid model

The simulation of average tide motion in the hybrid model indicates that the slight deposition at the edge of the mudflat lasts until the end. From the perspective of the complete intertidal flat, the elevation shows almost no change in the first 100-year simulation. The diffusion-dominated transport in this system leads to accretion at the edge due to the relatively large concentration discrepancy between the channel and mudflat edge. However, the minimal gradient in the mud concentration across the mudflat cannot back up the further deposition without the tidal varying within a tidal cycle. Meantime, the difference between the local and equilibrium concentration does not stimulate the accretion motion since the system is close to its equilibrium state. As such, there are no apparent variations of the whole mudflat.

Change in Grid Size and Time Step

Suppose we double the grid size (20 meters) and time step (0.4 minutes) in the model setup; the time-consuming is nearly half the original test. The specific complete profiles at different time steps are shown in Figure 4.33, taking a closer look

at the comparisons between the standard run and modified run more clear insights into nearly the same bed level for the two tests. Still, the profiles after adjusting are more rugged. This can be explained that there are fewer reservation points to define the shapes and thus a lack of information on bed levels at these places during evolution.

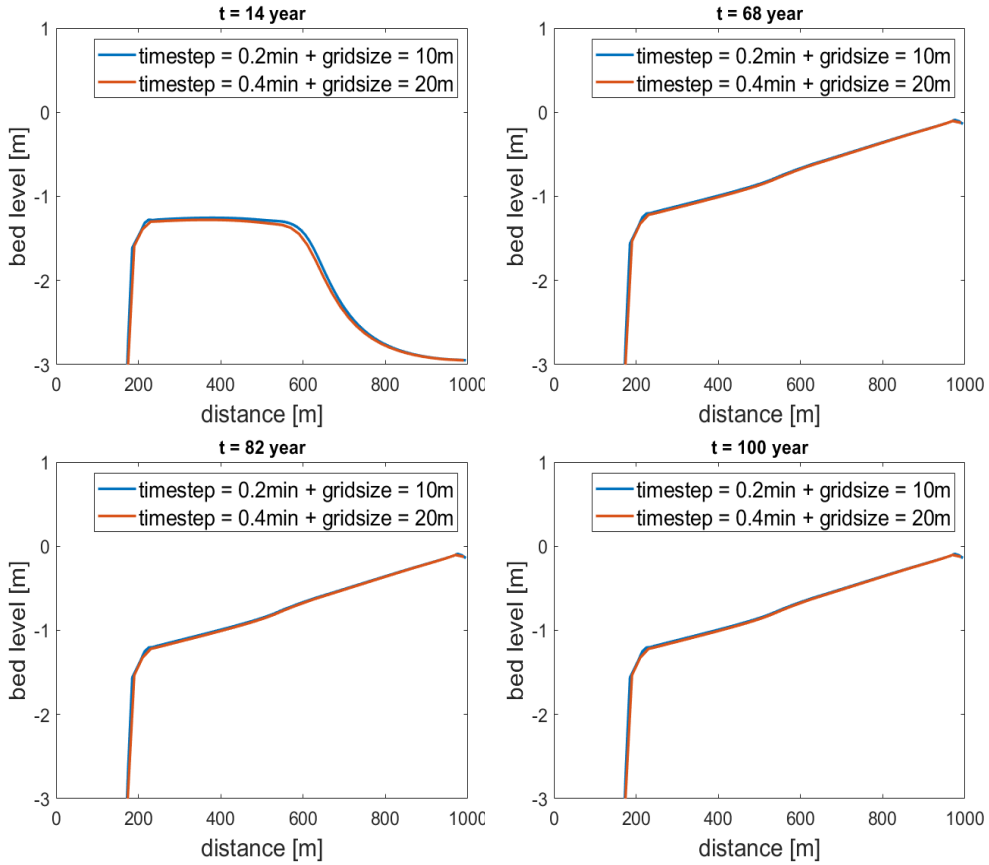

Figure 4.33: Full profiles of mudflat in 7, 14, 82 and 100 year under no **SLR** with the time step of 0.4 minutes and the grid size of 20 m in hybrid model

4.3.2 Sea Level Rise

The second set of experiments consider the influences from **SLR** on the equilibrium bed level generated in the previous runs.

Varying Tides

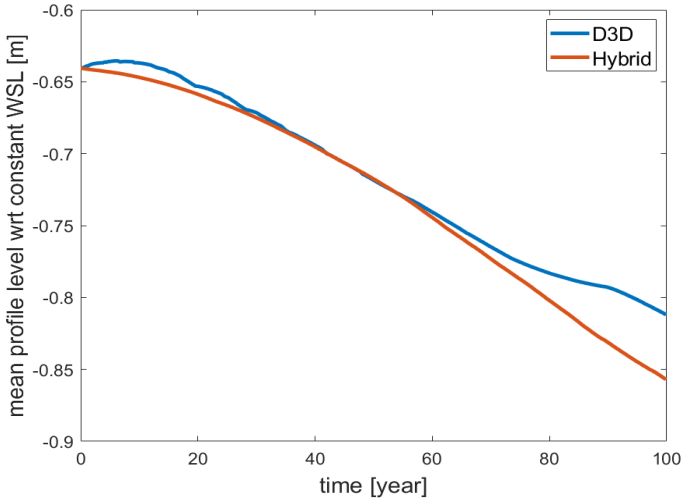

Figure 4.34: The comparison on the evolution of bed level between **D3D** and Hybrid model under **SLR** of 0.83 m/century

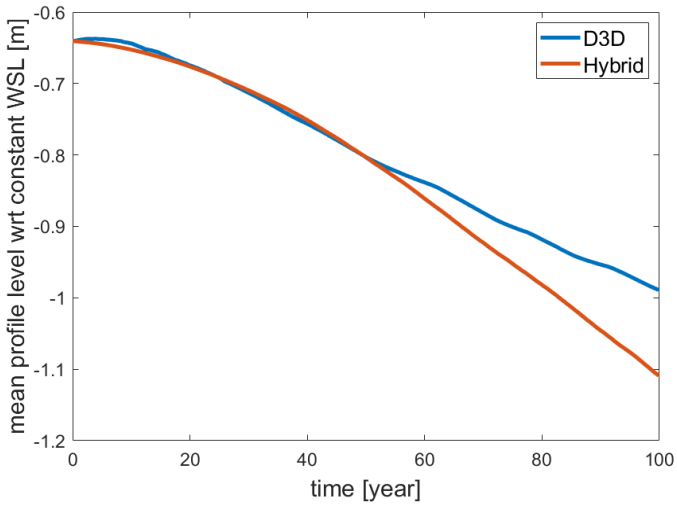

Figure 4.35: The comparison on the evolution of bed level between **D3D** and Hybrid model under **SLR** of 1.67 m/century

The standard run shows a similar evolution of the mean bed level before 50 years but apparent deviations after 50 years (Figure 4.34 and Figure 4.35). Closer analysis on the complete profiles (Figure 4.36 and Figure 4.37) reveals that the steeper slopes of the hybrid model, of which the landward end starts to have more deposition and slight erosion at the edge of mudflat compared with **D3D** at the post-run.

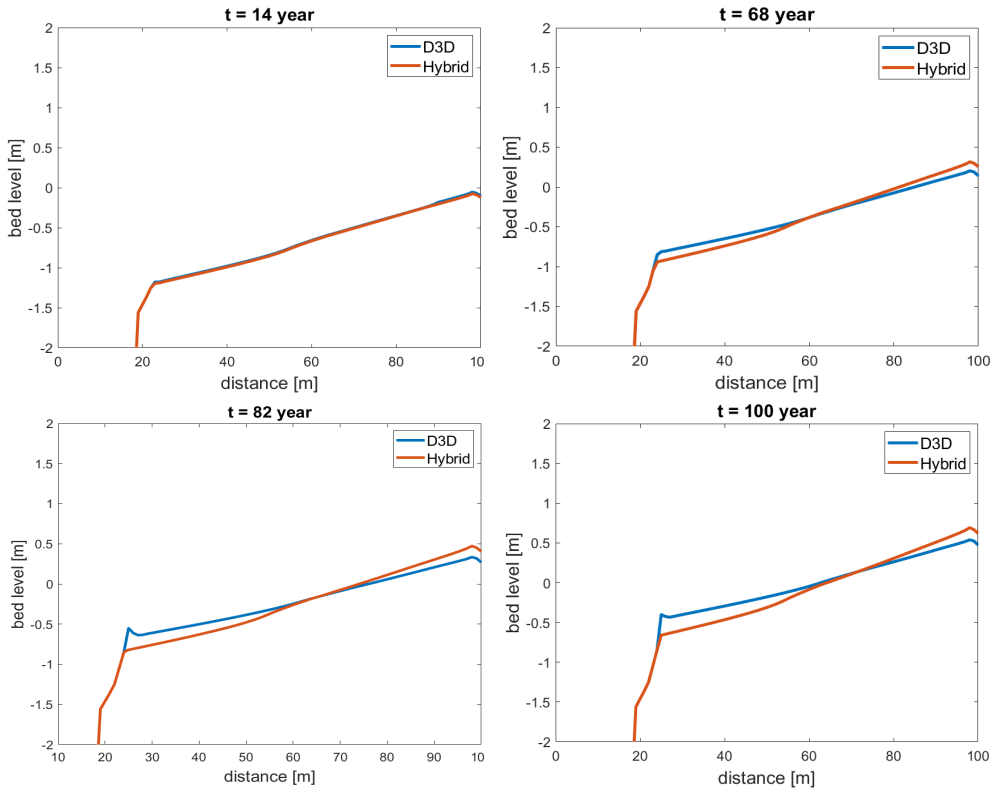

Figure 4.36: The comparison on the final profile between **D3D** and Hybrid model under **SLR** of 0.83 m/century in 14, 68, 82 and 100 year

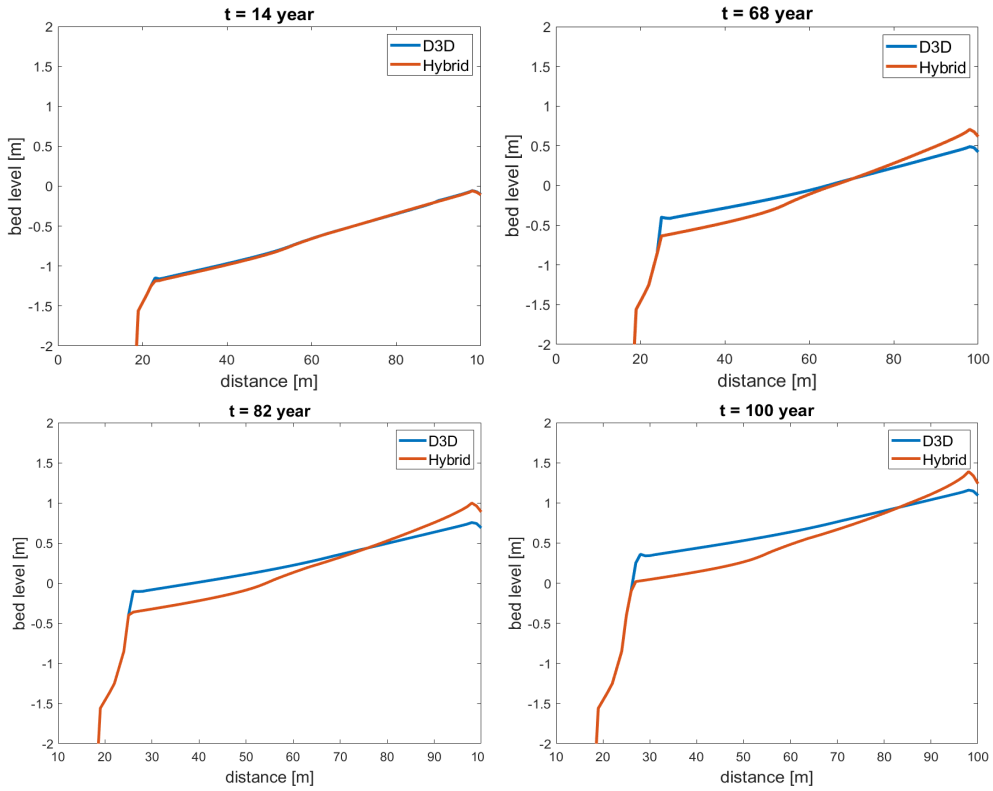

Figure 4.37: The comparison on the final profile between **D3D** and Hybrid model under **SLR** of 1.67 m/century in 14, 68, 82 and 100 year

From Figure 4.38, the strong fluctuations of concentration happen during the evolution of the process. The artificial channel bed level by dredging makes it easier to have the numerical instabilities, i.e., the spurious oscillations in the concentra-

tion. To improve the stability, lowering the time step to 0.1 minutes can efficiently decrease the degree of numerical wiggles (Figure 4.39). Nevertheless, the whole tendency of concentration keeps falling. It is because the concentration computation is dominated by the water depth variation (Equation 1.7), and the increase of the water depth leads to the continuous reduction in the concentration level. (Figure 4.39).

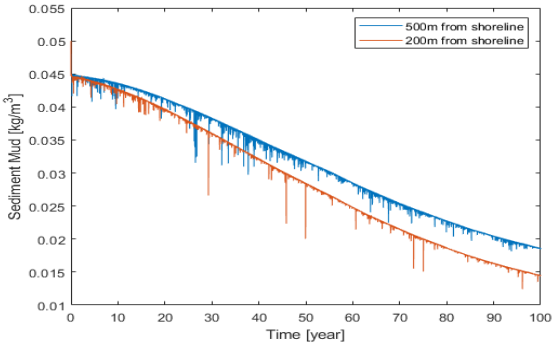

Figure 4.38: Evolution of **SSC** levels across the mudflat in hybrid model

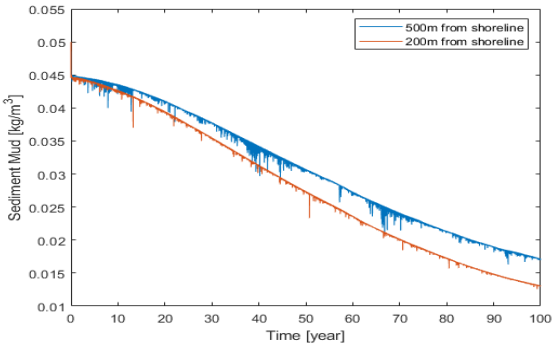

Figure 4.39: Evolution of **SSC** levels across the mudflat after decreasing time step in hybrid model

Time Averaging of Tide Motion

Firstly, we pay attention to the average elevation of the mudflat, provided in Figure 4.40. The case with the average tidal motion induces numerical instability in the evolution of the mean profile level. There is an abrupt increase in the mean bed level and the following sudden drop. The spikes of the curve occur between 20 and 50 years in the case of 0.83 m/century.

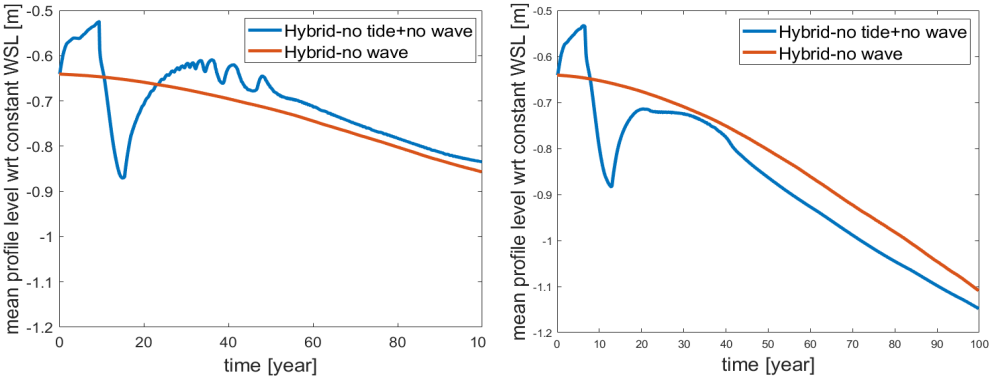

Figure 4.40: Comparisons of the bed level evolution between average tidal motion and varying tides, under **SLR** of 0.83 m/century and 1.67 m/century in hybrid model

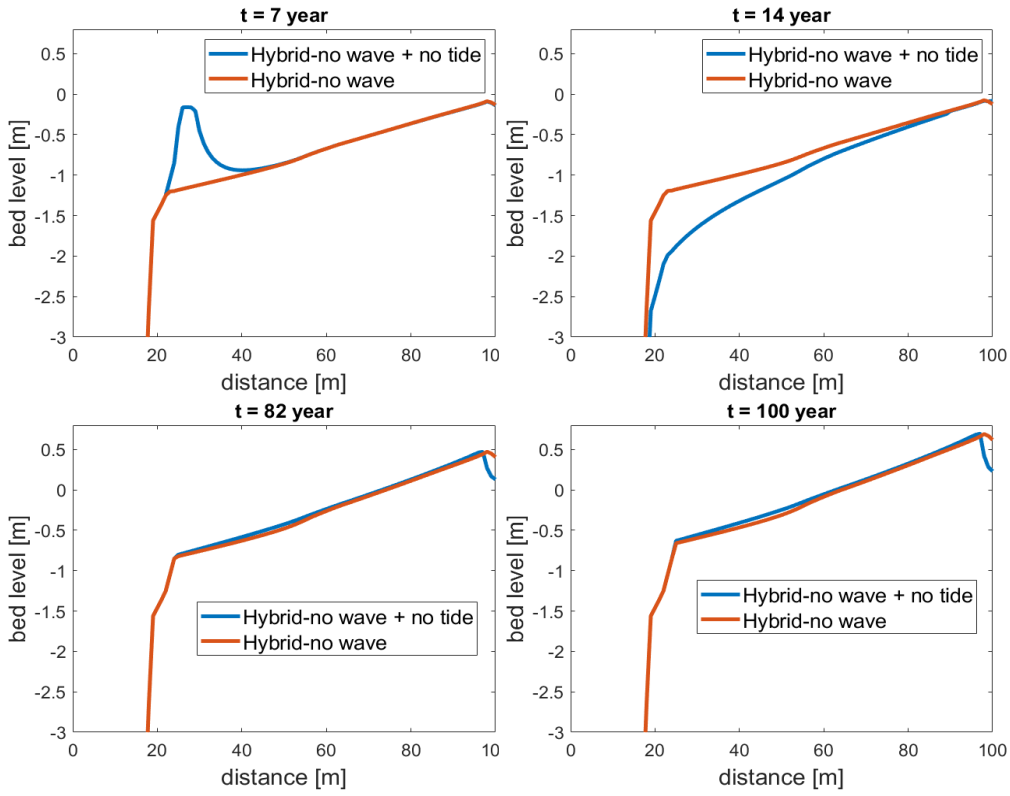

Figure 4.41: Comparisons of the full profiles between average tidal motion and varying tides in 7, 14, 82 and 100 year under 0.83 m/century **SLR** in hybrid model

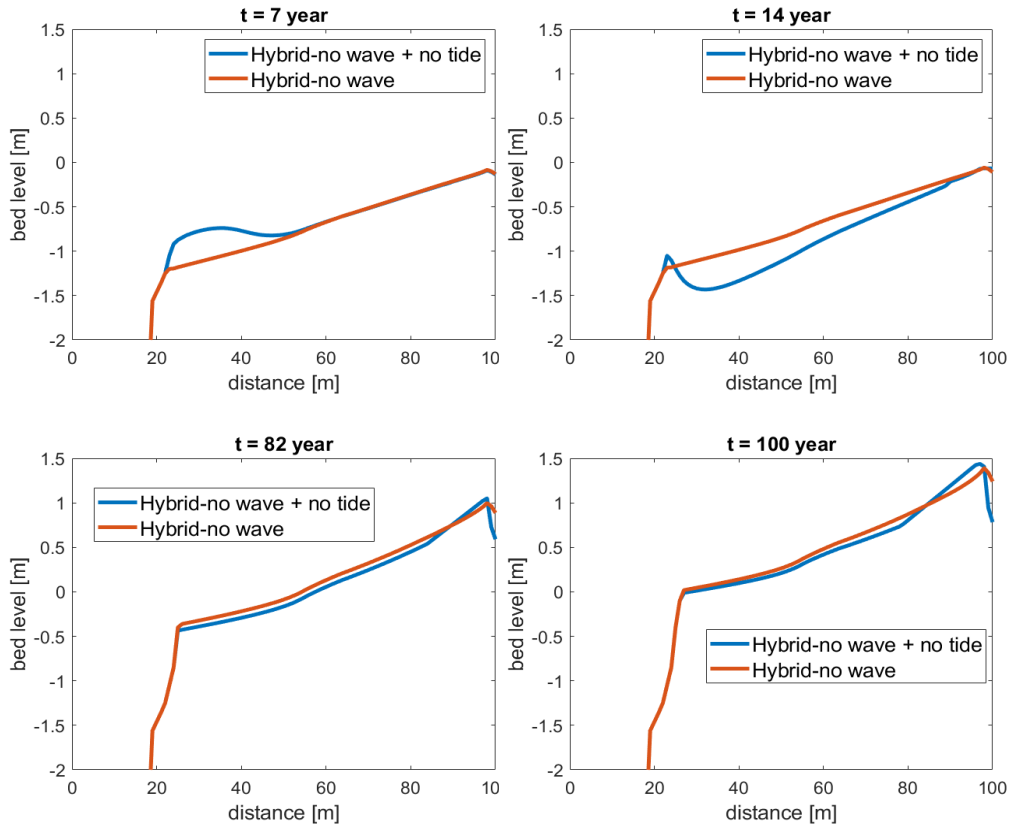

Figure 4.42: Comparisons of the full profiles between between average tidal motion and varying tides in 7, 14, 82 and 100 year under 1.67 m/century **SLR** in hybrid model

Initially, the unrealistically large deposition occurs at the edge according to the high mean bed level, and the sink is at the subtidal part of the mudflat afterward. Subsequently, the sink rebounds to be a certain level, and the (small) deposition front slowly moves towards the shoreline as the standard runs in the hybrid model and **D3D**. (Figure 4.41 and Figure 4.42).

The tides in this system can effectively prevent levee development at the mudflat edge, and waves re-suspend the sediments, after which they will be transported landward in the flood flows. The hybrid model with the average tide and no wave effects can only depend on the concentration differences, i.e., diffusion transport to distribute the sediments along the mudflat. There was a large gradient in the vicinity of the edge of the mudflat. This causes the faster process of transporting sediments from the channel to the tidal flat in essence. Still, a smaller gradient in the concentration within the mudflat results in the slow sediment transport process from the levee to the shoreline. This exactly explains the initial deposition at the edge of mudflats.

A closer investigation into the concentration level at different stations reveals the strong numerical instabilities before 50 years. Even if modifying the *Morphological Scale Factor (**MF**)* and time step [3], they cannot make a dominant effect on the eliminating of instabilities (4.44(b) and 4.44(c)). Moreover, the mudflat profiles and the concentration fields recover after 50 years.

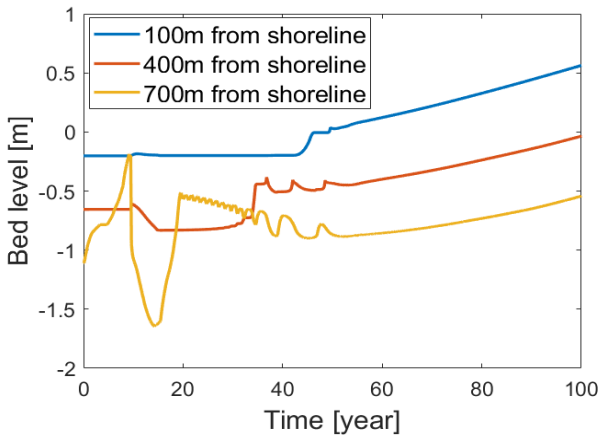

Figure 4.43: Evolution of bed level across mudflat in the hybrid model

An abrupt increase in the bed level of the levee enables the edge over the water level, and thus the drying results in the flop of available suspended sediments near the channel towards zero. The discrepancy between the equilibrium and almost zero local concentration stimulates a sharp decline in the elevation at the mudflat edge. This area is inundated again with an increasing water depth that generates the reverse increase in bed level of the levee, suggested in bed level variations at the 700 m from the shoreline where the position is close to the channel (Figure 4.43). The same position also indicates that the general reduction in the bed level with slight fluctuations. This is because the **SLR** is not apparent between 20-year and 50-year and bed level variation is closely correlated to the change in the concentration field. It exactly explains the wiggles. The evolution of bed level converges to be stable after 50 years in that the accelerated **SLR** is rapid enough so that the elevation of mudflat cannot catch up anymore, and the mudflat is gradually drowned. The tidal flat near the shoreline (Figure 4.43) suggests no early fluctuations on the bed

3 The Courant number ($C = \frac{u\Delta t}{\Delta x}$) is a dimensionless value representing the time in which a particle keeps in one cell of the mesh. It needs to be between 0.1 and 10 in**D3D**. Decreasing the time step, in this case, may improve the stability of the model.

level due to the slow process of sediment transport by diffusion transport from the edge of mudflat to fill in the storage area created by **SLR** before 50-year. The process explains the gap near the landward end in the 0.83 m/century **SLR** and 1.67 m/century **SLR** in the 100 year. For the slight wiggles during concentration evolution from 4.44(a), this could be caused by the artificial channel profile leading to numerical instabilities.

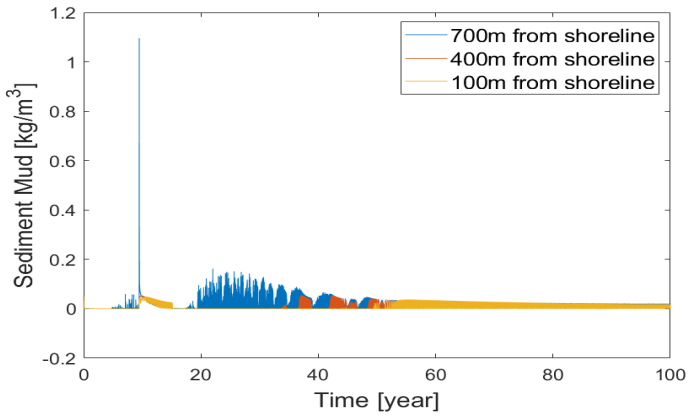

(a)

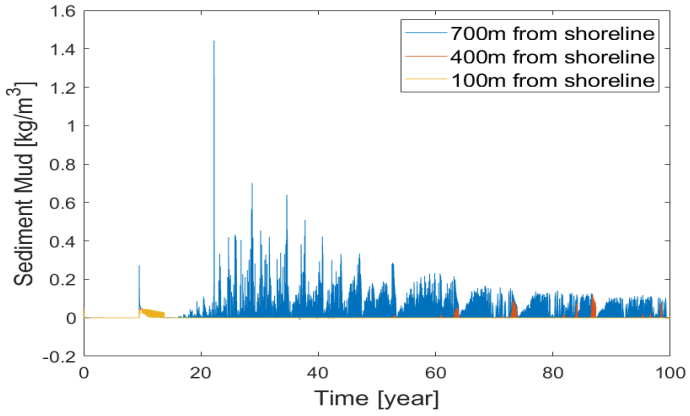

(b)

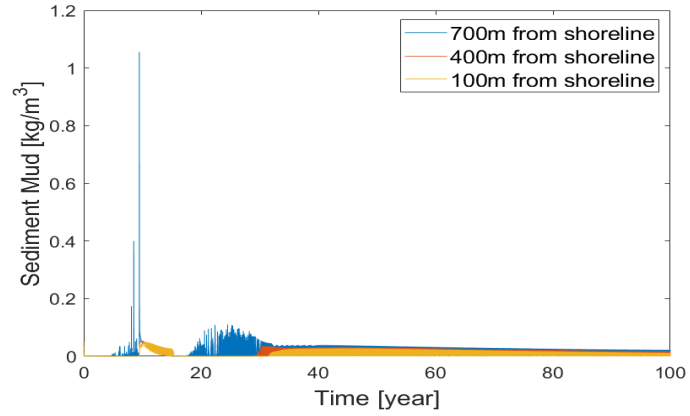

(c)

Figure 4.44: Evolution of **SSC** across mudflat (a) with standard parameter setup, (b) after modifying **MF**, (c) after modifying time step in the hybrid model

Change in Grid Size and Time Step

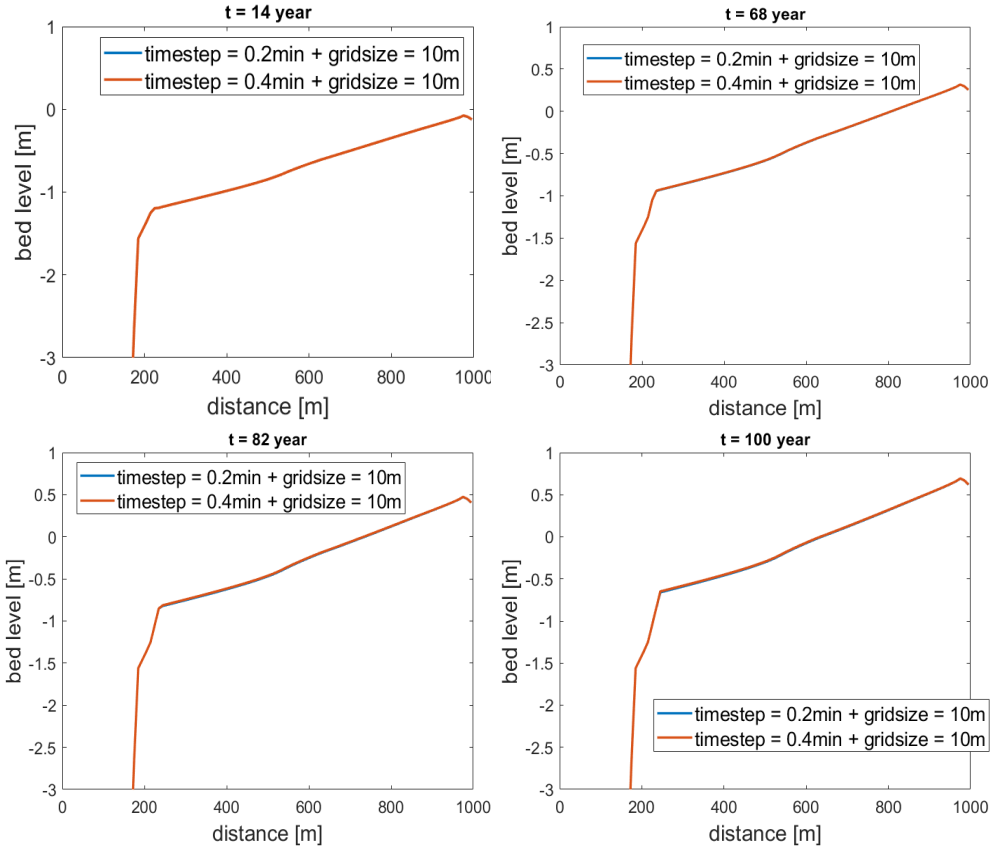

Figure 4.45: Full profiles of mudflat in 7, 14, 82 and 100 year in the 0.83 m/century **SLR** with the time step of 0.4 minutes in hybrid model

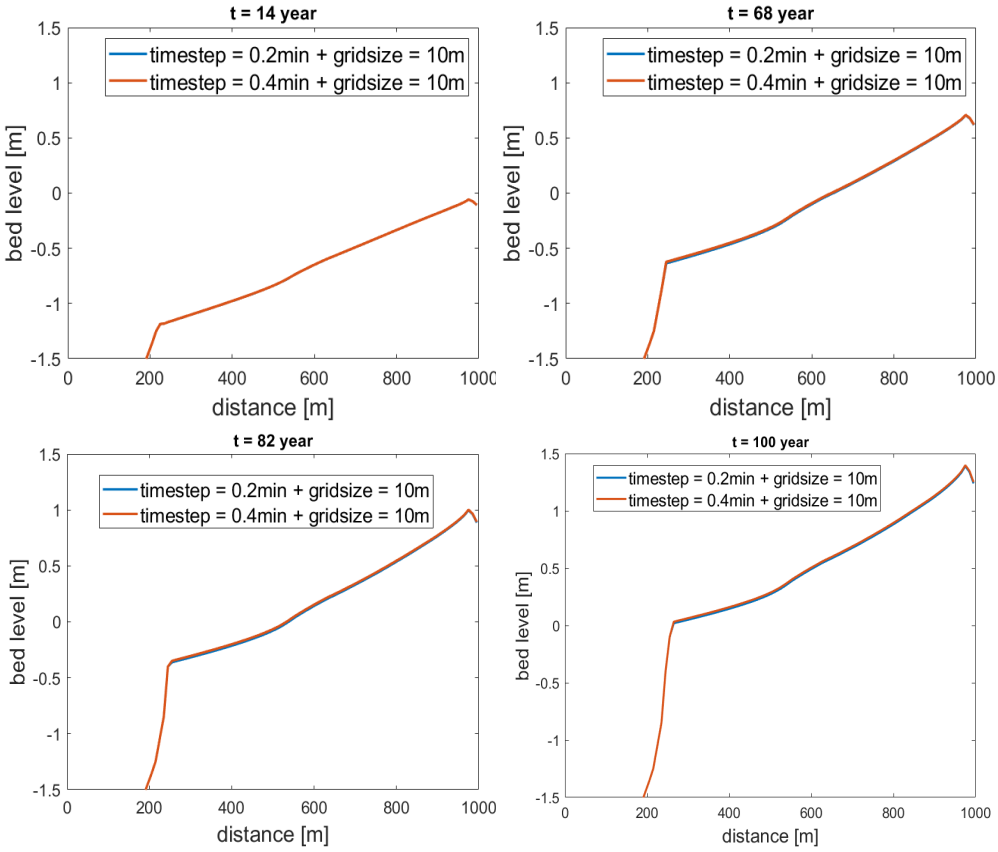

Figure 4.46: Full profiles of mudflat in 7, 14, 82 and 100 year in the 1.67 m/century **SLR** with the time step of 0.4 minutes in hybrid model

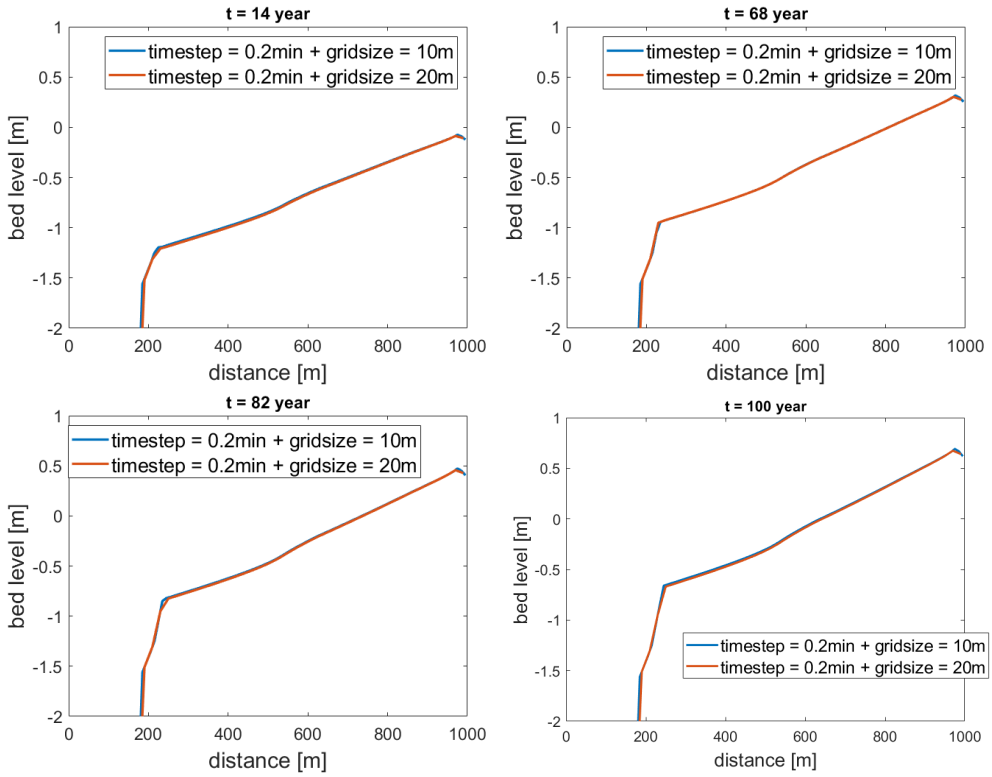

Figure 4.47: Full profiles of mudflat in 7, 14, 82 and 100 year in the 0.83 m/century **SLR** with the grid size of 20m in hybrid model

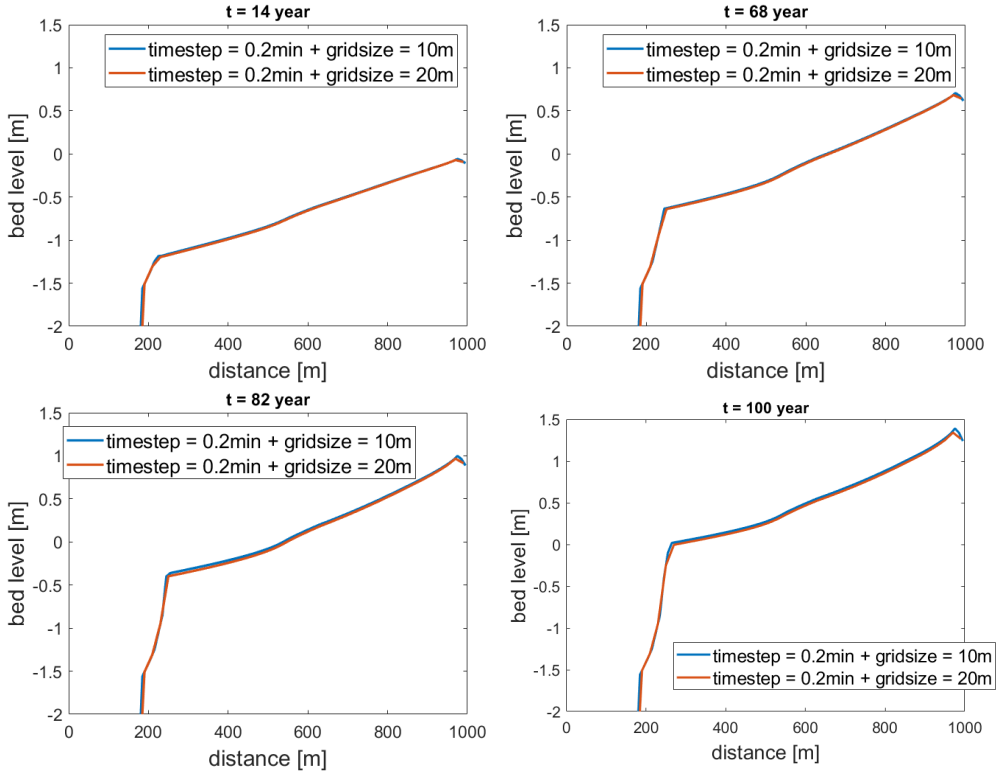

Figure 4.48: Full profiles of mudflat in 7, 14, 82 and 100 year in the 1.67 m/century **SLR** with the grid size of 20m in hybrid model

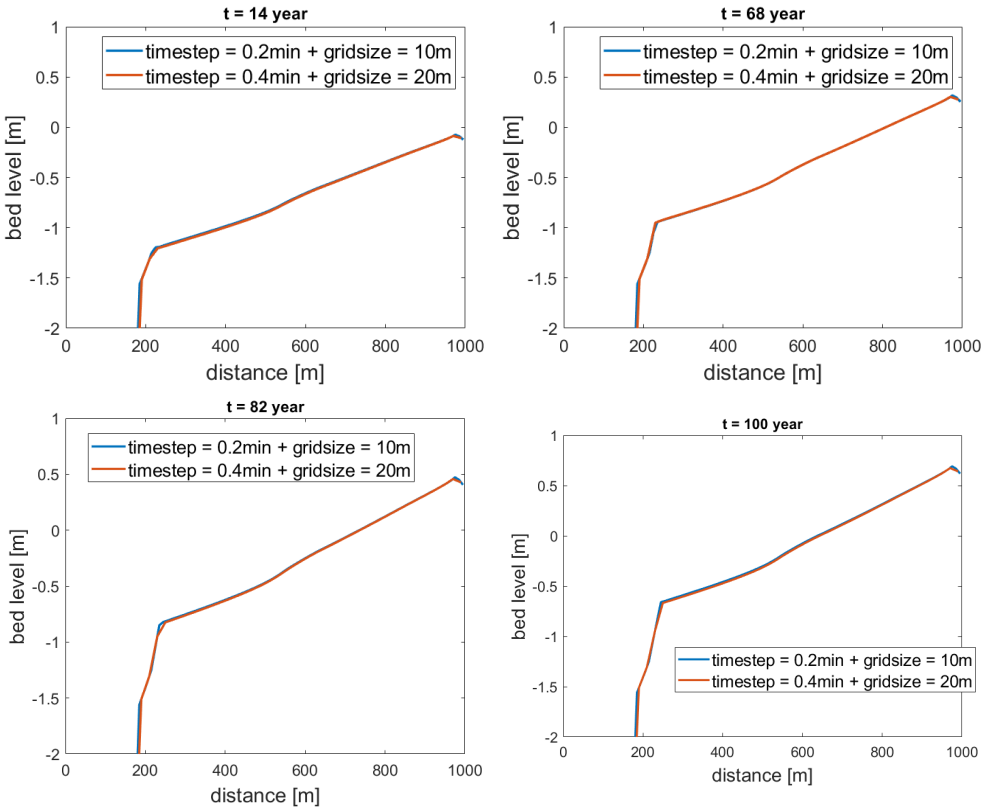

Figure 4.49: Full profiles of mudflat in 7, 14, 82 and 100 year under 0.83 m/century **SLR** with the time step of 0.4 minutes and grid size of 20m in hybrid model

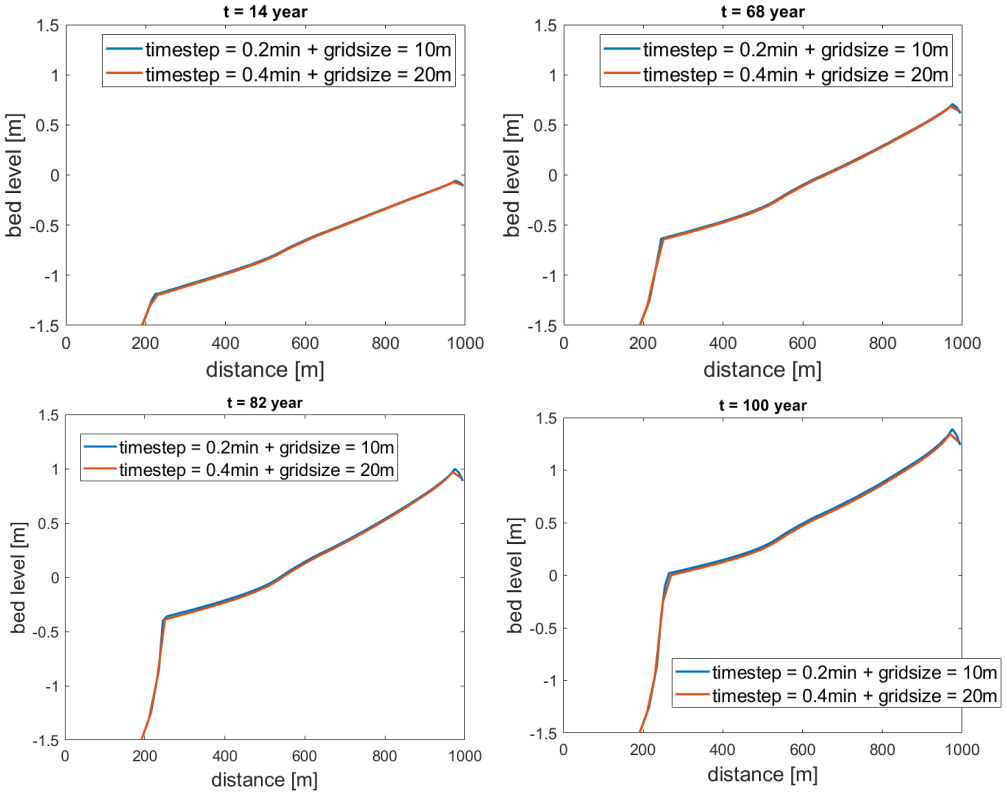

Figure 4.50: Full profiles of mudflat in 7, 14, 82 and 100 year under 1.67 m/century **SLR** with the time step of 0.4 minutes and grid size of 20m in hybrid model

Starting from the only change in the time step of 0.4 minutes, the executive results in the hybrid model (Figure 4.45 and Figure 4.46) suggests similar predictive pro-

files except for the slightly larger deposition after changes in the time step (the bed level difference is about 0.01 m for both **SLR**). Moreover, the simulation time (about 28 minutes) is shorter than the standard case.

Another run is doubling grid size to 20 m to lower the resolution level but keeping the time step constant at the same time. The numerical simulation is promising as well, suggested in Figure 4.47 and Figure 4.48. The almost overlapped figures indicate the feasibility of coarser grids application in the hybrid model to save computational time.

Finally, the simulation was executed with the time step of 0.4 minutes and grid size of 20 m in the 0.83 m/century and 1.67 m/century **SLR** (Figure 4.49 and Figure 4.50). The synchronous changes in the numerical parameters of time step and grid size can improve the efficiency of the simulation. The predicted accretion rate in the modified case is similar to the scenarios without numerical setup changes.

5 DISCUSSION

The discussion chapter mainly focuses on the different general points which are closely related to Chapter 4 and will be elaborated on in this chapter.

5.1 ASMITA

5.1.1 Average Elevation Prediction

Solely for the average elevation of mudflat under impacts of **SLR**, the reproduction projects from **ASMITA** modeling approach can reach a relatively accurate and satisfying level whatever the single element or multi-element models, except for the slight differences in the scenarios of 1.67 m/century **SLR** since the diffusion coefficients defined by calibrated ϵ in 3, 5 and 11-element models are applied for different interfaces between the adjacent elements, and thus it is difficult to determine the coefficient values at the exact location in another model if there are no usage of the coincident interfaces.

Firstly, our 1D modeling approach effort from **ASMITA** can reproduce the results of **D3D** in that the equilibrium state of mudflat can be well represented in **ASMITA** model. According to the simulation results from **D3D**, this provides the input parameters, α and β, which express the equilibrium relation. Moreover, the morphological timescale of the mudflat system is correctly represented by certain parameters. The parameter values chosen in this application attempts to find the best fit between **D3D** and **ASMITA**.

5.1.2 Full Profile Prediction

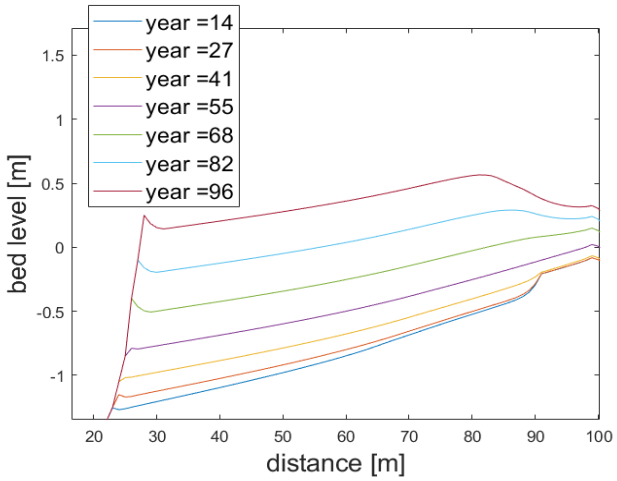

Figure 5.1: Evolution of mudflat in the case of 1.67 m/century and 50 % drop in **SSC** at the boundary in **D3D**

The multi-element model can roughly simulate the full profile evolution, but a single element model cannot achieve it due to the characteristics of aggregation in **ASMITA**. Meantime, more details about the shape of mudflats can be included if applying more elements, i.e., a 3-element model consisting of two elements predicting the mudflat can determine the general slope changes of mudflats while 5-element and the 11-element model suggests more detailed profiles with a pattern of the polyline. With regard to the slower water level rising, i.e., 0.83 m/century, the simulated mudflats in **ASMITA** can fit well with **D3D**. While in the scenario of 1.67 m/century **SLR**, it is apparent the application of δ values are too low so that the sediment input towards the shoreline direction can not catch up with the accretion rate of **D3D** in the rapid acceleration stages of **SLR** so that the steepness of hybrid model is mild. The diffusion coefficient is proportional to water depth values, and the application of water depth is the maximum. As such, the computational diffusion coefficient reaches the threshold[1]. To improve the steepness of the predicted tidal flat, we can appropriately expand the δ in the elements near the shoreline and lower those near the channel. However, the calibration efforts on regulating the diffusion parameters will grow with increases in the number of elements, and meanwhile, it is uncertain to determine what elements need to be revised and how much to adjust.

The considerable amount of elements involved in the prediction can improve the detail level of the full mudflat profile. While smaller-scale morphological changes begin to be essential, e.g., Van der Wegen et al. [2017] provides the insight into the generation of the gap near the shoreline due to a sudden drop in **SSC** level, it is doubtful that the predictive ability of **ASMITA** can keep the same level as well. As Figure 4.16, Figure 4.21 and Figure 4.26, the accretion of mudflat practically maintains the same rate for different parts of mudflat under impacts of **SLR** without important small-scale local changes. However, the developments of mudflat in the accelerated **SLR** and 50 % drop scenario, suggesting that the mudflat gradually sinks at the most sections except for the landward end with a slight deposition before the 14^{th} year due to the sudden **SSC** decrease at the boundary. The sediment input fills in the erosion, followed by the deposition due to the accelerated **SLR** indicated in Figure 5.1. Figure 4.3 shows the final profile of mudflat with a gap at the landward end, which is more dominant in the scenario of 1.67 m/century **SLR**. This is because the wave cannot re-suspend the sediments anymore at low water, and the deposition front migration from the edge to shoreline direction comes to a halt. Here neglecting the 3-element model is because this model indicates the mudflat slope by a straight line, which is impossible to reproduce at the landward end. The parameter setups in 5-element and 11-element are shown as follows, the application of water depth is the value of the 100th year in the simulation of **D3D**[2]:

Table 5.1: Overview of model parameters in 5-element model of **ASMITA** with 50 % drop in **SSC** at the boundary under 1.67 m/century **SLR**

Path	**H (m)**	**a (m)**	**T (s)**	L_b **(m)**	**u (m/s)**	ϵ	**D** (m^2/s)	δ (m^3/s)	**L (m)**	w_s **(m/s)**
1.67	m/century									
1to2	1.0133	1	44700	95	0.006589	0.1	10.0044	0.053355	190	0.001
2to3	1.1797	1	44700	285	0.016979	0.1	10.03401	0.062301	190	0.001
3to4	1.3348	1	44700	475	0.02501	0.1	10.08349	0.072754	185	0.001
4to5	2.07	1	44700	660	0.022409	0.1	10.10394	0.09728	215	0.001
5tooutside	21.67	1	44700	875	0.002838	0.1	10	1.7336	125	0

1 ϵ contributes a little bit to the value of D, which the order depends on the input value of 10 from **D3D**

2 It needs to be aware of is that the water depth of elements near the shoreline in the 11-element model, viz. Path 1 to 2 over the adjacent element is because the gap in the post runs lead to the final water depth at the landward end beyond the adjacent mudflat.

Table 5.2: Overview of model parameters in 11-element model of ASMITA with 50 % drop in SSC at the boundary under 1.67 m/century SLR

Path	H (m)	a (m)	T (s)	L_b (m)	u (m/s)	ϵ	D (m^2/s)	δ (m^3/s)	L (m)	w_s (m/s)
1.67	m/century									
1to2	1.3054	1	44700	35	0.001884	0.1	10.00046	0.186494	70	0.001
2to3	1.1377	1	44700	105	0.006486	0.1	10.00479	0.162606	70	0.001
3to4	1.0064	1	44700	175	0.012221	0.1	10.01503	0.143988	70	0.001
4to5	1.0758	1	44700	245	0.016006	0.1	10.02756	0.154109	70	0.001
5to6	1.1506	1	44700	315	0.019241	0.1	10.0426	0.165072	70	0.001
6to7	1.216	1	44700	385	0.022252	0.1	10.06021	0.17476	70	0.001
7to8	1.2743	1	44700	455	0.025095	0.1	10.08025	0.183504	70	0.001
8to9	1.3275	1	44700	525	0.027795	0.1	10.10256	0.191588	70	0.001
9to10	1.3776	1	44700	595	0.030355	0.1	10.12694	0.146851	95	0.001
10to11	2.07	1	44700	690	0.023427	0.1	10.11361	0.113163	185	0.001
11tooutside	21.67	1	44700	875	0.002838	0.1	10	1.7336	125	0

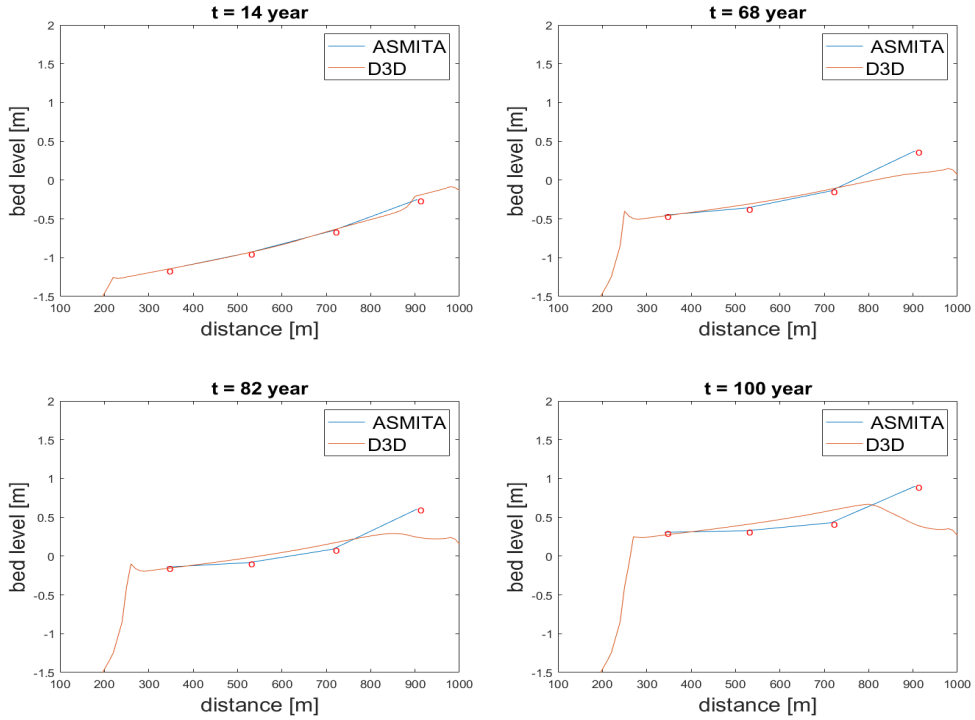

Figure 5.2: Full profiles of 5-element model in 7, 14, 82 and 100 year under 1.67 m/century SLR and 50 % drop in SSC at the boundary

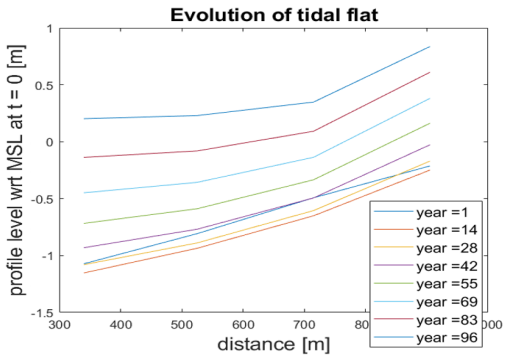

Figure 5.3: Full profile evolution under sudden 50 %drop in SSC and 1.67 m/century SLR case in 5-element ASMITA model

Figure 5.2 indicates that 5-element model roughly simulates the initial erosion at the side near the channel slope under **SLR** and **SSC** decrease impacts. It is because of the decrease in **SSC** level and the application of larger equilibrium water to stimulate the sink of mudflat in **ASMITA** model. The bed level change is determined by the difference between the equilibrium and local concentration in **ASMITA**. The larger equilibrium water depth increases equilibrium concentration and, accordingly, the erosion tendency of bed level. The erosion in the landward elements is unapparent because of the small difference between the new equilibrium and the initial state. The following deposition is caused by **SLR** impacts. However, for keeping the curved mudflat profiles, the element near the shoreline predicts a higher bed level than **D3D** in post runs. The sink cannot be tracked in **ASMITA**, by contract, **ASMITA** shows more accretion on the bed level in the landward end. The application value of water depth in the 5-element model is the maximum existing in the evolution process. However, after correcting the water depth of 0.18m and accordingly δ turning to $0.00948 m^3/s$, the model is capable of simulating the relatively unapparent deposition in the pre-operation and the gap near the shoreline at the same time, with a much lower diffusion coefficient, shown in Figure 5.5 and Figure 5.4.

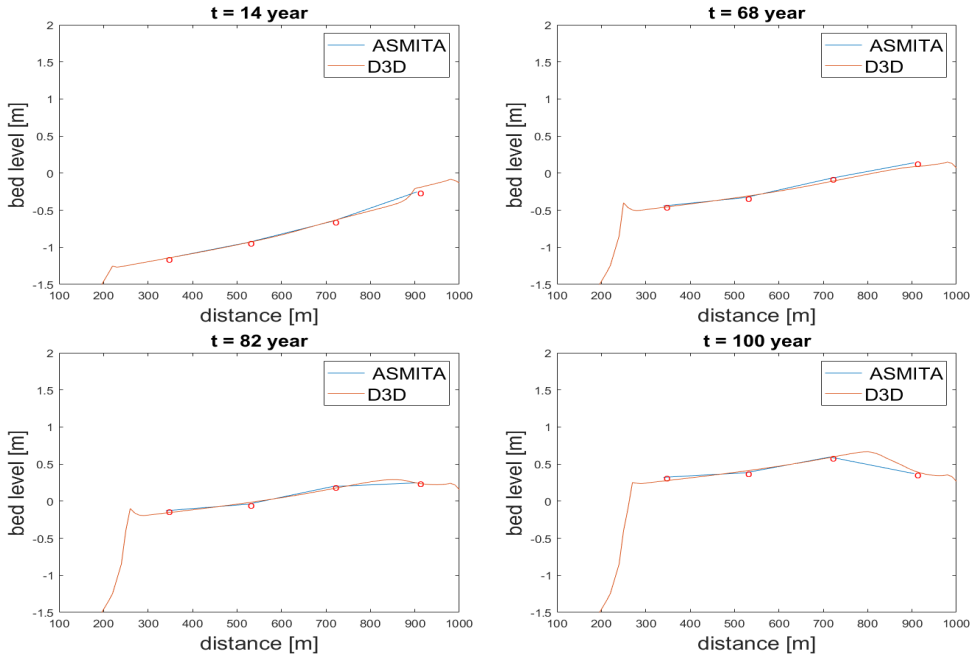

Figure 5.4: Full profiles of 5-element model with the modified δ values of the elements near the shoreline after 7, 14, 82 and 100 years under 1.67 m/century **SLR** and 50 % drop in **SSC** at the boundary

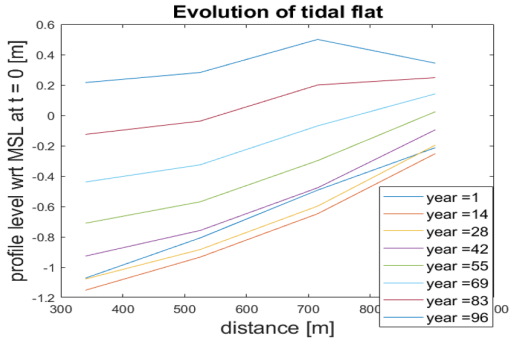

Figure 5.5: Full profile evolution with the modified δ values in the elements near the shoreline under sudden 50 %drop in **SSC** and 1.67 m/century **SLR** case in 5-element **ASMITA** model

The 11-element model with smaller elements near the shoreline should have enough ability to track a certain area in detail. But for the original setup of water depth with maximum, the volume of the elements near the shoreline **ASMITA** model drops to zero in the first simulation year, and thus the program reports errors. This is because the large diffusion coefficients result in a low morphological timescale, especially for the elements with the volume of the order of 1. Slightly modifying the diffusion coefficients of Element 1, Element 2 and Element 3, suggests the similar outputs as **D3D** (Figure 5.7 and Figure 5.6). The modified parameters are shown in Table 5.3:

Table 5.3: Overview of modified model parameters in 11-element model of **ASMITA** with 50 % drop in **SSC** at the boundary under 1.67 m/century **SLR**

Path	**H (m)**	**a (m)**	**T (s)**	L_b **(m)**	**u (m/s)**	ϵ	**D** (m^2/s)	δ (m^3/s)	**L (m)**	w_s **(m/s)**
1.67	m/century									
1to2	0.06	1	44700	35	0.040998	0.1	10.01008	0.00858	70	0.001
2to3	0.065	1	44700	105	0.113532	0.1	10.08378	0.009364	70	0.001
3to4	0.446	1	44700	175	0.027577	0.1	10.03392	0.06393	70	0.001
4to5	1.0758	1	44700	245	0.016006	0.1	10.02756	0.154109	70	0.001
5to6	1.1506	1	44700	315	0.019241	0.1	10.0426	0.165072	70	0.001
6to7	1.216	1	44700	385	0.022252	0.1	10.06021	0.17476	70	0.001
7to8	1.2743	1	44700	455	0.025095	0.1	10.08025	0.183504	70	0.001
8to9	1.3275	1	44700	525	0.027795	0.1	10.10256	0.191588	70	0.001
9to10	1.3776	1	44700	595	0.030355	0.1	10.12694	0.146851	95	0.001
10to11	2.07	1	44700	690	0.023427	0.1	10.11361	0.113163	185	0.001
11tooutside	21.67	1	44700	875	0.002838	0.1	10	1.7336	125	0

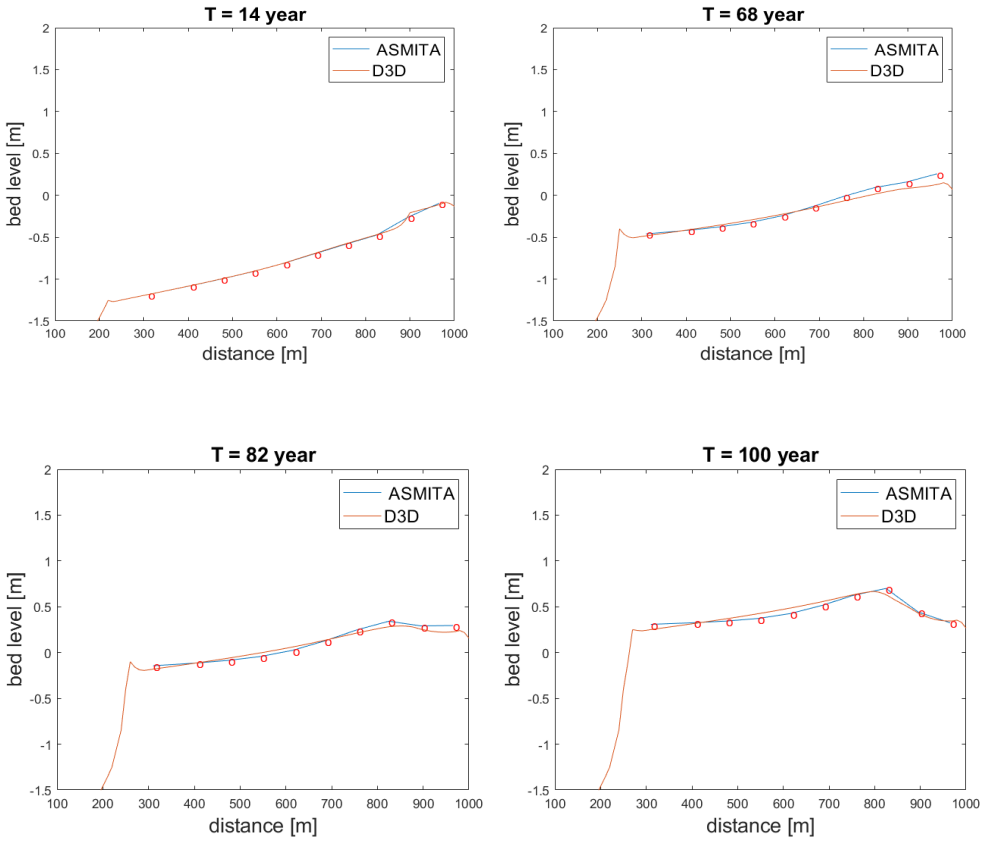

Figure 5.6: Full profiles of 11-element model with the modified δ values of the elements near the shoreline after 7, 14, 82 and 100 years under 1.67 m/century **SLR** and 50 % drop in **SSC** at the boundary

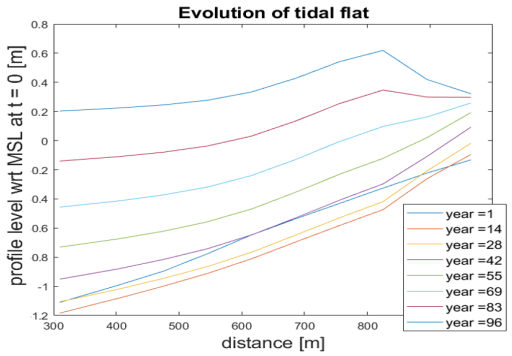

Figure 5.7: Full profile evolution with the modified δ values in the elements near the shoreline under sudden 50 % drop in **SSC** and 1.67 m/century **SLR** case in 11-element **ASMITA** model

The outcomes in Figure 5.4 and Figure 5.6 imply that **ASMITA** model can reproduce the local morphological changes through reasonably modifying the diffusion coefficients to ensure the correct morphological timescale for every element. The inclusion of many elements in **ASMITA** model can be more specific to plot the morphodynamics in detail but with more calibration efforts.

5.2 HYBRID MODEL

5.2.1 Steepness of Mudflat in Hybrid model

From Chapter 4, the predictive profiles in the hybrid modeling approach are almost the same as **D3D** at the beginning, while the deviation in the steepness becomes more and more obvious after 20 years, i.e., the mudflat profile of **D3D** is gentler than the hybrid model. The main differences between the two modeling approaches lie in the sediment transport module.

In the beginning, **MSL** does not have an apparent rise so that the morphological variations of the mudflat are slight, and the discrepancies between **D3D** and hybrid modeling approaches can be negligible (Figure 5.8). However, the accretion rate in the landward end starts to exceed the level at the edge of mudflat after 30 years. The variation in water depth can directly be reflected in the computation of equilibrium concentration in the hybrid model. In contrast, the equilibrium concentration and availability of sediments are closely related to the empirical sediment transport capacity in **D3D** which have noticeable fluctuations in every tidal cycle.

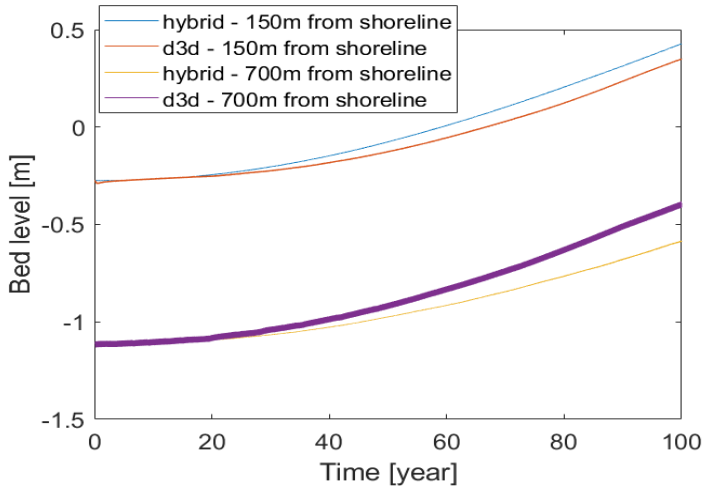

Figure 5.8: Comparison on the evolution of mudflat bed level between **D3D** and hybrid model at the 150 m and 700 m from shoreline under 0.83 m/century **SLR**

Figure 5.9 indicates that **SSC** level of **D3D** from overall trend in the shallow water is less sensitive than hybrid modelling approach. The tidally average **SSC** level, which is at 150 m from the shoreline, nearly keeps the constant with the water level rising in **D3D** model. From more direct and intuitive influences of water level changes, this results in the larger sediment concentration gradient along the mudflat in the hybrid model, and accordingly, the diffusion-dominated transport can transport more sediments towards the landward direction. This is because the concentration discrepancy between the deep water and shallow water grows over time (Figure 4.38). The mechanism explains the steeper mudflat profile in the hybrid model since more sediments deposit near the shoreline. Closer analysis on the tidally average **SSC** in **D3D** (Figure 5.10) reveals the smaller sediment concentration gradient along the mudflat during the evolution. The tidally average **SSC** at different parts of mudflat do not dominantly vary during the evolution process, and this thus results in the almost parallel accretion on the mudflat.

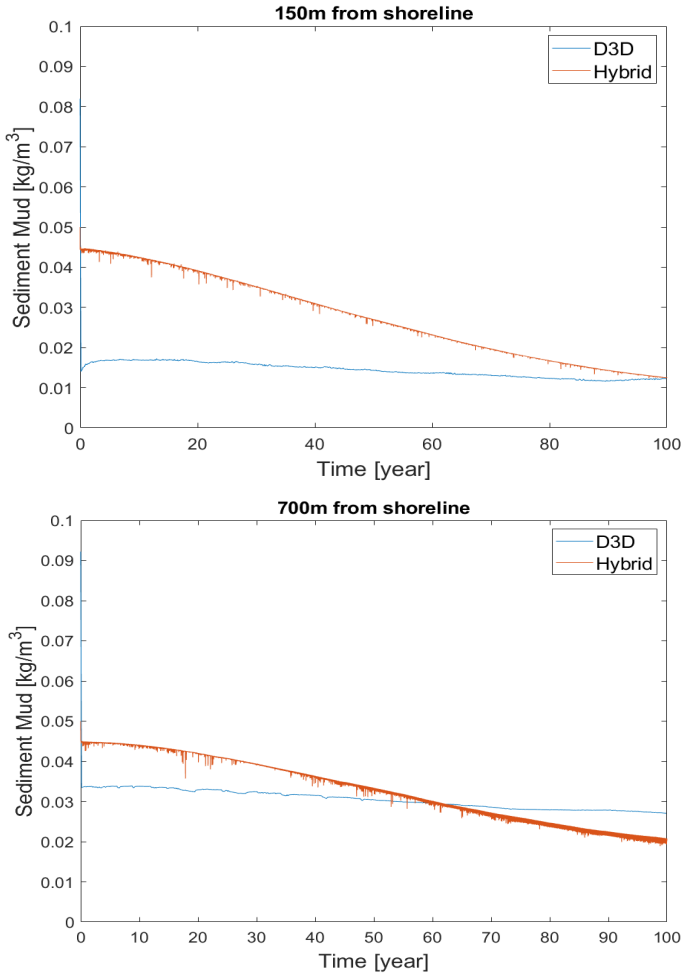

Figure 5.9: Comparison on the (tidally average) **SSC** between **D3D** and hybrid model at the 150 m and 700 m from shoreline under 0.83 m/century **SLR**

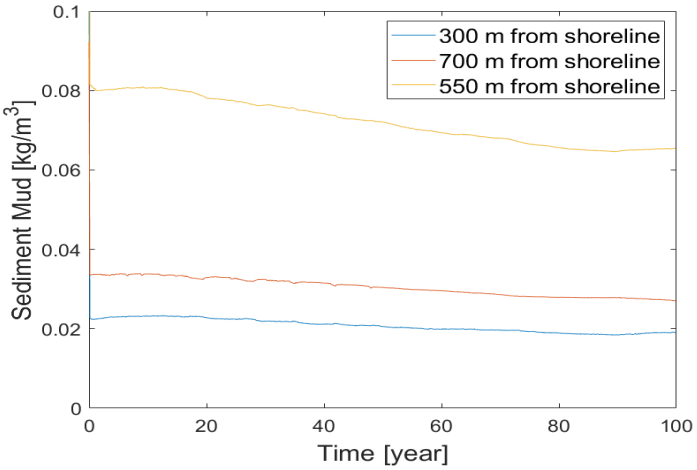

Figure 5.10: Evolution of tidally average **SSC** across the mudflat in **D3D** under 0.83 m/century **SLR**

In order to lower the slope of predictive mudflat, it is vital to decrease the concentration gradients inside mudflat in the hybrid model. The first possible solutions on the steeper profile are as follows. The computation of equilibrium concentration does not depend on the sediment characteristics and flow velocity in the hybrid model. Instead, the relation between the actual water depth and equilibrium state (Equation 5.1). This implies that the equilibrium concentration is sensitive to the

application of power values, n. Therefore, we can try to run the hybrid model again but with different powers (n = 2 and n = 4) to verify if the parameter can influence the steepness of mudflats. With increasing in the water depth in the scenario of **SLR**, the equilibrium concentration level accordingly declines.

$$c_e = c_E(\frac{h_e}{h})^n \tag{5.1}$$

As indicated in Figure 5.11, the final complete profile level lowers with the reduction in the power value. This is because c_e is less sensitive to the ratio h_e/h in the case of smaller n (Figure 5.12) so that the rate of descent in c_e and accordingly the accretion rate of bed level, which is determined by the difference between the equilibrium concentration and the actual concentration field, slow down. The opposite case appears in the more significant n application ($n = 4$), and there is more deposition on the whole mudflat. Furthermore, a lower level of sensitivity for the complete tidal flat with a larger power leads to a lower concentration gradient within mudflat. This is since the larger power reduces the orders of magnitude of the right part in Equation 5.1 and accordingly the difference in the sensitivity between the shallow water and deep water. This mechanism contributes to the milder profile with larger power values (n = 4).

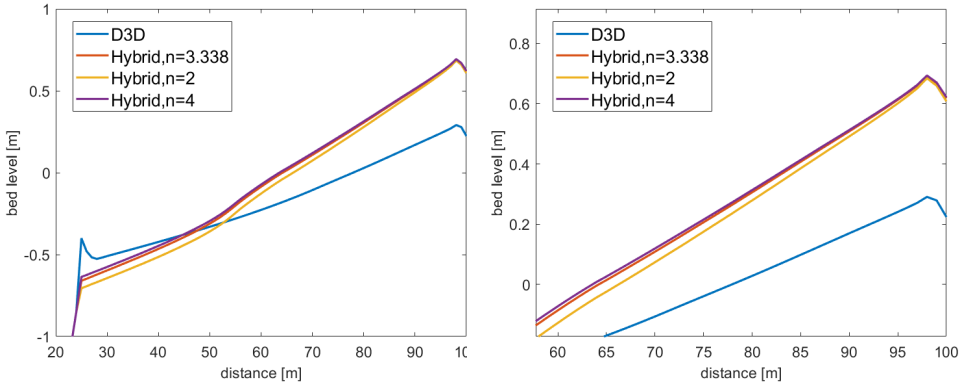

Figure 5.11: Scenarios on the different powers under **SLR** rate of 0.83 m/century and its close-up in the 100th year (Blue line represents the profile predicted by **D3D**)

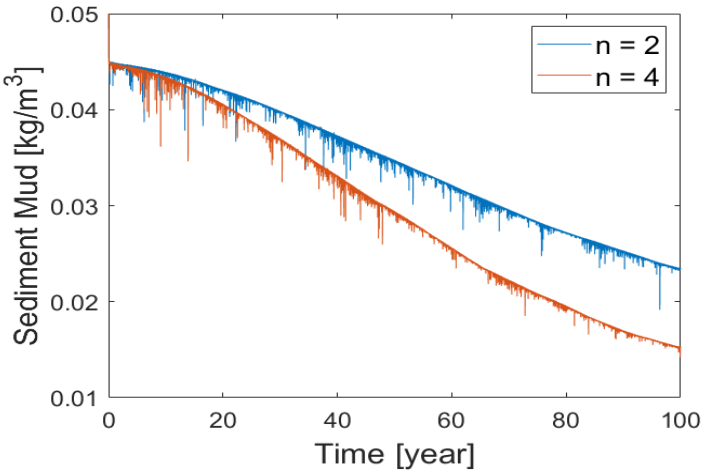

Figure 5.12: Comparison on the concentration between different power applications at the 500 m from shoreline under 0.83 m/century **SLR**

The adjusted mudflat profiles are still steeper than **D3D** modeling approach, and the power n does not have pronounced effects on the change of the steepness of mudflat in the hybrid model. Raising the reference **MSL**, as the second method, can

reduce the sensitivity of the hybrid model by rising in the water depth. A higher equilibrium water depth corresponds to the higher reference level, lowering the sensitivity of concentration variations with a slower deposition rate on the mudflat. Figure 5.14 indicates that a reference level of + 0.5 m reduces the variations of concentration over time in comparison with the reference level of 0 m. Thus, a lower whole bed level is expected in the hybrid model run. Moreover, the shallow section of mudflat becomes relatively insensitive to the water level change, which makes the slope milder.

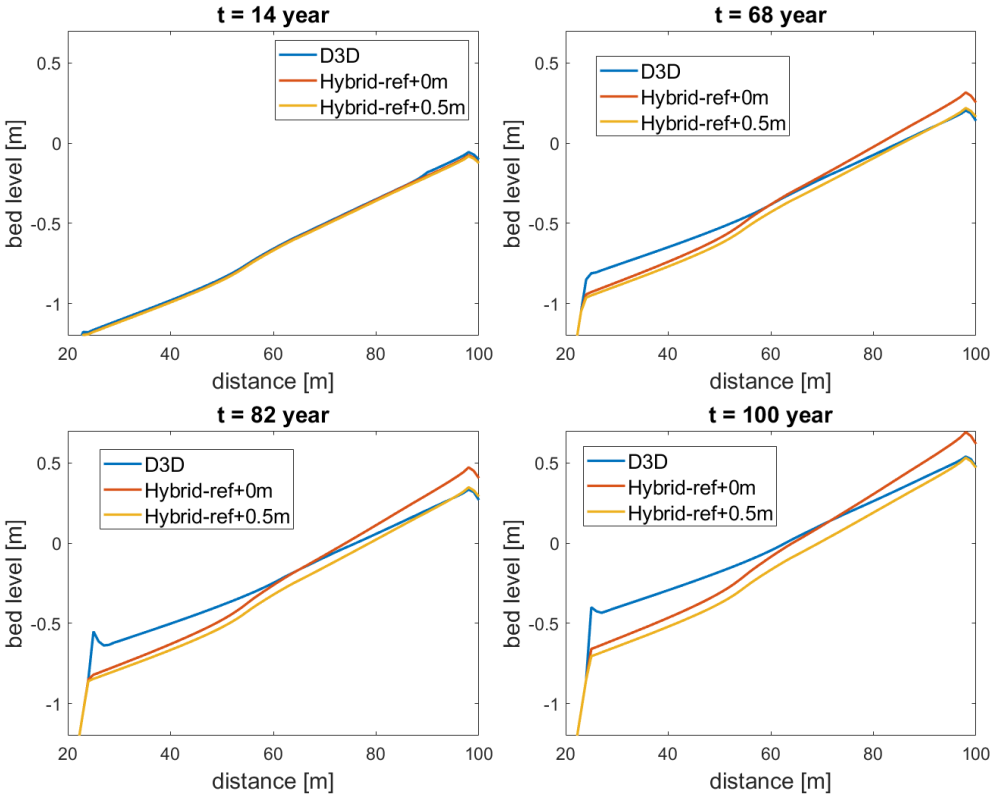

Figure 5.13: Comparison among the hybrid model runs with different reference levels and D3D run under 0.83 m/century SLR after 14, 68, 82 and 100 years

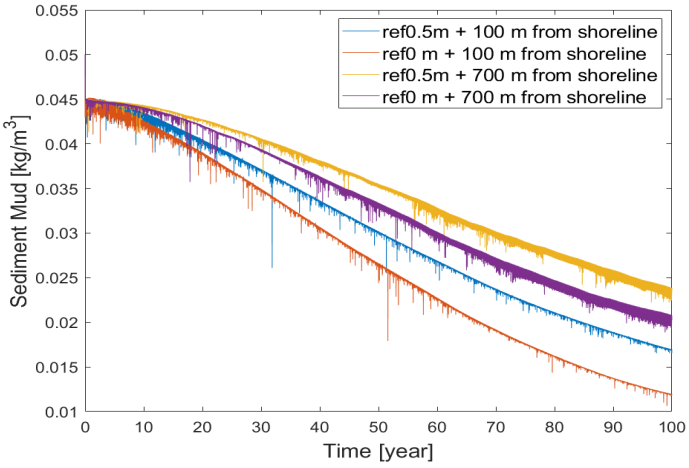

Figure 5.14: Comparison on the concentration evolution among the hybrid model runs with different reference levels across the mudflat under 0.83 m/century SLR

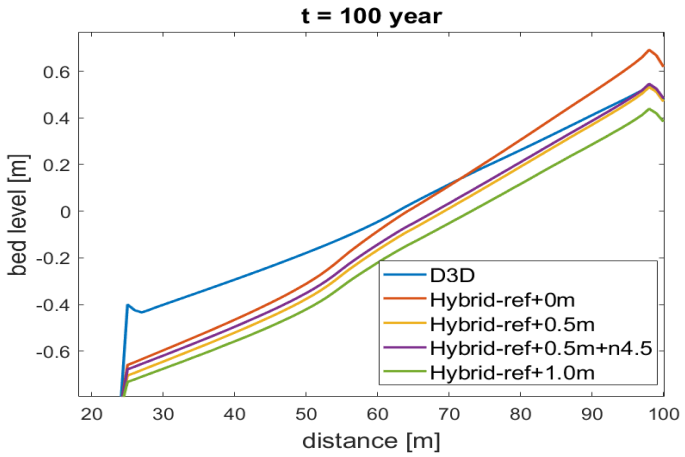

Figure 5.15: Comparison among the hybrid model with different reference levels as well as powers and **D3D** model under 0.83 m/century **SLR**

Figure 5.13 indicates that the rise in the reference level to + 0.5 m slightly decreases mudflat slope without too low bed level. Further lowering the steepness by + 1.0 m reference level, as indicated in Figure 5.15, the complete tidal flat with low deposition does not reach the same elevation as the one in **D3D** model. The first solution of applying large power can improve the total elevation but reduce the slope. We conducted the run with n of 4.5 and a reference level of + 0.5 m. The result in Figure 5.15 suggests that the combination of large power and reference level can reduce the steepness with a higher bed level to some extent.

5.3 RELATIONSHIP AMONG THREE MODELLING APPROACHES

In this research, the further runs in **ASMITA** and hybrid model are based on the setup and results of **D3D** in essence. This is because:

- **D3D** contributes to the parameter calibration in **ASMITA** consisting of the parameters determining the equilibrium state of profile and adaption time scale.
- The parameters originated from **ASMITA** e.g., global equilibrium concentration, c_E and the power, n, applied in the relation between equilibrium and actual morphology, and the rough structure of **D3D** modeling approach, as well as equilibrium elevation in the numerical grids, can be extracted in the sake of building the hybrid model.

The timescale computation in Chapter 4 suggests that diffusion transport is more evident than advection. Moreover, we can gain insights into the tide motion impacting less dominantly on the equilibrium state as well as the adaption process in the sensitivity analysis exerted in **D3D**, but the case with the average tidal motion may not activate the development of mudflat. Due to the different sediment exchange computation in the hybrid model from **D3D**, the computational model provides the opportunity to neglect wave effects in the simulations of the hybrid model and thus improve the computational efficiency. However, the simulations after averaging tidal motion are not promising with the unrealistic bed level developments and unstable concentration fields, which indicate that tides play an essential role in the restriction of the accretion at the edge of mudflat under **SLR**. The improvement in the time step or (and) grid size is to verify if the methods can improve the operational efficiency in the hybrid model.

The simulation results from **ASMITA** and hybrid model suggest that two modeling

approaches have (limited) abilities to reproduce the results of **D3D**. From the perspective of run time, **ASMITA** has the overwhelming advantages in which the run needs a few minutes, compared with the hybrid model and **D3D**. The modeling approach can thus shorten plenty of time in the case of long-term morphological development. Nevertheless, the predictive landward edge of mudflat under larger **SLR** cannot obtain enough sediments transported from the edge near the channel by diffusion sediment transport. Thus this results in the gentler profile if following the existing instructions to set up the diffusion coefficient. This can be optimized by improving the values of diffusion coefficient near the land boundary, which needs more calibration efforts, especially for the application of **ASMITA** model with a larger number of elements.

The hybrid modeling approach, which is closer to the structure of **D3D**, can be used to seek the possibilities to optimize **D3D** run. The simulations of expanding time step and grid size scenarios in Chapter 4 suggest that the hybrid model can shorten the run time while ensuring the stability and accuracy of runs. However, the run results from the hybrid model also indicate that the predictive profiles are gentler than **D3D** with the original configurations. The parameters input needs to be further calibrated. The simulation with the reference level of + 1m to predict a milder slope (Figure 5.15) inspires that the hybrid model could give good results in the case of the mudflats with a relatively larger depth, which can be tested in further study.

6 CONCLUSION-RECOMMENDATIONS

This research aims to compare the behaviors of three modeling approaches in the case of long-term morphological evolution of inter-tidal flat under impacts of **SLR**. The study can be divided into three phases: Phase 1 analyzed the existing **D3D** model applying for a transect in the South San Francisco Bay and conducted the extensive sensitivity analyses on which wave, tide, and **SSC** were tested how they influence the morphological timescale and equilibrium state of mudflat system. Phase 2 mainly investigated the feasibility of reproduction of **D3D** results by one-element model and multi-element model. Phase 3 focused on the hybrid model to simulate the same scenarios as **D3D** but with a series of optimizations.

This study is concluded by answering the research questions indicated in Chapter 1. The main question is as follows:

What are the comparison results among process-based modeling approaches, aggregated modeling approaches, and hybrid models for a case that has been modeled successfully with the process-based model D3D: the development of tidal flat cross-section profile under the influence of sea-level rise?

The main research question can be answered by explaining the sub-questions, which are done below.

6.1 RESEARCH QUESTIONS

Do the three modeling approaches predict the same behavior of the tidal flat responding to sea-level rise?

Generally speaking, **D3D** model is capable of computing the flows, sediment transports, waves, and morphological developments in every numerical grid so that it enables the full profile of mudflat simulated and accordingly covers more details about the behaviors of tidal flat developments. **ASMITA** modeling approach, with a higher aggregation level than **D3D**, only focuses on the prediction of the variables with aggregated characteristics, e.g., the aggregated water depth in the limited range. This leads that one-element **ASMITA** cannot predict the full mudflat profile in the evolution process. Instead, the average bed level of the complete mudflat is predicted. The one-element model aggregates the mudflat and a certain part of the channel with its slope as a whole. However, the spatial scale of Dumbarton mudflat is 1000, which is much smaller than the whole tidal basin involving different elements, e.g., channels and shoals. As such, it brings the possibilities that the whole mudflat can be roughly plotted by **ASMITA** model under the impacts of **SLR**, if using more elements to divide the mudflat into smaller parts. Same behavior as **D3D**, the simulation results of **ASMITA** indicate that generates the accretion on the mudflat responding to **SLR**. Nevertheless, the rate of deposition at the landward end, which is indicated by the increase in the aggregated parameters, i.e., water depth relative to **MSL**, cannot keep up with **SLR** in **D3D** model in the case of 1.67 m/century. For this monotonous deposition and erosion, **ASMITA** can be regarded as a useful tool to make predictions with a certain degree of accuracy and plot the

rough profiles of the mudflat. For the local morphodynamics, Chapter 5 suggests that **ASMITA** has the ability to reproduce **D3D** as well.

The hybrid model is a new long-term morphological modeling approach implemented in **D3D**. The phase 3 runs in the hybrid model can predict the accretion of mudflat responding to **SLR**, but the profile is steeper than **D3D** and the steepness increases over time.

What are the requirements for the parameter settings in the aggregated modelling in order to reproduce quantitatively the same results as the process-based modelling?

The application of parameters in the process-based model is of importance to reproduce qualitatively and quantitatively the same morphological developments of mudflat as **D3D** in the aggregated model. The first series of parameters are related to the equilibrium state of the intertidal flat system. The calibration of these parameters needs to be based on a long-term morphological development available. Here **D3D** model has been calibrated by the historical data which the model results could reproduce the 2011 measured profile quite well, and accordingly, the simulations provide the morphological equilibrium. The numerical information can thus achieve the parameter input, and the equilibrium state is well represented in the aggregated model. In addition, the calibration of parameters defining the morphological timescale of the mudflat system consists of the power indicating the relation between the equilibrium morphology and actual morphology, the global equilibrium concentration suggesting the sediment need for the whole mudflat system, the diffusion coefficient reflecting the horizontal transport and settling velocity, need to represent the correct morphological timescale. Chapter 3 presents the specific calibration suggestions.

How far can the spatial aggregation go?

Due to the limitation of this research that only focuses on a 1-dimensional transect of mudflat and the lack of **D3D** model simulations for the 2-D or 3-D space, the application in this research cannot expand the mudflat profile to multidimensional space. Nevertheless, the mudflat can be specified separated into a certain amount of sections as the aggregated elements in **ASMITA** to answer how far the spatial aggregation can go. The results of Phase 2 in the case of **SLR** scenarios indicate that the simulations are promising under 0.83 m/century water level rise for multi-elements. However, the doubling **SLR** (from 0.83 m/century to 1.67 m/century) leads that the prediction at the landward end deviates from **D3D** due to the smaller deposition rate. This can be made up by the modification of diffusion coefficients in **ASMITA** model. The relatively flat profiles with monotonic deposition under slower **SLR** impacts during evolution enable the predictions by **ASMITA** easier, and the spatial aggregation scale can be small with the magnitude of the order of 1, e.g., 11-element model. Considering the local deposition and sink of mudflat in the cases of, e.g., the abrupt drop in **SSC** level at the boundary, the predictions in **ASMITA** still have the capacity of reproducing the mudflat evolution as **D3D**. Chapter 5 indicates that the reproduction of filling up the erosion near the channel in the pre-operation and the gap generated in the landward end are possible in 5-element and 11-element **ASMITA** models. However, the diffusion coefficients in multi-element models need to be modified as well, similar to the cases of **SLR** alone. This can be achieved by reducing the applied water depth in δ to simulate the sink at the landward end with a slower deposition rate. As indicated in the 11-element model, **ASMITA** model run abruptly stops in that the application of excessive water depth leads to numerous sediments transported to the elements near the shoreline with the initial volume

of the magnitude of the order of 10. It, therefore, cannot simulate the dominant gap in the later stages suggested in D3D model. The application of the diffusion coefficients needs to be given thorough consideration, especially for the elements representing the partial variations with the small original volume configuration.

What is the best way of combing the three modelling approaches?

The foundation in this study is the simulations in D3D modeling approach, which has been successfully applied in South San Francisco Bay. D3D provides not solely the available information to calibrate the parameters in ASMITA model, but also the similar model setups and inspirations to decrease the unnecessary processes and thus raise the operation efficiency in the hybrid model. ASMITA model with the least time-consuming characteristics is adequate to simulate the longer-term morphodynamics of mudflat responding to SLR. This provides rough predictions of profile development, i.e., the general steepness. The number of elements determines the level of detail in the profile of the intertidal flat, the multi-element ASMITA models are promising to predict the partial morphological changes. Moreover, ASMITA has the capacity of modeling the morphological developments of the mudflat under different SLR scenarios. We need to pay attention to the further calibration of diffusion coefficients in the scenarios of the larger SLR and local bed level changes. The simulation duration of the hybrid model shall be longer than ASMITA model. Yet, the optimization methods applied in the hybrid model, e.g., larger time steps or neglecting the unnecessary processes, can significantly improve the run efficiency. It is therefore concluded that the hybrid model can be used to optimize the simulation of D3D in that it is more robust than D3D and effectively avoid the spin-up time, so that makes it possible to keep the numerical stability and modeling efficiency at the same time. However, the hybrid model, which is sensitive to the water depth, predicts the shallow mudflat being inaccurate with a faster accretion rate. Accordingly, the complete slope is steeper than D3D. The steepness can be slightly alleviated, to some extent, by enlarging the power, n, and reference level of MSL.

What are the comparison results among process-based modelling approaches, aggregated modelling approaches and hybrid models for a case that has been modelled successfully with the process-based model D3D: the development of tidal flat cross-section profile under influence of sea-level rise?

Phase 2 and Phase 3 fully demonstrate different comparisons among the three modeling approaches. One-element ASMITA model perfectly reproduce the average bed level evolution from D3D model. The aggregation feature in ASMITA allows predicting the aggregated variables. Multi-element ASMITA models obtain not only the adaption process of the mean profile level but also the full profile by fitting the curves to simulate the morphology of mudflat. The comparison results are promising even if the smaller steepness of mudflat is observed under large SLR. The gentler slopes only occur in the post-run with the fast acceleration of SLR. Slight calibration in the diffusion coefficient shall offset the shortcomings. Moreover, concerning the situation of the local changes in the bed level, ASMITA model has the capacity of accurately tracking the morphodynamics of the mudflat as well. Phase 3 focuses on the comparisons among D3D, the hybrid model with the standard runs, and the modified runs. The hybrid model consisting of the tide motion predicts a relatively steeper profile in contradistinction to D3D. The problem can be mildly solved by the regulation of the power value and reference water level. The average tides induce the numerical instabilities at the edge of mudflat in the pro-phase, which induces an unrealistic deposition near the channel. However, the mudflat evolution converges to be stable after the 50-year. This implies that varying

tidal motion plays a significant role in preventing the accretion in the levee even if the diffusion transport is dominant. Moreover, the adjustments in the numerical setup are capable of shortening the simulation time, and the double time step and grid size is a good attempt.

6.2 RECOMMENDATIONS

6.2.1 2D model

The modeling exercise implemented different modeling approaches in the case of the 1-Dimension transect, instead, 2D configurations. It limits the application of the morphological models without enough certifications to verify if **ASMITA** and the hybrid model can successfully reproduce **D3D** in the broader area as well. Further studies on the long-term morphological developments of mudflats prediction can be expanded to 2D in **ASMITA** and the hybrid models. For **ASMITA**, it can specify and separate the mudflat in the numerous small-scale aggregated elements to predict the morphological developments in the multi-dimension, instead of integrating over a certain length of the intertidal flat. The hybrid model can test different optimizations and save more time in a 2D model. The comparisons among different modeling approaches in the multidimensional model can be exerted. Based on the simulations with expanding the spatial range, the sub-question, **how far the spatial aggregation can go** can be re-answered. The further runs will gain more insights into the spatial range of which the morphological modeling approaches can be applied, simultaneously, with a certain level of feasibility and efficiency.

6.2.2 Sensitivity of the Hybrid model

The hybrid model newly developed has not many studies on the behaviors in the case of **SLR**. In this research, the mudflat in the shallow water is more sensitive to the variation of water level and cannot give a good result in the reproduction of the **D3D** model. The calibration in the power and reference level is not practical to regulate the steepness of the mudflat in South San Francisco Bay by reducing the sensitivity of shallow mudflats. As such, we can test the hybrid model in the prediction of morphodynamics in relatively deep water.

6.2.3 Optimization in the Hybrid Model

The optimizations in the hybrid model in this research start from neglecting the advection transport, and expanding the grid size as well as the time steps. Some attempts prove the validity and feasibility of the optimizations applied in the hybrid model, suggested in the promising outcomes. The further runs in the hybrid model can carry on the further promotion of the time step and the grid size within the allowable error range to reproduce **D3D**.

BIBLIOGRAPHY

Ariathurai, R. and Krone, R. (1974). Finite element mode for cohesive soils. *Journal of Hydraulic Engineering, Div. ASCE*, 104:279–283.

Bearman, J. A., Friedrichs, C. T., Jaffe, B. E., and Foxgrover, A. C. (2010). Spatial trends in tidal flat shape and associated environmental parameters in south san francisco bay. *Journal of Coastal Research*, 26(2):342–349.

Bosboom, J. and Stive, M. J. (2012). *Coastal dynamics I: lectures notes CIE4305*.

Cheng, R. T., Casulli, V., and Gartner, J. W. (1993). Tidal, residual, intertidal mudflat (trim) model and its applications to san francisco bay, california. *Estuarine, Coastal and Shelf Science*, 36(3):235–280.

Conomos, T., Smith, R., and Gartner, J. (1985). Environmental setting of san francisco bay. In *Temporal dynamics of an estuary: San Francisco Bay*, pages 1–12. Springer.

de Vriend, H. J. (1996). Mathematical modeling of meso-tidal barrier island coasts part i: empirical and semi-empirical models. In *Advances in coastal and ocean engineering*, pages 115–149. World Scientific.

Dissanayake, D., Ranasinghe, R., and Roelvink, J. (2012). The morphological response of large tidal inlet/basin systems to relative sea level rise. *Climatic change*, 113(2):253–276.

Elmilady, H., Van der Wegen, M., Roelvink, D., and Jaffe, B. (2019). Intertidal area disappears under sea level rise: 250 years of morphodynamic modeling in san pablo bay, california. *Journal of Geophysical Research: Earth Surface*, 124(1):38–59.

Fleming, K., Johnston, P., Zwartz, D., Yokoyama, Y., Lambeck, K., and Chappell, J. (1998). Refining the eustatic sea-level curve since the last glacial maximum using far-and intermediate-field sites. *Earth and Planetary Science Letters*, 163(1-4):327–342.

Foxgrover, A. C., Higgins, S. A., Ingraca, M. K., Jaffe, B. E., and Smith, R. E. (2004). Deposition, erosion, and bathymetric change in south san francisco bay: 1858–1983. *US Geological Survey Open-File Report*, 1192:25.

Herman, P., Middelburg, J., Van de Koppel, J., and Heip, C. (1999). Ecology of estuarine macrobenthos. *Advances in ecological research*, 29(780):195–240.

Kemp, A. C., Horton, B. P., Donnelly, J. P., Mann, M. E., Vermeer, M., and Rahmstorf, S. (2011). Climate related sea-level variations over the past two millennia. *Proceedings of the National Academy of Sciences*, 108(27):11017–11022.

Kragtwijk, N., Zitman, T., Stive, M., and Wang, Z. (2004). Morphological response of tidal basins to human interventions. *Coastal engineering*, 51(3):207–221.

Lesser, G. R., Roelvink, J. v., van Kester, J. T. M., and Stelling, G. (2004). Development and validation of a three-dimensional morphological model. *Coastal engineering*, 51(8-9):883–915.

Lodder, Q. J., Wang, Z. B., Elias, E. P., van der Spek, A. J., de Looff, H., and Townend, I. H. (2019). Future response of the wadden sea tidal basins to relative sea-level rise—an aggregated modelling approach. *Water*, 11(10):2198.

Parris, A. S., Bromirski, P., Burkett, V., Cayan, D. R., Culver, M. E., Hall, J., Horton, R. M., Knuuti, K., Moss, R. H., Obeysekera, J., et al. (2012). Global sea level rise scenarios for the united states national climate assessment.

Schoellhamer, D. H. (1996). Factors affecting suspended-solids concentrations in south san francisco bay, california. *Journal of Geophysical Research: Oceans*, 101(C5):12087–12095.

Townend, I., Wang, Z. B., Stive, M., and Zhou, Z. (2016). Development and extension of an aggregated scale model: Part 1–background to asmita. *China Ocean Engineering*, 30(4):483–504.

Van der Wegen, M., Jaffe, B., Foxgrover, A., and Roelvink, D. (2017). Mudflat morphodynamics and the impact of sea level rise in south san francisco bay. *Estuaries and Coasts*, 40(1):37–49.

Van der Wegen, M., Roelvink, J., and Jaffe, B. E. (2019). Morphodynamic resilience of intertidal mudflats on a seasonal time scale. *Journal of Geophysical Research: Oceans*, 124(11):8290–8308.

Van Goor, M., Zitman, T., Wang, Z., and Stive, M. (2003). Impact of sea-level rise on the morphological equilibrium state of tidal inlets. *Marine Geology*, 202(3-4):211–227.

Walters, R., Cheng, R., and Conomos, T. (1985). Time scales of circulation and mixing processes of san francisco bay waters. In *Temporal dynamics of an estuary: San Francisco Bay*, pages 13–36. Springer.

Wang, Z. B., De Vriend, H. J., Stive, M. J., Townend, I. H., Dohmen-Jansen, C., and Hulscher, S. (2008). On the parameter setting of semi-empirical long-term morphological models for estuaries and tidal lagoons.

Wang, Z. B., Elias, E. P., van der Spek, A. J., and Lodder, Q. J. (2018). Sediment budget and morphological development of the dutch wadden sea: impact of accelerated sea-level rise and subsidence until 2100. *Netherlands Journal of Geosciences*, 97(3):183–214.

Wang, Z. B., Townend, I., and Stive, M. (2020). Aggregated morphodynamic modelling of tidal inlets and estuaries. *Water Science and Engineering*, 13(1):1–13.

A EQUATIONS OF SEDIMENT TRANSPORT IN PROCESS-BASED MODEL AND AGGREGATED MODEL

The main difference between ASMITA and the process-based model (e.g., Delft3D) is in the level of aggregation in spatial and temporal scales. ASMITA model is based on the same principle as the process-based model in the case that the suspended sediment transport is dominant, suggesting in the advection-diffusion equation (Townend et al. [2016]; Wang et al. [2018]). For 3D convection-diffusion equation:

$$\frac{\partial c}{\partial t} + \frac{\partial (uc)}{\partial x} + \frac{\partial (vc)}{\partial y} + \frac{\partial (wc)}{\partial z} - \frac{\partial}{\partial x}(\epsilon_x \frac{\partial c}{\partial x}) - \frac{\partial}{\partial y}(\epsilon_y \frac{\partial c}{\partial y}) = w_s \frac{\partial c}{\partial z} + \frac{\partial}{\partial z}(\epsilon_z \frac{\partial c}{\partial z}) \quad \text{(A.1)}$$

Where:

c=sediment concentration;

t =time;

u, v = horizontal flow velocity components;

x, y = horizontal coordinates;

w = vertical flow velocity;

z = vertical coordinate;

ϵ = turbulent diffusion coefficient;

w_s =settling velocity.

To solve the equation, a bed boundary condition is needed: the sediment concentration where the downward flux can be obtained by the concentration multiplying with settling velocity, or the sediment concentration gradient where the upward flux is the result of the product of the gradient and vertical diffusion coefficient. For sand, the asymptotic solution of the equation is the sediment exchange between the bottom and water column. For mud, this can be obtained by Krone-Partheniade formula (Ariathurai and Krone [1974]).

The equation can be integrated into the vertical direction to get the depth-averaged advection-diffusion equation:

$$\frac{\partial h\bar{c}}{\partial t} + \frac{\partial (\alpha_x \bar{u} h \bar{c})}{\partial x} + \frac{\partial (\alpha_y \bar{v} h \bar{c})}{\partial y} - \frac{\partial}{\partial x}(D_x h \frac{\partial \bar{c}}{\partial x}) - \frac{\partial}{\partial y}(D_y h \frac{\partial \bar{c}}{\partial y}) = E - D_b \quad \text{(A.2)}$$

Where:

α = coefficient counting for the effects of the shapes of the vertical distribution of flow velocity and sediment concentration;

D_x, D_y = dispersion coefficients;

E = erosion at the bottom;

D_b = deposition to the bottom

This is used for process-based model as the first-level of aggregation. It can also be written as:

$$\frac{\partial(h\bar{c})}{t} + \frac{\partial s_x}{\partial x} + \frac{\partial s_y}{y} = E - D_b \tag{A.3}$$

Where s_x, s_y indicate the suspended sediment transport rate in x- and y- direction. This equation can be further aggregated in the scale of a morphological element. By using Green's theorem:

$$\frac{\partial(VC)}{\partial t} = \sum_i S_i + Source - Sink \tag{A.4}$$

Herein, V is the volume of the water body of the area and S_i denotes sediment transport at open boundary (positive is import).

The equation used in ASMITA need to aggregate this equation in time:

$$\sum S + Source - Sink = 0 \tag{A.5}$$

Here Source and Sink terms cannot be computed by the independent formula for sediment transport and bed erosion in that there is no available detained information on flow strength due to aggregation. Therefore, both models try to represent the same physical process but at different levels of aggregation.